UNIVERSIDADE DE LISBOA
FACULDADE DE CIÊNCIAS
DEPARTAMENTO DE FÍSICA


# Synthesis, characterization, and biological evaluation of peptides capable of interfering with RANK-TRAF6 pathway using nuclear imaging

Kyle Manuel Ferreira Gonçalves

**Mestrado em Engenharia Biomédica e Biofísica**

Dissertação orientada por:
Dr. João Domingos Galamba Correia
Dr. Nuno Matela

2022

# Acknowledgements

First and foremost, I'd like to express my gratitude towards Dr. João Domingos Galamba Correia, Dr. Nuno Matela, and Rúben Silva.

To Dr. João Domingos Galamba Correia, who provided me with the unique opportunity to carry on his wonderful project. His contagious enthusiasm, vision, knowledge, and patience to guide me was a pivotal experience in my academic journey.

Rúben Silva, who at the time of writing this got accepted to carry on his doctorate thesis. Rúben was there from the beginning, teaching me the fundamentals of experimental chemistry. Without his knowledge, attentiveness, and guide, this thesis would not be possible.

To Prof. Nuno Miguel de Pinto Lobo e Matela, who brought this project to my attention and guided me not only during my thesis, but my entire graduate degree. Not to mention the fantastic trip to Belgium. Those beers were delicious!

To my mother, father, and sister for their unwavering support throughout my life. They shaped who I am today, and I am grateful to have them. A special mention to my great-grandmother, who will always have a special place in my heart. Unfortunately, she is no longer with us, but will never be forgotten.

To the trio: Gonçalo Ribeiro, Henrique Almeida, and Inês Marques, who were there during many sleepless nights studying.

To Ana Abreu, my girlfriend and best friend, who puts up with me throughout the day and night.

Last but not least, to the whole $C^2$TN-UL community, and all the friends I made along the way: Ana Rita *Sorrisos* (the great company when getting coffee), Rúben Silva (the brainiac), Salete Baptista (the sensible one), João Machado (a great friend, but thinks he's funny when clearly not), Joana Duarte (the one who makes great memes), Catarina Pinto (the one who so graciously deals with all of us), Miguel Tarita (Alt + F4), Afonso André (Mr. 3pm), Sofia Martins, Sérgio Figueiredo (what a wonderful *bacalhau* that restaurant we had), Dr. António Paulo, Dr. Lurdes Gano, Elisabete Correia and Paula Campello.

*"The important thing is to not stop questioning. Curiosity has its own reason for existing. One cannot help but be in awe when contemplating the mysteries of eternity, of life, of the marvelous structure of reality. It is enough if one tries merely to comprehend a little of this mystery each day. The important thing is not to stop questioning;"*

Albert Einstein
"Old Man's Advice to Youth: 'Never Lose a Holy curiosity'". LIFE Magazine (2 May 1955) p. 64. ("What Einstein's journals teach us about Focus, Play, and Creativity") ("What Einstein's journals teach us about Focus, Play, and Creativity")

# Abstract

The RANK-RANKL interaction, and consequently, the RANK-TRAF6 pathway, is involved in several fundamental biological cycles, such as cell growth, apoptosis, osteosteoclastogenesis and inflammatory responses. As a result of partaking in such important processes, it is also implied that this pathway is related to severe pathologies, such as osteoporosis and breast or prostate cancer-induced bone metastasis. Currently, one of the therapeutic approaches to treat such diseases lies in the inhibition of RANK-RANKL interaction. Nonetheless, considerable interest arose in an alternative route, namely the inhibition of the RANK-TRAF6 pathway. This process is achievable, for example, by the interference of RANK's interaction with TRAF6 using decoy peptides (e.g., L-T6DP-1).[8] Thus, the objective of this project was to synthesize, purify and biologically evaluate two peptides (3A and its negative control, 3B) containing a cell penetrating sequence (KLFMALVAFLRFLT), combined with sequences designed *in silico* to interfere with the RANK-TRAF6 pathway (RQM**A**T**A**DE**A** and RQMP**T**E**D**E**Y**). Furthermore, biodistribution studies of peptides 3A and 3B, modified with a gallium-67 chelator were aimed to be achieved, in in vivo animal models, by micro-PET-SPECT-CT imaging. The aforementioned studies were not performed, as during the process, several issues arose. Some include long amino acid coupling times and difficulty radiolabeling peptide 3A. These adversities led to an overall unsuccessful procedure, requiring further optimization. Although the image acquisition of the synthesized peptides was impossible at this time, it was deemed that the equipment validation should still be made using an alternative compound that is currently being investigated by the C$^2$TN-IST group: a $^{67}$Ga-radiolabeled gold nanoparticle named $^{67}$Ga-AuNP-BBN-Pt1.

**Keywords:** Receptor Activator of Nuclear Factor Kappa B (RANK); Tumor Necrosis Factor Receptor Associated Factor 6 (TRAF6); Nuclear-Factor Kappa-B (NF-κB); Solid Phase Peptide Synthesis (SPPS); Nuclear Imaging.

# Resumo

A interação RANK-RANKL, e consequentemente a via RANK-TRAF6, encontra-se envolvida em diversos ciclos biológicos fundamentais, tais como o crescimento celular, apoptose, osteoclastogénese, e respostas inflamatórias. No seguimento da interferência em tais processos, é implícito que a disrupção do normal funcionamento desta interação possa resultar em patologias severas, das quais se destacam osteoporose, ou, em casos mais extremos, metástases ósseas resultantes de cancro da mama ou da próstata. Considerem-se, por exemplo, pacientes diagnosticados com cancro da mama ou da próstata. As células tumorais deste tipo de cancros expressam fatores osteoclastogénicos capazes de alterar o microambiente do osso, como interleucinas(IL)-6 e IL-8, proteínas relacionadas com a hormona paratiroideia (PTHrP), fatores de necrose tumoral-α (TNF-α), entre outros. PTHrP e IL-11 induzem expressão de RANKL, enquanto suprimem a atividade do seu fator inibitório, a osteoprotegerina (OPG). Tal favorece a interação de RANKL com o seu recetor, RANK. A interação de RANK com o seu ligando, desencadeia uma cascata de eventos, que culmina com a ativação do fator nuclear kappa-β (NF-kβ), um complexo proteico que regula mecanismos de resposta inflamatória, crescimento celular e apoptose. Dentro destes mecanismos, encontra-se a expressão genética osteoclástica e consequente osteoclatogénese que leva à reabsorção óssea. Encontramo-nos assim perante um *loop* de *feedback* positivo, no qual a alteração no microambiente do osso promove o crescimento de células cancerosas, que, por sua vez, promovem a expressão de RANKL e inibição da osteoprotegerina, desencadeando assim a via RANK-TRAF6, que ativa NF-κB, promovendo a expressão genética osteoclástica.[16, 23-24]

Atualmente, uma alternativa terapêutica para o tratamento de patologias que promovam degradação óssea (e.g. osteoporose) baseia-se na inibição da interação RANK-RANKL por ação do anticorpo monoclonal humano Denosumab. Este anticorpo mimetiza a função da osteoprotegerina (OPG), impedindo o RANKL de interagir com o seu recetor, RANK. Ao inibir a interação de RANK com RANKL, favorece-se o mecanismo de remodelação óssea. Apesar de ser uma terapia inovadora, a paragem na administração de Denosumab pode levar a uma reversão rápida da sua ação farmacológica, *turnover*, muitas vezes para níveis ainda mais críticos que os anteriores ao tratamento – também designado como 'efeito *rebound*'.[31] Não obstante, e tendo como inspiração o mecanismo de atuação do Denosumab, tem surgido um interesse crescente por vias alternativas. De entre as várias possibilidades, uma opção exequível passa pela inibição da via RANK-TRAF6. Este processo pode ser alcançado pela inibição da interação de RANKL com TRAF6, utilizando-se por exemplo *decoy peptides* (e.g., L-T6DP-1).[8]

Adicionalmente, considerando o nosso interesse no uso de péptidos como potenciais fármacos para terapia-alvo, ou como vetores de metalofármacos para várias aplicações biomédicas, o objetivo deste projeto contempla a síntese, purificação e avaliação biológica de um péptido (3A; KLFMALV AFLRFLTRQMPTEDEY-$NH_2$) e o seu controlo negativo (3B; KLFMALVAFLRF LTRQMATADEA-$NH_2$) que contêm uma sequência capaz de interferir com a interação proteína-proteína RANK-TRAF6 bem como sequências "penetradoras" (do inglês: *cell penetrating sequence;* KLFMALVAFLRFLT).

Após a preparação dos péptidos 3A (KLFMALVAFLRFLTRQMPTEDEY-$NH_2$) e 3B (KLFMAL VAFLRFLTRQMATADEA-$NH_2$), o objetivo final do estudo consistia na obtenção de imagens SPECT da biodistribuição dos péptidos radioativos sintetizados em ratinhos saudáveis, pela técnica de imagiologia multimodal micro-PET-SPECT-CT.

Numa fase inicial do projeto, experimentaram-se três tipos diferentes de síntese peptídica em fase sólida: (i) síntese 'clássica' ('*Classica*l' SPPS); (ii) síntese com assistência de ultrassons ('*US-assisted SPPS'*), e (iii) síntese com assistência de micro-ondas ('*MW-assisted SPPS'*). Nesta fase, procedeu-se à síntese de um segmento do péptido 3B (S3B; RQMATADEA-$NH_2$), com o objetivo de comparar os métodos de síntese peptídica em fase sólida 'clássica' e o mais recente método com auxílio a ultrassons.

Ao finalizar a síntese pelos dois processos, verificou-se por análise RP-HPLC analítico que os rendimentos dos "resíduos brutos" eram de 84% para o método 'clássico', e 72% para o método com auxílio a ultrassons. Apesar de se ter obtido um menor rendimento de síntese, deve ser salientado que a síntese pelo método com auxílio de ultrassons foi finalizada em cerca de um quarto do tempo. Como tal, para a realização das sínteses subsequentes (dos péptidos 3A e 3B, e dos seus conjugados), escolheu-se o método de síntese peptídica em fase sólida com auxílio de ultrassons.

Para a síntese do péptido 3A (KLFMALVAFLRFLTRQMPTEDEY), foram realizadas duas tentativas: a primeira com um suporte polimérico MBHA Rink Amide, e a segunda com a resina NovaPEG Rink Amide. No primeiro procedimento (com MBHA Rink Amide), a síntese foi terminada. No entanto, após análise com RP-HPLC analítico (ver figura 4.4), verificou-se que mesmo que o péptido tivesse sido sintetizado, que o processo foi concluído com um rendimento muito baixo. Visando otimizar a síntese do péptido 3A, optou-se por utilizar, numa segunda instância, um novo suporte polimérico com um maior *loading* ($Loading_{MBHA}$ = 0.38 mmol/g *versus* $Loading_{NovaPEG}$ = 0.47 mmol/g). Durante a síntese com a nova resina, verificou-se que nos primeiros 12 aminoácidos os acoplamentos foram mais rápidos. Contudo, ao acoplar a segunda arginina do péptido (KLFMALVAFL**R**FLTRQMPTEDEY), decidiu-se dar como terminado o procedimento, dado que o tempo de acoplamento ultrapassava 8 h. Tendo chegado a um impasse, optou-se por realizar as sínteses dos péptidos 3A e 3B, consecutivamente, pelo método de síntese peptídica em fase sólida com auxílio a micro-ondas. Por fim, os péptidos foram sintetizados por este método, com um rendimento moderado (53% para 3A, e 47% para 3B).

Após purificação por RP-HPLC semi-preparativo, procedeu-se ao acoplamento do *linker* ($PEG_2$) e do quelante bifuncional (NODAGA), seguindo o método de síntese peptídica em fase sólida com auxílio a ultrassons. Subsequentemente, realizou-se a clivagem dos péptidos, purificação, e por fim, espectrofotometria UV-Vis para determinação de concentrações, em preparação para radiomarcação. Durante o procedimento de espectrofotometria UV-Vis, verificou-se que o péptido precipitava subitamente e frequentemente, a temperatura ambiente. O baixo rendimento da primeira síntese, e uma precipitação súbita a temperatura ambiente durante, levou a atribuir ao péptido 3A uma tendência a agregar, característica de péptidos com certas sequências. Apesar de não ter sido realizada uma análise detalhada a tal fenómeno, adotaram-se medidas preventivas, tal como a adição de uma pequena quantidade de ácido trifluoracético à solução durante UV-Vis, e realização da técnica *flash freeze* após cada utilização do péptido.

A dificuldade em manusear o péptido 3A e o seu conjugado, tornou-se especialmente evidente durante a radiomarcação com $^{67}Ga$, a qual em condições *standard* se mostrou como uma impossibilidade. Devido a restrições de tempo, não foi possível realizar a otimização do processo de síntese dos péptidos 3A e 3B, bem como dos correspondentes conjugados, em quantidades suficientes para se fazerem estudos de otimização da radiomarcação. Como tal, tomou-se a decisão de suspender a utilização dos mesmos na fase final do projeto, até que as metodologias fossem revistas e otimizadas, processo esse que se encontra de momento a ser realizado.

Para além deste trabalho experimental de síntese, procedeu-se paralelamente à validação do equipamento pré-clínico de imagem FLEX™ Triumph™ micro-PET-SPECT-CT, recentemente adquirido e instalado no $C^2$TN-IST. O processo de validação envolveu duas fases, tendo-se iniciado com a utilização de diversos fantomas, tais como tubos de Eppendorf e seringas contendo soluções radioactivas. Este trabalho preparatório culminou numa segunda fase, na aquisição de uma imagem SPECT-CT de ratinhos com tumor (Balb/c com xenotransplantes celulares PC-3 de adenocarcinomas da próstata de origem humana) após administração localizada de nanopartículas radiomarcadas com $^{67}Ga$ ($^{67}Ga$-AuNP-BBN-Pt1). Os resultados das imagens pré-clínicas adquiridas (figuras 4.25 e 4.26) mostram uma diferença substancial na migração do composto 24 h p.i, que parece fixar-se durante um longo período (> 24 h) no tumor.

O trabalho descrito nesta dissertação, teve como objetivo a síntese de um péptido e a sua conjugação a um agente quelante bifuncional, visando a sua marcação radioativa com $^{67}$Ga e posterior avaliação da sua biodistribuição em ratinhos por imagiologia pré-clínica multimodal FLEX™ Triumph™ micro-PET-SPECT-CT. Em simultâneo, pretendeu-se validar e calibrar o equipamento pré-clínico multimodal micro-PET-SPECT-CT recentemente adquirido pelo C$^2$TN-IST. Uma vez que não foi possível a aquisição de imagens nucleares com radiopéptidos inicialmente propostos, em alternativa, e após validação do equipamento, fez-se um estudo imagiológico de nanopartículas radiomarcadas com $^{67}$Ga ($^{67}$Ga-AuNP-BBN-Pt1), em ratinhos Balb/c com xenotransplantes celulares PC-3 de adenocarcinomas da próstata de origem humana.

Em conclusão, pode dizer-se que o trabalho experimental realizado contemplou a utilização de inúmeras diferentes técnicas e metodologias, englobando diversos métodos de síntese peptídica em fase sólida, purificação, técnicas de radiomarcação e muito mais. Adicionalmente, foram também realizadas aquisições e tratamentos de imagens multimodais SPECT-CT de modelos animais. Esta abrangência permitiu ao mestrando tomar contacto com muitos aspetos essenciais da Medicina Nuclear, mais especificamente com os relacionados com a radioquímica farmacêutica e equipamento de imagiologia pré-clínica.

**Palavras-chave:** Recetor ativador do fator nuclear kappa-B (RANK); Recetor-associado 6 do fator de necrose tumoral (TRAF6); Fator Nuclear-Kappa B (NF-κB); Síntese Peptídica em Fase Sólida (SPPS); Imagiologia Nuclear.

# Contents

# List of Figures

## Section 2

## Section 3

## Section 4

# List of Tables

# List of Abbreviations

| | |
|---|---|
| **AA** | Amino acid |
| **ACN** | Acetonitrile |
| **BFC** | Bifunctional Chelate |
| **BM** | Bone Metastasis |
| **CPP** | Cell Penetrating Peptide |
| **DBF** | Dibenzofulvene |
| **DCM** | Dichloromethane |
| **DIPEIA** | N, N.-Diisopropylethylamine |
| **DMF** | Dimethylformamide |
| **ESI-MS** | Electrospray Ionization - Mass Spectrometry |
| **Fmoc-SPPS** | Fluorenylmethyloxycarbonyl-Solid Phase Peptide Synthesis |
| **HBTU** | (2-(1H-Benzotriazol-1-yl)-1,1,3,3-Tetramethyluronium Hexafluorophosphate |
| **HF** | Hydrofluoric Acid |
| **HPLC** | High Performance Liquid Chromatography |
| **IkB proteins** | Inhibitor of the Nuclear Factor Kappa-B proteins |
| **IKK kinase** | Inhibitor of the Nuclear Factor Kappa-B kinase |
| **MBHA** | 4-Methylbenzhydrylamine |
| **MeOH** | Methanol |
| **MW-SPPS** | Microwave-assisted SPPS |
| **N-Fmoc** | N-Fluorenylmethyloxycarbonyl group |
| **NF-κB** | Nuclear Factor-Kappa B |
| **OCP** | Osteoclast Precursors |
| **PP** | Piperidine |
| **PPIs** | Protein-Protein Interactions |
| **RANK** | Receptor Activator Of Nuclear Factor Kappa-B; TNF-Related Activation-Induced Cytokine Receptor (TRANCER); NF-κB Activator; |
| **RANKL** | RANK Ligand; TNF-Related Activation-Induced Cytokine (TRANCE); |
| **RP-HPLC** | Reverse Phase – High Performance Liquid Chromatography |
| **SPPS** | Solid Phase Peptide Synthesis |
| **TFA** | Trifluoroacetic Acid |
| **Tis** | Triisopropylsilane |
| **TNF** | Tumour Necrosis Factor |
| **TRAF6** | Tumour Necrosis Factor Receptor-Associated Factor 6 |
| **TRANCE-R** | TNF-Related Activation-Induced Cytokine Receptor |
| **US-SPPS** | Ultrasound-Assisted Solid Phase Peptide Synthesis |

Section 1

# Introduction

## 1.1 Motivation

The bone is the organ most frequently associated with solid cancer metastasis. Although a definite number is unknown, it is estimated that about 400,000 new instances of malignant bone metastasis are diagnosed *per* year in the United States alone. These forms of metastases are a prevalent complication of metastatic breast and prostate cancer, affecting 65 to 80 percent of these patients. Furthermore, the incidence of bone metastases (BM) has also been documented as having increased in other types of cancer, which could be linked to a general increase in the life expectancy of cancer patients arising from advancements in diagnosis and therapeutic interventions.[1-4]

BM can have a variety of consequences as it progresses. Some include greater risks of serious skeletal-related events (SREs) – fractures, pain, hypercalcemia, and nerve-compression syndromes, which lead to increased morbidity and decreased survival. Once tumours metastasize to bone, bone remodelling deregulation occurs, becoming incurable. The expanding cluster of metastasizing tumour cells alters the bone microenvironment, promoting bone invasion and enhancing subsequent growth.[2, 3]

The use of certain drugs, including bisphosphonates (BPs), radiopharmaceuticals (Samarium-153-Lexidronam and $^{223}RaCl_2$), and antibodies (Denosumab) that target osteoclastogenesis, are the classical treatments for patients with metastatic bone cancer. Nevertheless, 30 to 50 percent of patients who undergo these types of treatments relapse, often worsen their condition, as bone marrow serves as a receptacle for dormant tumour cells that are resistant to chemotherapy. Therefore, the need for innovative therapies becomes evident. Several techniques have in fact been surging, notably those based on nanoparticles. Bone-targeted doxorubicin-loaded nanoparticles for skeletal metastases, as well as mesoporous silica nanoparticles, are two of several examples.[2, 4-6]

Protein-protein interactions (PPIs) are known to be the foundation of a wide array of biological processes, such as cell-to-cell interactions, communication, and metabolic and developmental control. Particular interest lies in the RANK-TRAF6 pathway, a PPI that has been identified as being essential for osteoclastogenesis control - by inducing osteoclast differentiation and activation, which leads to bone resorption.[6, 7]

Following this interest, this project aimed at synthesizing new radioactive molecules based on sequences previously identified as able to interfere with the RANK-TRAF6 pathway, coupled to a cell-penetrating sequence, as well as to obtain a final pre-clinical m-PET-SPECT-CT image.[8, 9]

## 1.2 Objectives

The main goal of this thesis is to synthesize, evaluate, and obtain a final pre-clinical micro-PET-SPECT-CT image of radiolabelled peptides designed to interfere with the RANK-TRAF6 pathway. To achieve this aim, specific objectives were defined and divided into two sets, namely Peptide Synthesis and Nuclear Imaging.

Regarding the Peptide Synthesis, the first objective is to compare the methods of ‘classical’ solid phase peptide synthesis (‘classical’ SPPS), and ultrasound-assisted solid phase peptide synthesis (US-assisted SPPS). This is achievable by synthesizing the model peptide S3B (RQMATADEA-$NH_2$) by each method, and assessing the following: i) Duration of the synthesis and ii) Crude yield of each synthesis obtained by analytical RP-HPLC. Peptide S3B was chosen for this comparison as it is the

targeting sequence constituting peptide 3B (KLFMALVAFLRFLTRQMATADEA-$NH_2$). Additionally, as the peptide sequence grows, coupling times can widely vary with the amino acid sequence, and size. As such, it seemed it was a good stopping point to infer data, and take conclusions for the assessment.

After evaluating and selecting the most efficient method of synthesis, the objective will shift towards synthesizing peptides 3A (KLFMALVAFLRFLTRQMPTEDEY-$NH_2$) and 3B (KLFMALVAFLRFLTRQMATADEA-$NH_2$), their respective conjugates and preparation of the corresponding $^{67}$Ga-labeled peptides. Finally, the biodistribution of the radiopeptides prepared will be evaluated in normal mice by multimodal Nuclear Imaging.

## 1.3 Thesis Structure

This thesis is organized in five sections:

- **Section 1** briefly expresses the motivation that led to the development of the present project, its objectives, and contributions.
- **Section 2** establishes the groundwork necessary to understand the project. As it involves concepts from biology, physiology, chemistry, radiochemistry and nuclear imaging, this section begins with basic concepts whose connections between fields are established throughout each individual section. Described initially are the main molecules currently associated with metastization of breast and prostate cancer to the bone – RANK, RANKL, OPG and TRAF6. The basic concepts to synthesize a molecule capable of interfering in this process are presented, referring to several methods for its synthesis, as well as nuclear imaging techniques that can be chosen. Finally, section 2 ends by intersecting all concepts explained, by combining the molecular structures needed for a peptide to be visible by nuclear imaging.
- **Section 3** presents the experimental part.
- **Section 4** includes the results and discussion.
- **Section 5** summarizes the achievements, and gives suggestions for future projects.

Section 2

# From Peptides to Nuclear Imaging

## 2.1 RANK, RANK-Ligand and Osteoprotegerin

RANK (Receptor Activator of Nuclear Factor kappa-B, also known as NF-κB activator) belongs to the subfamily type 11 of the tumour necrosis factor receptor superfamily (TNFRSF) and is a type I homotrimeric transmembrane protein. RANK expression was initially detected on osteoclast precursors (OCPs), mature osteoclasts, and dendritic cells. More recently, the expression of RANK has also been reported in mammary glands and some cancer cells, including breast and prostate cancers, two types of tumours with high bone metastasis potential. Functionally, RANK has no intracellular enzymatic activity. As its name indicates, RANK's actions on the cell are mediated through binding and activating other proteins, which can then trigger several signalling pathways (Figure 2.1). It has been shown that the interaction of RANK with its ligand (RANKL) is the final common pathway through which bone resorption is regulated.[10-13]

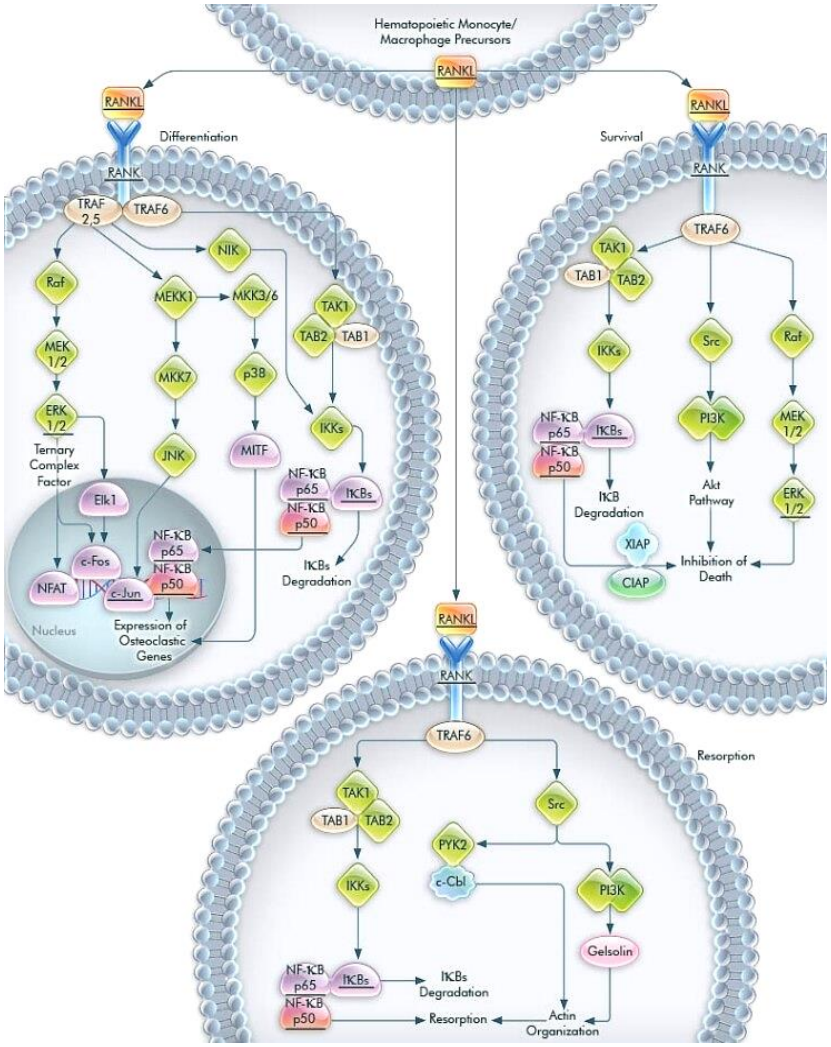


**Figure 2.1:** Schematic representation of RANK signalling pathways in differentiation, resorption, and survival mechanisms. Adapted from [14].

RANKL – also known as osteoprotegerin ligand (OPGL) or osteoclast differentiation factor (ODF), can be expressed in different molecular forms: trimeric transmembrane proteins and two different secreted forms. Lymph nodes, mammary glands, thymus, lungs, bone marrow, and spleen are among the tissues where this protein is strongly expressed. In adult bone tissue, however, osteocytes are the primary source of RANKL. Being referred to as osteoprotegerin ligand, a link with osteoprotegerin (OPG) is implied. In fact, OPG serves as a natural inhibitor of RANKL, competing with RANK to bind to RANKL. Thus, the ratio of RANKL to OPG determines the balance between bone formation and resorption, meaning that the triad RANK-RANKL-OPG interaction affects osteoclast differentiation, activation, and survival. This has already been proven in mice with OPG deficiency, who develop osteoporosis, whereas overexpression of OPG in mice results in fewer osteoclasts and higher bone mass.[11, 15-19]

## 2.2 Tumor Necrosis Factor Receptor-Associated Factor 6 (TRAF6)

Tumour necrosis factor receptor-associated factors (TRAFs) are a family of adaptor proteins that share a similar structural domain at their C-terminus. This region allows TRAFs to interact with cell surface receptors or other signalling molecules, serve as adaptor proteins for a wide variety of receptors involved in regulating cell death and survival, and provide cellular responses to stress.[20]

It has been demonstrated that a particular member of this family, TRAF6, displays a key role in bone resorption, through a signalling pathway denominated RANK-TRAF6 pathway. For example, severe osteopetrosis with defects in bone remodelling and tooth eruption - caused by impaired osteoclast formation - was found in TRAF6 deficient mice, which led to death at an early age.[19-21]

The significance of TRAF6s' interaction with RANK can be explained by the fact that RANK proteins contain three potential TRAF6-binding sites, all of which are involved in interaction and signal transduction. As presented in Figure 2.2, structure-based sequence alignment of human (h) and mouse (m) TRAF6-binding sites, shows that RANK (TRANCE-R) and other TNFR members have a preserved amino acid sequence pattern of Proline(P)-X-Glutamic acid(E)-X-X-Aromatic residue(Ar)/Acid residue(Ac).[8, 22]

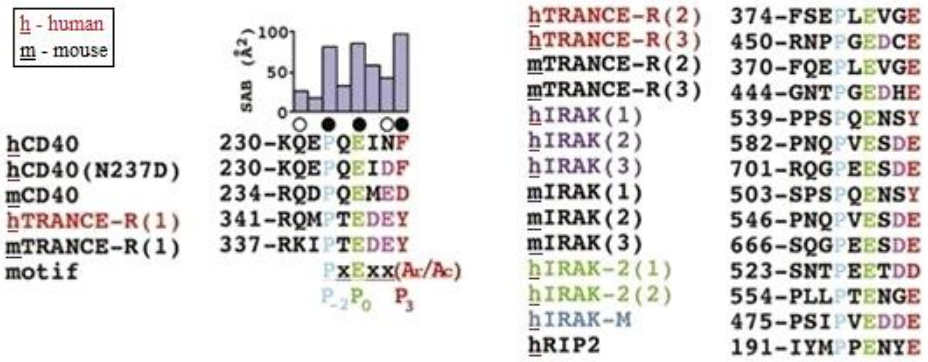


**Figure 2.2:** TRAF6-binding sites for TNFR family members in human (h) and mouse (m), as well as TRAF6-binding motif P-X-E-X-X-(aromatic/acid residue). Adapted from [8].

Hence, special attention is given to the sequence of P-X-E-X-X-Ar/Ac.

## 2.3 RANK-TRAF6 Pathway: From RANKL to Metastatic Bone Cancer

Having addressed the primary entities responsible for bone remodelling, it is essential to understand how a mechanism that ensures bone maintenance can lead to the development of metastatic bone cancer.

Generally, there is an overall balance in the process of bone formation and reabsorption, in a process known as bone remodelling. This balance can be disrupted by metastatic tumour cell development in

the bone, either resulting in osteolytic metastases (excessive bone resorption) or osteoblastic metastasis (excessive bone formation). The cancer cells have the ability to express several osteoclastogenic factors that profoundly alter the bone microenvironment. Some of these factors include interleukins-6 (IL-6) and 8 (IL-8), parathyroid hormone-related proteins (PTHrP), prostaglandins E2 (PEG2), CSF-1 (macrophage colony-stimulating factor), and TNF-alpha (TNF-α). Tumour-derived PTHrP and bone-derived IL-11 induce both RANKL overexpression, and suppression of OPG. This leads to RANK-TRAF6 pathway promotion of osteoclast gene expression, as depicted in Figure 2.3. [16, 23-24]

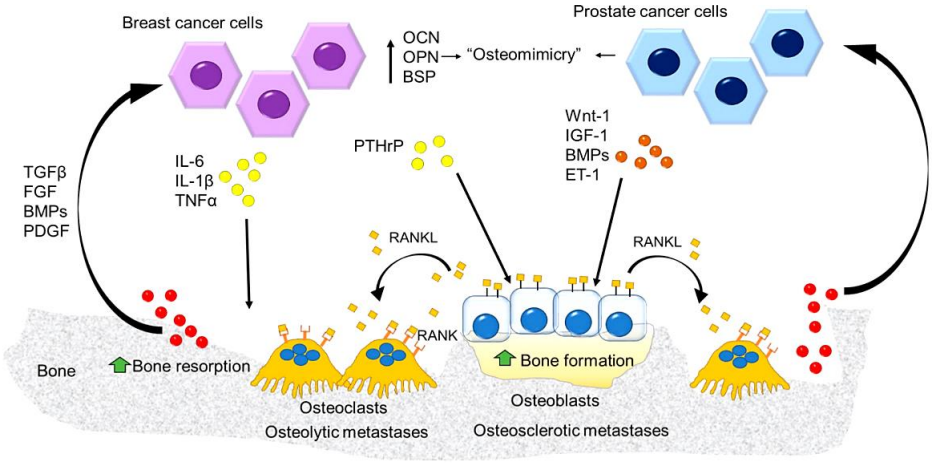


**Figure 2.3:** Depiction of the vicious cycle of bone metastization. Tumour cells express osteoclastogenic factors by promoting RANKL overexpression and inhibiting OPG. Overexpression of RANKL and OPG inhibition leads to osteoclast gene expression, promoting bone resorption, which will further fuel tumour cell development. Adapted from [25].

By interpretation of Figures 2.1 and 2.3, it is perceivable that once RANKL is free to interact with its receptor in the osteoclast membrane, signalling transduction pathways are triggered. This leads to the activation of nuclear factor-kappa B (NF-κB), which triggers osteoclast gene expression. [26, 27]

As a response to an accentuated bone resorption, tumour cell growth is further fuelled with mitogenic factors released from the bone matrix – tumour growth factor (TGF)-β, insulin-like growth factors (IGFs), fibroblast growth factors (FGFs), platelet delivered growth factors (PDGF), and $Ca^{2+}$ – promoting the so-called "vicious cycle of bone metastization". [23, 28]

## 2.4 Denosumab

Denosumab is a monoclonal antibody used to prevent bone loss by mimicking OPG's function. As such, this therapeutic can be used to prevent skeletal-related events. [29,30] It is indicated for the following therapeutic applications:

1) Treatment of osteoporosis in women that underwent menopause – which have an increased risk of bone fractures.
2) Treatment of men with increased risk of fractures.
3) Treatment of bone loss in men who are being treated for prostate cancer, due to medications that cause bone density loss.
4) Treatment of women with breast cancer receiving certain medications that increase bone fractures.
5) Treatment of patients with bone tumours (Giant Cell Tumour of Bone – GCTB).
6) Treatment of patients unresponsive to certain medications with high calcium levels caused by cancer. [29]

Denosumab prevents the formation, function, and survival of osteoclasts upon inhibition of the interaction RANKL-RANK. As a result, the RANK-TRAF6 pathway will not mediate signalling responses, hindering osteoclast gene expression. The mechanisms of normal bone remodelling, denosumab treatment, and effects after treatment discontinuation, are depicted in Figure 2.4. [30]

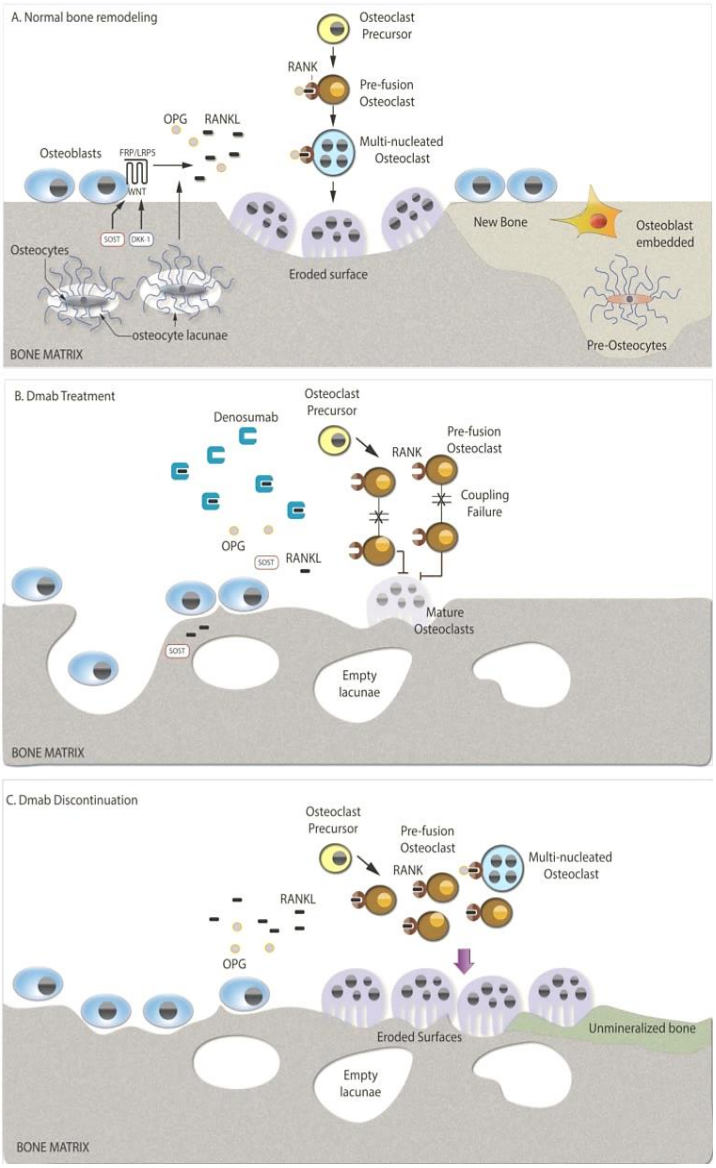


**Figure 2.4:** Representation of A) Normal bone remodelling; B) Denosumab treatment; C) Denosumab discontinuation. Adapted from [31].

Although denosumab has had a significant impact in the treatment of metastatic bone cancer, its effects can rapidly turnover when the administration is discontinued (see Figure 2.4 C) – sometimes to even worse levels as pre-treatment - referred to as a "rebound phenomenon".[31] All considered, Denosumab is both an inspiration and a motivator for a surge of alternative RANK ligand inhibitor medications.

## 2.5 Introduction to Peptides and Proteins

Undoubtedly, the scientific community has been increasingly devoting attention to peptides, protein therapeutics and applications.

Proteins and peptides are a result of the condensation of amino acid residues that differ in their side chains:

- When the condensation of two or more amino acids occurs, the product of the reaction is considered a peptide or protein, depending on the size. Represented in Figure 2.5, are the chemical structures of aspartate (Asp), and a segment of one of the peptides to be synthesized (Aspartate-Glutamate-Alanine, or DEA).
- A linear chain of twenty to thirty amino acids, is usually called an oligopeptide, or simply a peptide.
- Proteins are one or more polypeptide chains of over hundreds of amino acids.[32]

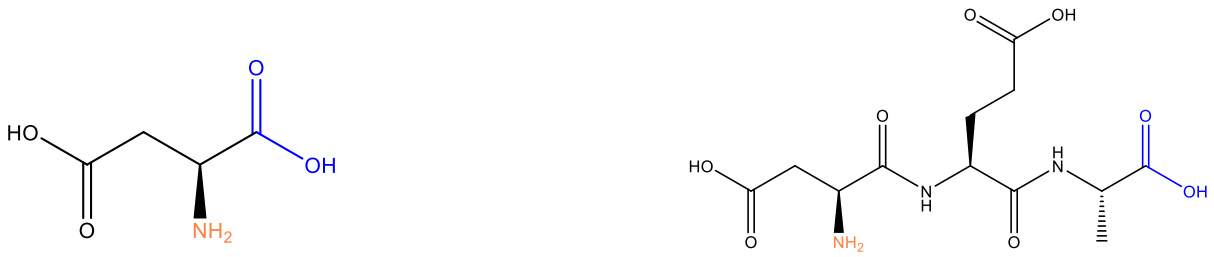


**Figure 2.5**: Representation of the chemical structures of Aspartate [Left] and Aspartate-Glutamate-Alanine (Asp-Glu-Ala) [Right]. Highlighted in orange is the α-amine group (N-terminal), and in blue, the α – carboxyl group (α-carbon).

Conventionally, when writing the notation of a peptide, the N-terminal is implied as positioned on the left, and the C-terminal on the right.[33,34] This is an important concept to have in mind when synthesizing peptides, as there are various techniques available – for instance, *tert*-butyloxycarbonyl (Boc) SPPS and fluorenylmethoxycarbonyl (Fmoc) SPPS – which will be explained further. By understanding this convention, further simplifications of the peptide structure notation can be made, as seen below.

$$1 \rightarrow \text{Asp} - \text{Glu} - \text{Ala} \leftarrow 2$$

By examining the sequence above (Asp-Glu-Ala or DEA), it is apparent that there are two ways to synthesize the exemplified orthogonal peptide:

- The conventional direction (1) implies that the N-terminal of the aspartate will be protected, meaning the succeeding amino acids will be coupled by their N-terminal to their precursor.
- The second option is the opposite direction (2). This translates into all alanine's terminals being protected, except its amine group, where the following amino acid will be coupled. Hence, the required peptide will be obtained at the end of the synthesis by coupling α-carboxyl groups to the free α-amine group of the previous amino acid.

## 2.6 Solid Phase Peptide Synthesis (SPPS)

Solid Phase Peptide Synthesis (SPPS) can be defined as a process in which a peptide anchored to an insoluble polymer matrix is assembled, by successively adding the amino acids constituting its sequence (see Figure 2.6). This is the method of choice for polypeptide synthesis, as it is simple, repetitive, and punctuated only by washing steps, to remove excess reactants and by-products. During SPPS, any functional groups in the amino acid side chains must contain temporary protecting groups. This approach

serves a range of objectives, which include synthesis control, limitation of amino acid polymerization, and prevention of unfavourable side reactions during the procedure.[35-38]

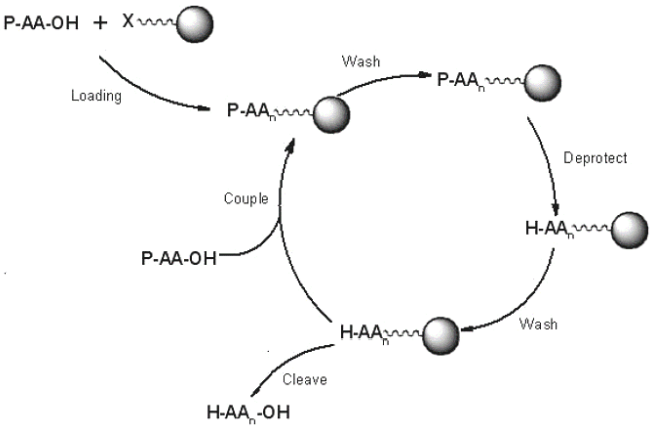


**Figure 2.6:** Simplified schematic representation of SPPS protocol. The initial amino acid is coupled to the insoluble polymer matrix and, by succeeding deprotections and couplings, the peptide will be synthesized. When the sequence is finalized, the peptide is removed from the polymer matrix. Adapted from [39].

As summed in Figure 2.6, SPPS is comprised of a series of cycles, which are in general terms divided into the following steps:

1. **Cleavage of protecting group (Deprotection)** – The amino acids used in SPPS usually have one of their terminals protected. As a result, to synthesize the desired sequence, the terminal groups must be removed whenever a new amino acid is to be coupled.
2. **Resin wash (1)** – Washing the resin and reactor is a vital step in SPPS, to avoid any by-products of the reaction.
3. **Test to confirm the protecting groups were removed (1)** – There are several tests to detect the cleavage of the protecting groups was successful. For instance, the Kaiser test, a colorimetric assay based on the reaction of ninhydrin with amines. The Kaiser test is used to detect primary amines, perceived by the intense blue colour it radiates.
4. **Coupling** – SPPS is a cycle of sequential addition of amino acids. After deprotecting the first amino acid, a second one is coupled to said first. This reaction is assisted by an activator and a basic catalyst.
5. **Resin wash (2)**
6. **Kaiser test (2)** – In practice, after a coupling attempt, amino acids may or may not have been bound to the resin. Therefore, after the coupling step, the second test of confirmation should take place. If the Kaiser test was chosen for the procedure, the confirmation should be given by a translucid colour. If in this step a blue solution is obtained, the amino acid was not able to fully bind to the sequence, meaning the coupling step must be repeated.
7. **Final cleavage** – After the sequence is complete, the peptide must be removed from its solid support.[39]

### 2.6.1 Principles of SPPS

Multiple chemical reactions must occur to synthesize a peptide. These reactions should be understood for a swift and consistent synthesis. For instance, after obtaining the desired peptide sequence immobilized to the polymeric support, the amino acids still contain protecting side groups. Therefore, selecting a resin that is removed under the same conditions as the peptide side chains is, in most cases, of interest.

In the following subchapters, some concepts regarding the experimental procedures of SPPS will be addressed.

#### 2.6.1.1 Selective Protection

Many amino acids are reactive when left unprotected, allowing the formation of side products. A common example is cysteine, that when deprotected has a great tendency to form disulphide bonds with other cysteines. Therefore, to increase the yield and quality of peptide synthesis, the amino acids must contain protecting groups that can be removed only when needed. Additionally, the α-amine protecting group should contain protecting groups that are removed under different conditions of the other protecting groups. Although there exist many types of protecting groups, the two most associated to peptide synthesis are:

A. **Boc/Bzl**– By using Boc protecting scheme, a tert-butoxycabonyl (Boc) group is employed to temporarily protect the α – amino groups, whilst benzyl-based protecting groups are used for the side chains. Despite some advantages, the Boc-strategy requires continuous use of trifluoroacetic acid (TFA), which may induce degradation or modification of certain peptide sequences. Furthermore, Boc-SPPS makes use of HF. As a result, specialized laboratory equipment is necessary.

B. **Fmoc/tBu –** The Fluorenylmethoxycarbonyl(Fmoc)-SPPS approach uses Fmoc protected α – amines, and tert-butyl or trityl protected side chains. This type of chemistry provides mild deprotection methods, by using a base to expose the α-amino group - typically piperidine (20–50%) in *N*,*N*-Dimethylformamide (DMF). By being more sustainable and providing safer reaction conditions (achieved by replacing TFA for piperidine during deprotection, and TFA instead of HF for final resin cleavage), this type of SPPS has replaced Boc chemistry almost entirely.

While the common methods of peptide synthesis have significant differences, they all follow the same method of adding amino acids sequentially to the expanding peptide chain, beginning with the C-terminal of the desired sequence, and ending with the first amino acid. Nonetheless, in this thesis, the focus will be shifted towards Fmoc-SPPS from this point forward, as it was the simplest and safest option availible.[40-43]

#### 2.6.1.2 Resins

SPPS is generally carried out on beaded resins. The most common solid supports used during routine SPPS are crosslinked polystyrene (PS)-based resins, with good swelling characteristics in organic solvents such as Dimethylformamide (DMF) and Dichloromethane (DCM). There are, however, a wide variety of different other solid support options, such as crosslinked polyamide (PA), composite PS-Polyethylene glycol (PEG)–based, hydroxymethyl, Wang, Merrifield, amongst others. Depending on the method and peptide to synthesize, each resin has different properties that can be of use. Hence, optimizing the resin choice is an important step in obtaining the desired peptide with the maximum yield, whilst following the most cost and time-effective method. By choosing certain combinations of chemistry (Boc/Fmoc) and resins, peptide cleavage can be achieved at the same time as the removal of the side chain protecting groups constituting the peptide sequence. In the case of Fmoc-SPPS, the most popular resins are the amide-forming products Rink Amide, PAL and Sieber Amine resins, which offer high acid lability and mild cleavage conditions. [34, 44]

### 2.6.1.3 Fmoc Deprotection

The Fmoc group removal in SPPS is divided in a multi-stepped chemical reaction:

1) Removal of the acidic proton at position 9 of the fluorene ring system.
2) Generated anion moves to adjacent atom, resulting in carbon dioxide and dibenzofulvene (DBF) products by β-elimination.
3) Neutralization of DBF intermediate products.

The deprotection reaction is characterized by the removal of the protecting group from the amine in which the desired peptide bond is to be formed. This reaction is generally performed in a polar electron donor solvent with a mild base – e.g., 20% piperidine in DMF. Piperidine is usually the chosen deprotection agent, as it forms a stable adduct with the DBF by-product, preventing reactions with the substrate (see Figure 2.7). [44, 45]

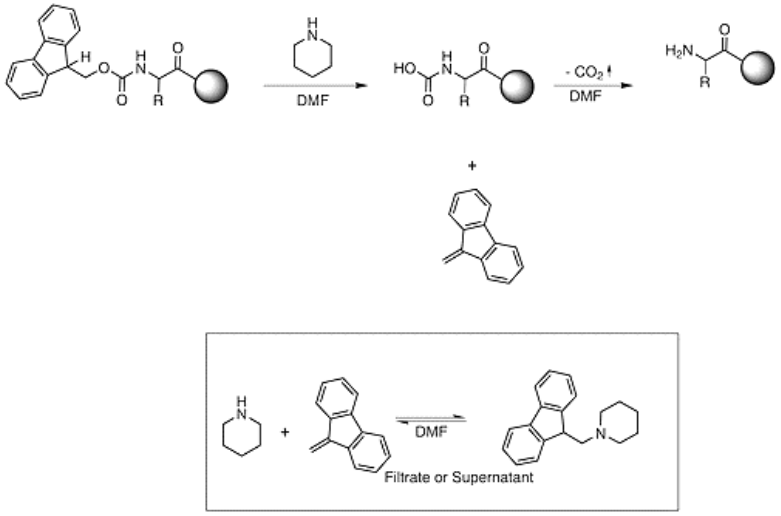


**Figure 2.7:** Schematic representation of the Fmoc-deprotection reaction. Initially, the piperidine removes the acidic proton of the fluorene ring system. As a result of this reaction, a DBF-piperidine adduct will be formed, leaving the peptide's amine deprotected, and releasing carbon dioxide. Adapted from [46].

### 2.6.1.4 Kaiser Test

Since the process of coupling amino acids is not discernible to the naked eye, it is essential to qualitatively examine the reactions. One way of doing so is by a colorimetric test known as Kaiser test. The Kaiser test is based on the reaction of ninhydrin with the free primary amines, which can result in one of several outcomes depending on the reaction's current state:

a) **Intense blue colour** – shows the presence of excess free primary amines, indicating that the amino acid has been deprotected, or that the coupling has failed.
b) **Light blue** – The presence of light blue could either indicate an incomplete deprotection or coupling. As such, if incomplete deprotection occurs, either the piperidine should be replaced and/or deprotection duration should be increased. In the case of incomplete coupling, the coupling stage should be redone.
c) **Yellow or translucid colour** – Either coupling was complete, or deprotection unsuccessful. In the case of the latter, it is important to check the quality of the piperidine in use.
d) **Red-Brown or other –** secondary amines in solution produce a red-brown colour. This can indicate one of the following: (a) The reactor was incorrectly washed, leaving piperidine residues in the resin; (b) The N-terminal amino acid is either proline, asparagine, serine, aspartic acid, pipecolic acid, or tetrahydroisoquinoline-3-carboxylic acid. Other tests, such as the Isatin test or the chloranil test, should be used in this case.[35, 48, 49]

### 2.6.1.5 Activation and Coupling

The term coupling refers to the formation of a peptide bond between two amino acids, and in overview goes as demonstrated in Figure 2.8.

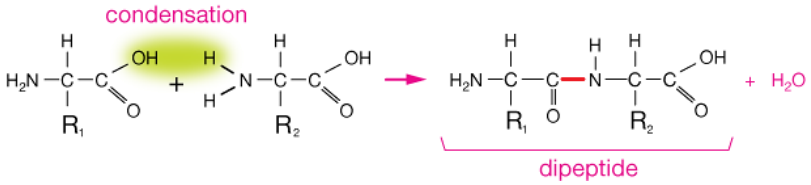


**Figure 2.8:** Schematics of a peptide bond formation. The amine group of one amino acid reacts with the carboxyl of the other, originating the dipeptide and a free water molecule. Adapted from [49].

Although seemingly straightforward, amino acid coupling involves a complex sequence of reactions. While in nature, condensation of amino acids is mediated by enzymes and various mediators of reaction, in peptide synthesis, several methods have been developed to bypass this phenomenon.

One of the techniques of choice is using uronium salts. The two most commonly used uronium salts are Hexafluorophosphate Benzotriazole Tetramethyl Uronium (HBTU) and Hexafluorophosphate Azabenzotriazole Tetramethyl Uronium (HATU). In Figure 2.9, the activation mechanism using uronium reagents is shown.

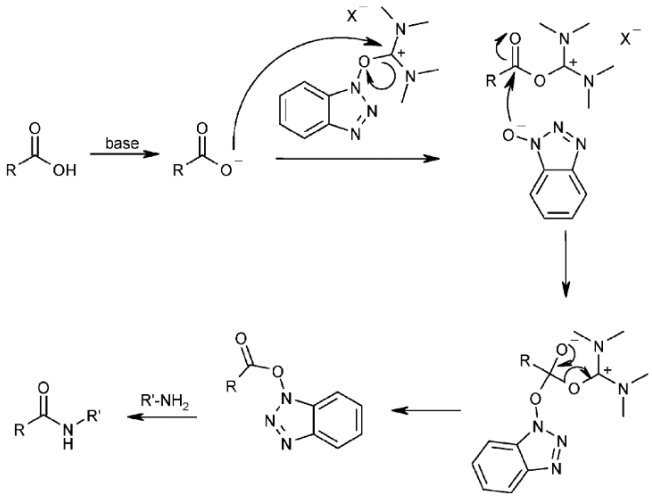


**Figure 2.9:** Mechanism of amino acid activation using uronium-type salts. Adapted from [51].

HBTU and HATU will mediate the amide bond formation by reacting with the carboxylic acid, originating an activated ester. Activated esters are more prone to nucleophilic 'attacks' of unpaired electrons of the primary amine, allowing easier reactions with amines and, consequently, the formation of amide bonds.[50, 51]

### 2.6.1.6 Cleavage and Peptide Isolation

Having finalized the synthesis of the desired peptide sequence, the last challenge in SPPS is the simultaneous removal of the side chain protecting groups, whilst separating the peptide from its solid support - the cleavage. Typically, to remove peptides anchored to amine linkages, a treatment of the peptide-resin with 95% trifluoracetic acid for 1 to 3 hours is made.

During cleavage, by simultaneously removing several protection groups as well as the resin's linker, extremely reactive cationic species are generated. Consequently, inhibiting these products is fundamental to avoid any unwanted reactions. This can be achieved by adding to the TFA solution a

cocktail of scavengers. The prepared scavenger solution will vary with the peptide sequence and the protecting groups of the amino acids used. Regardless, the most commonly used scavengers are:

- **Water** – effective at scavenging t-butyl cations and arylsulphonyl-based protecting groups from cleavage products.
- **1,2-Ethanedithiol (EDT)** – the best scavenger for t-butyl cations, also offering some protection to unprotected tryptophan against sulphonation. Additionally, it assists the cleavage of cysteine's trityl protecting groups.
- **Triisopropylsilane (TIS)** – can be used as an alternative to EDT, especially when synthesizing peptides containing Arginine(Pmc), Arginine(Pbf) and Tryptophan(Boc). TIS is also particularly effective with stabilized cations released on the cleavage of Trt and the Rink amide linker.

Following the cleavage, the peptide will be dissolved in a 90-95% TFA and 5-10% scavenger solution. The peptide is isolated by precipitation and final wash. The approach involves, for instance, evaporation of excess TFA and volatile scavengers with a gentle stream of nitrogen gas, directly in the reactor. After evaporating excess reagents, ice-cold diethyl or t-butyl methyl ether is added to precipitate the peptide, with subsequent centrifugation. The chosen method will, of course, depend on the synthesized peptide, which may result in different yields. Still, it is preferable to have a slightly lower yield but avoid the possibility of unwanted biproducts occurring due to reaction reversibility.[48, 52]

### 2.6.1.7 Manual, Ultrasound and Microwave-Assisted SPPS

The 'classical' solid phase peptide synthesis method was achieved on a custom-built system of standard laboratory glassware, as depicted in Figure 2.10.

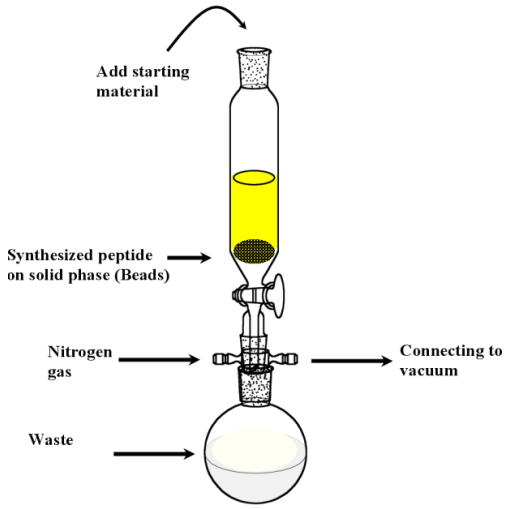


**Figure 2.10:** Representation of the system used for manual SPPS. The system consists of a glassware column (reactor) protected with a specialized filter. The filter allows the resin containing the peptide to be retained at the top. At the bottom, lies a vessel to where the waste is removed. Adapted from [53].

For the manual synthesis procedure, a sintered filter is put on the bottom of the reactor, blocking the passage of the resin. The reactor's tap is then set to a *closed* position, and the reagents are added at the top of the vessel. Subsequently, the valve is turned to the inert gas position (usually Nitrogen gas), generating a nitrogen flow that agitates its contents. After a certain time, the gas flow is interrupted, and the reactor is set to an *open* position, which allows waste removal. This cycle is repeated until the peptide sequence is finished.[52]

The *'classical'* SPPS has several limitations, some of which are evident. Repeated transfers of liquid during deprotection, washing and coupling are both time-consuming, and will lead to resin loss either

by spill or by resin bead adhesion to the glass of the vessel. The necessity of temperature and humidity control is also a limiting factor, as racemization may occur. Additionally, the reactor must contain orifices that allow the addition of reagents, making the solution prone to contamination.

With the advancements in technology, alternative methods for SPPS surged, namely with the development of the first automated microwave synthesizers, and with the pioneering work of Takahashi and Shimonishi, that introduced ultrasonic waves in SPPS.[54]

One commonly used SPPS method is the microwave(MW)-assisted SPPS. MW-assisted SPPS is an automated method that provides efficient results and moderates to high yields. During microwave irradiation, microwaves superheat molecules either by dipolar polarization or ionic conduction, two fundamental mechanisms for energy transfer to the irradiated substance. Consisting of electromagnetic radiation of the electromagnetic spectrum, polar molecules (for example water) will orient themselves with the oscillating electric field of the microwaves. As the dipoles realign with the changing electric field, differences in phase will be created, resulting in loss of energy by molecular friction and collision. Additionally, if there are ions in the solution, there will be an oscillation of these charged particles under the electric field of the microwaves (see Figure 2.11). [55-57]

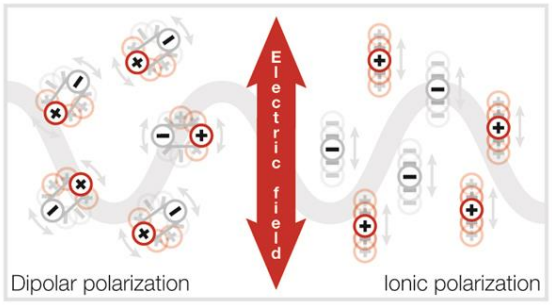


**Figure 2.11:** Representation of the phenomena associated with microwave-assisted SPPS. The electromagnetic energy from the microwave is converted into kinetic energy, which in turn, leads to heating the of the solution. Adapted from [57].

Besides the well-established microwave-assisted SPPS, numerous scientific papers also surged regarding an alternative method that also proves to be quite efficient, the ultrasound(US)-assisted SPPS. Recent studies have shown that the usage of US-assisted SPPS can lead up to a 4-fold time reduction in comparison with the *'classical'* method, achieving the synthesis of a 25-mer peptide within a *'working day'*. The principle in which the US-assisted SPPS is based on is the cavitation phenomenon: when applying ultrasounds to a liquid, a cycle of compression and rarefaction waves are induced in the medium. These alternating pressures will lead to the formation and eventual collapse of the cavitation bubbles, which generate energy for chemical and mechanical effects (see Figure 2.12).[54, 58-60]

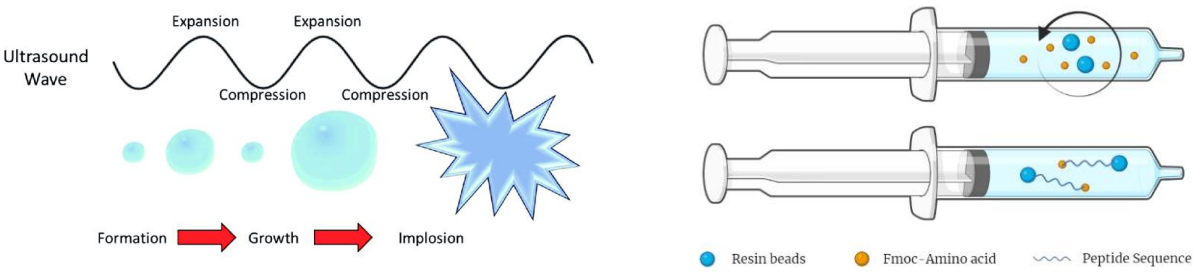


**Figure 2.12:** On the left, the cavitation phenomenon during US-assisted SPPS. The cycle of compressions and rarefactions induces the collapse of bubbles, which generate energy.[60] On the right, the representation of the reactor used in ultrasound(US)-assisted SPPS, consisting in a laboratory syringe, with a specialized filter at the bottom. Adapted with BioRender.com.

## 2.7 Nuclear Medicine

According to the Radiological Society of North America (RSNA), Nuclear Medicine is the clinical discipline that includes the use of radionuclides for diagnostic and therapeutic purposes.[101] Specially designed cameras allow doctors to track the movement of the radioactive tracers in the body. Although there are several other types of techniques, focus is drawn to Single Photon Emission Computed Tomography (SPECT) and Positron Emission Tomography (PET).[61] In the past years such nuclear modalities have been combined with Computed Tomography (CT) resulting in multimodality PET-CT or SPECT-CT imaging systems. Such systems combine in the same equipment the high sensitivity of the nuclear imaging techniques with the high spatial resolution of CT.

### 2.7.1 Principles of Computed Tomography (CT)

As illustrated in Figure 2.13, during CT, the patient rests on a bed positioned to observe a certain area of the body. Subsequently, an X-ray tube rotates around said area, firing X-rays through the patient and into a radiation detector positioned on the opposite side of the equipment.

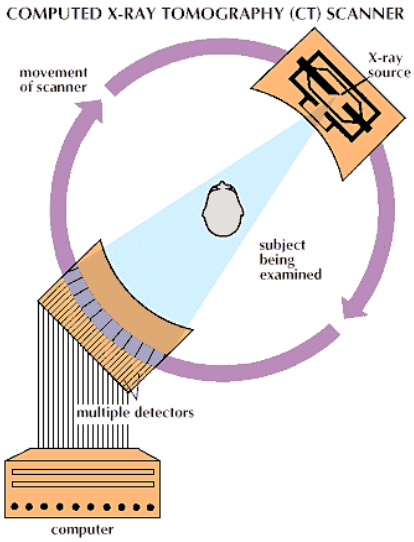


**Figure 2.13:** Schematic representation of CT scan. The X-ray source rotates around the object to be observed, and fires X-rays that will be detected by X-ray camera detectors. These signals can then be reconstructed into the images to be observed. Adapted from [62].

During the irradiation, several projections are acquired from different angles, and can subsequently be seen in slices, or reconstructed as a 3D image (see Figure 2.14). Hence, computed tomography.[76]

**Figure 2.14**: Example of a 3D reconstructed acquisition of a water-filled Eppendorf tube used for the FLEX™ Triumph™ equipment's CT camera validation. Inside the phantom, an air bubble detected by the camera can be clearly seen.

Although CT presents itself as an important tool for anatomical imaging, the usage of X-ray imaging alone has its limitations. For instance, the ease that X-rays pass through soft tissue. Consequently, the visualization of most organs becomes difficult, unless a contrast agent is used. Additionally, PET and SPECT imaging modalities can be used to complement the CT scan.[63]

### 2.7.2 Principles of Positron Emission Tomography (PET)

A PET scan is a procedure that employs the use of radiotracers to assess organ and tissue function.[101] PET imaging begins with the injection of a biological radiotracer with a positron-emitting isotope (for instance $^{68}$Ga, $^{64}$Cu or $^{18}$F). As the radiotracer is administered to the patient, it will enter the bloodstream and accumulate in certain area(s) of the body. Radioisotopes, as it is known, decay after a certain interval in what can be several types of nuclear reactions.[76, 77] In the case of positron-imaging isotopes, the nuclear reaction is as described in equation 2.1:

$$p \rightarrow n + \beta^{+} + v \quad (2.1)$$

Where $p$ is the proton, $n$ the neutron, $\beta^{+}$ the positron, and $v$ a neutrino. The ejected positron almost immediately reacts with an electron, resulting in an annihilation reaction that produces two photons with an energy of 511 keV emitted in opposite directions. These photons are subsequently detected by a ring of detectors that surround the patient. Because the photons are detected almost *simultaneously*, the annihilation must have occurred along a straight line connecting the said detectors. As a result, by combining several lines from different particle decays, the location of the radioelement accumulation can be determined (see Figure 2.15).[64]

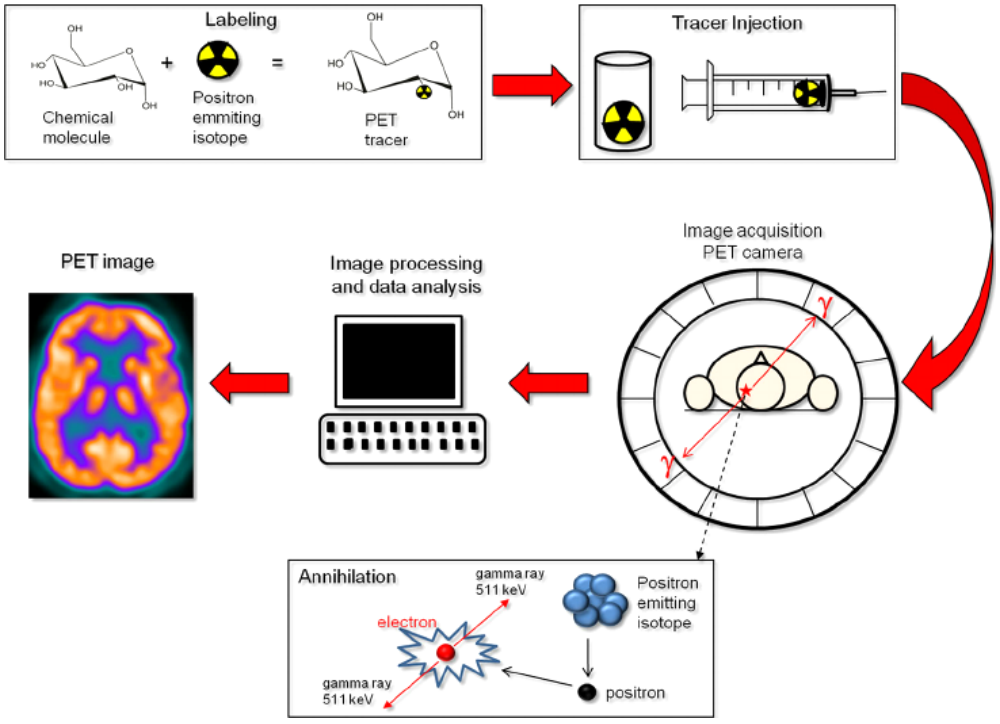


**Figure 2.15:** Schematics of PET imaging. The chemical molecule is radiolabelled with a positron-emitting isotope and injected into the patient. Then, the radioisotope will accumulate in the regions of interest, and decay. Resulting from the decay, the signals originated from the annihilation can be processed and reconstructed into a final PET image. Adapted from [77].

It is worth noting that the word *simultaneously* was left in italic, as a simultaneous detection of photons is highly unlikely. Therefore, software calculations need to take place to correlate the so-called lines of response (LOR) to the most likely event.

### 2.7.3 Principles of Single Photon Emission Computed Tomography (SPECT)

SPECT is a medical imaging technique that ultimately originates a tomographic image based on the detection of gamma(γ) photons. As said for PET, in SPECT, a radiopharmaceutical is administered to the patient. The substance will accumulate in certain area(s) and undergo nuclear decay. This decay will enable a detector (or set of detectors) to collect data that will be reconstructed into the final image. The primary distinction between PET and SPECT, is the type of decay of the chosen radioisotope. In a PET scan, positron-emitting radioisotopes are used, whereas, during SPECT, the choice is amongst gamma(γ)-emitter radiopharmaceuticals. When a nucleus decays, it is frequently left in an excited energy state. By emitting high-energy photons, this nucleus can decrease its energy level (see equation 2.2).[65]

$$ {}^{A}_{Z}X^{*} \rightarrow {}^{A}_{Z}X + \gamma \quad (2.2) $$

In equation 2.2, X* depicts the nucleus in an excited state. Photons emitted in this process are also called gamma rays, and their energy can be as high as 1 GeV. These specific reactions can occur in several situations. For instance, after a violent collision with another particle, or, more commonly, by virtue of a nucleus that is in an excited state after alpha or beta decay. Being used in about two-thirds of all nuclear medicine diagnostic procedures worldwide[1], $^{99m}$Tc is one of the most frequently used gamma-ray emitters. This radioisotope sees a broad usage, as it can be chemically incorporated into small molecule ligands and proteins. Its decay is shown in equation 2.3.[66, 78]

$$ {}^{99m}_{43}Tc \rightarrow {}^{99}_{43}Tc + \gamma\ (140\ keV) \quad (2.3) $$

During a SPECT acquisition, a gamma head (or a set of gamma heads) rotates around the patient collecting several 2D images, or slices. These cameras are made up of several components: (a) led collimator; (b) scintillator crystals and (c) photomultiplier tube (PMT). As the radiopharmaceutical emits energy through nuclear decay, gamma radiation will reach the led collimator. The collimator will only allow radiation to pass through its window if it follows a path parallel to the collimator's orifice. As the gamma rays traverse the collimator, they will eventually hit the scintillator crystal matrix (for example Cadmium Zinc Telluride crystals). These crystals convert high-energy photons to low-energy photons, which in turn are converted to electrons by a photomultiplier tube. Therefore, electrical signals that provide information about the position where the photon collides with the crystal matrix will be obtained, and thus, the distribution of the radioactivity within the object of study. Even so, this data is still stored as what is known as a sinogram, which is not an ideal form of visual information about anatomical structures or function. As such, the reconstruction of the obtained sinogram is the final step to obtaining a tomographic image, as exemplified in Figure 2.16.[80]

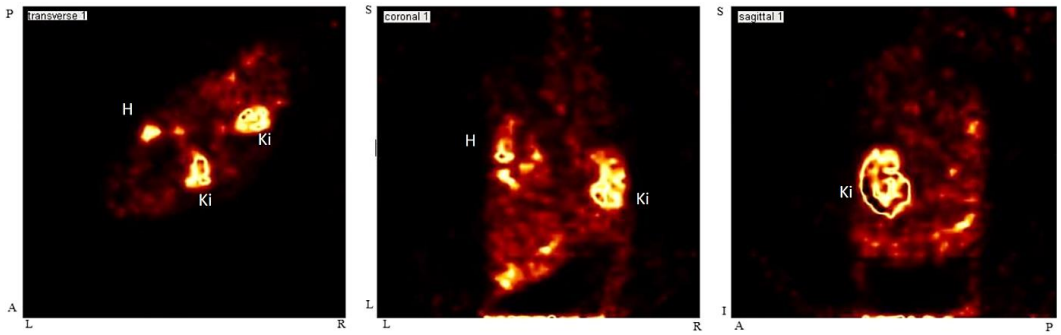


**Figure 2.16:** Example of a SPECT image obtained using the FLEX$^{TM}$ Triumph$^{TM}$ equipment. In this Figure, a SPECT image of a mouse after injection of $^{99m}$Tc-tetrofosmin (1.2 mCi) can be seen. The acquisition was made 2 h p.i. Accumulation of activity is visible in the Kidneys (Ki) and heart (H). The used reconstruction method was 3D-OSEM (10 iterations, 16 subsets).

[1] As of latest, the ratio of the procedures using $^{99m}$Tc has further increased.

### 2.7.4 Target-specific peptides as SPECT Agents for Imaging

Thus far, some of the basic mechanisms that lead to the development of metastatic bone cancer have been addressed, as well as sequences that can interfere with the RANK-TRAF6 pathway. Additionally, the synthesis of peptides was addressed to have at least a general understanding of peptide synthesis. Just after, the basic principles of the medical imaging modalities CT, PET and SPECT were introduced. After laying the groundwork for all these different fields of science, the final bridge can be built by understanding how targeting peptides are labelled with radiometals, so that they can be seen and traced in nuclear medicine images. The general structure of a target-specific biomolecule is demonstrated in Figure 2.17.

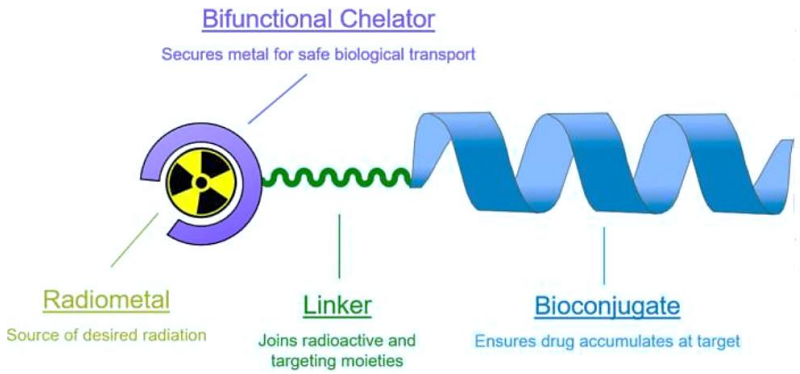


**Figure 2.17: S**chematic representation of a target-specific radiopharmaceutical prepared for radioimaging. The radiopharmaceutical consists of several sequences, namely the target-specific biomolecule, linker, bifunctional chelator agent, and radiometal. Adapted from [68].

By analysing the structure of the target-specific radiopharmaceutical depicted above, it is understood that only the target-specific biomolecule sequence (bioconjugate) was addressed up until this subchapter. The last steps needed to prepare the target-specific radiopharmaceutical are the addition of a linker, and a bifunctional chelator agent, that will hold the radioisotope chosen for the nuclear image.

#### 2.7.4.1 PEGylation

Besides the targeting molecule, which in this study is the peptide coupled to a cell-penetrating sequence, linkers are also employed to avoid unwanted interactions. The objective of coupling a linker is to spatially separate the functional sequence of the molecule that will be interacting with the target receptor, from the sequence of the molecule that contains the radiometal. This separation is often achieved by using polyethylene glycol (PEG) chains.[68]

PEGylation is defined as the modification of a molecule by linking one or more polyethylene glycol (PEG) chains, an inert polymer comprised of repeating units of $CH_2CH_2O$ (see Figure 2.18).[69]

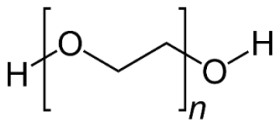


**Figure 2.18:** Polyethylene glycol (PEG) repeating structure. In the square brackets is the $CH_2CH_2O$ unit, which is repeated *n* times, depending on the chosen PEG. Adapted from [70].

When producing and injecting biomolecules, unfavourable characteristics such as low solubility, instability and rapid clearance by the organism can arise. Coupling a PEG chain to the sequence not only provides separation from the bifunctional chelating agent but also improves solubility and stability of molecules, allowing a better control against protein aggregation - a major challenge during protein development.[71-75]

### 2.7.4.2 Bifunctional Chelating Agents

The use of radiometals has been predominant in medical diagnosis, being well-known examples $^{67}$Ga, $^{68}$Ga, $^{64}$Cu and $^{99m}$Tc. These isotopes are often diluted in an aqueous solution and must be captured and integrated into the peptide structure. From the Greek word *chelè*, which translates into 'claw', the process of sequestration of the radiometal ions from the aqueous solution can be done using chelating agents (see Figure 2.19). Bifunctional chelators (BFCs) are simply chelators with reactive functional groups that can be coupled to targeting molecules (e.g., peptides or antibodies).[76]

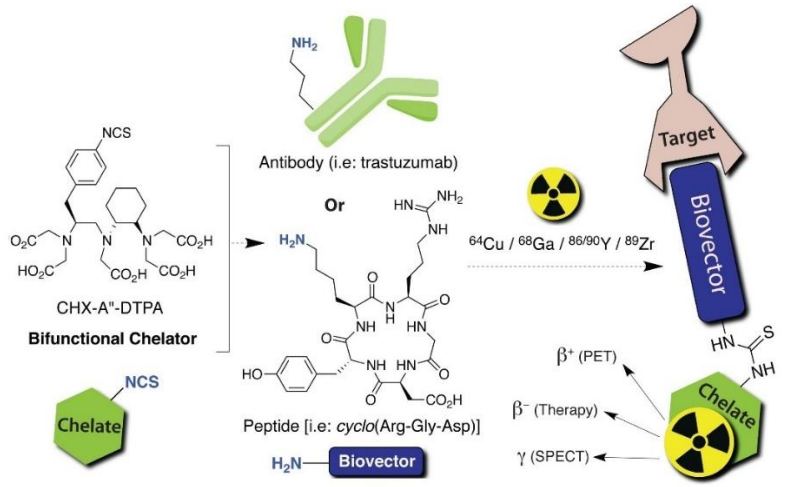


**Figure 2.19:** Schematics of radiolabelling using BFCs. The radioactive metal is captured by the bifunctional chelating agent. Adapted from [77].

The intricate part in radiolabelling occurs when determining the ideal combo of BFC and radiometal, as each radioactive metal complex is stabilized by donor atoms of different nature (e.g., N, O, S), coordination number and geometry. The most extensively evaluated BFC's for peptide radiolabelling are acyclic and cyclic polyaminopolycarboxylic ligands (see Figure 2.20), such as diethylenetriaminepentaacetic acid (DTPA), 1,4,7,10-tetraazacyclododecane-1,4,7,10-tetraacetic acid (DOTA), 1,4,8,11-tetraazacyclododecane-1,4,8,11-tetraacetic acid (TETA) and 1,4,7-triazacyclononane-1,4,7-triacetic acid (NOTA). These chelating agents are particularly interesting, as one of the carboxylic arms of polyaminopolycarboxylic ligands can be used for the coupling of the peptide, typically by formation of amide bonds with primary amines from lysine residues or the N-terminus of peptides.[78-82]

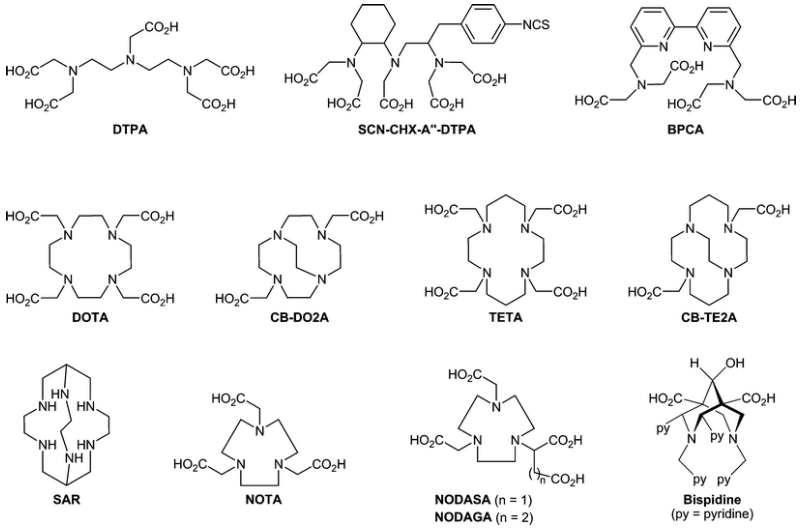


**Figure 2.20:** Acyclic and cyclic polyaminocarboxylic ligands. Adapted from [78].

Peptide labelling with $^{67}Ga/^{68}Ga$ has been typically achieved using DOTA or NOTA derivatives as bifunctional chelators. More particularly, Ga(III)-NOTA complex shows exceptional stability, having thermodynamic stability (pM = 26.4) higher than the one of Ga(III)-DOTA (pM = 15.2). As an additional advantage, the complexation of Ga(III) is faster for NOTA than for DOTA, having the latter the necessity of longer reaction times and higher temperatures. For this reason, although there has been a significant increase of BFC derivatives, NOTA-like chelators remain the paragon for $^{67/68}Ga$ peptide labelling.[78] Considering its similar structural properties and accessibility in $C^2TN$, NODAGA and $^{67}Ga$ were chosen as a combo for the present research.

Section 3

# Materials and Methods

Table 3.1 provides a list of the nomenclature used for the synthesized peptides. Hereafter, all peptides will be referred to by their respective nomenclature.

**Table 3.1:** Nomenclature of the synthesized peptides.

| Nomenclature | Peptide |
|---|---|
| **S3B** | RQMATADEA-$NH_2$ |
| **3A** | KLFMALVAFLRFLTRQMPTEDEY-$NH_2$ |
| **3B** | KLFMALVAFLRFLTRQMATADEA-$NH_2$ |
| **C3A** | NODAGA-$PEG_2$-KLFMALVAFLRFLTRQMPTEDEY-$NH_2$ |
| **C3B** | NODAGA-$PEG_2$-KLFMALVAFLRFLTRQMATADEA-$NH_2$ |

## 3.1 Peptide Synthesis

### 3.1.1 Materials and Equipment for 'Classical', US and MW-Assisted SPPS

Dicloromethane (DCM) (≥ 99.85%) and N,N-Dimethylformamide (DMF) (≥ 99%) were purchased from Riedel-de Haën™ (Hannover, Germany), being used without further purification. Trifluoracetic acid (TFA) (≥ 99%), triisopropylsilane (TIS) (≥ 98%), 1,2-ethanedithiol (EDT) (≥ 99%), piperidine (≥ 99%) and N,N-diisopropylethylamine (DIPEA) (≥ 99%) were purchased from Merck®. Novabiochem™ and Iris Biotech GmbH supplied all Fmoc-L-AA-OH (with the corresponding side chain protecting group orthogonal to Fmoc-based SPPS) and 2-(1H-Benzotriazol-1-yl)-1,1,3,3-tetramethyluronium hexafluorophosphate (HBTU) (≥ 99.9%), respectively. Rink Amide MBHA resin LL (100-200 mesh) with a loading of 0.38 mmol/g, and NovaPEG Rink Amide resin (35-100 mesh) with a loading of 0.47 mmol/g were acquired from Novabiochem®. For synthesis control, three fresh Kaiser test solutions (A, B and C) were prepared according to AAPPTec technical bulletin 1188, using SIGMA-ALDRICH® reagents. Final reagents were prepared as follows:

- **Reagent A:** 1 mL of a 0.66 g/L solution of potassium cyanide (KCN) (≥ 98%) in distilled water, diluted in 49 mL of pyridine (≥ 99%).
- **Reagent B:** 50 g/L solution of ninhydrin in n-butanol (≥ 99.5%).
- **Reagent C:** 2000 g/L solution of phenol (≥ 99.5%) in n-butanol.[83]

The 'classical' SPPS (employed in the synthesis of S3B) was held in a glass reactor with a porous fritted glass, as shown in Figure 3.1 [Left]. Solutions were stirred by a controlled $N_2$ gas flow, and all procedures were carried on at room temperature. The US-assisted SPPS (Figure 3.1 [Centre]) was performed using a polymeric syringe with an incorporated frit (PP— 5 mL reactor with PE frit, Multisyntech GmbH) and a removable cap to avoid contamination with water from the ultrasound bath. Sonication for SPPS was made using an ultrasonic frequency of 37 kHz, in a Fisherbrand™ S-Series FB15051, (240 × 137 × 150 mm bath dimension and 2.75 L maximum volume) ultrasonic water bath by Fisher Scientific. Throughout the procedure, the water bath volume was kept at a volume of approximately 1.5 L, and the temperature at 30 ± 5 ºC. Ultrasonic output was 200 W, with a peak at 320

W. Additionally, the reactor was positioned inside the equipment in the area where cavitation phenomenon was the strongest, identified by an aluminium foil test as per supplier recommendation. Finally, the MW-assisted SPPS was performed in CEM Liberty 908505 automated microwave peptide synthesizer (Figure 3.1 [Right]), including CEM provided accessories (bottle tubing, Teflon bottle caps, bottles, reaction vessel calibration stand).[59]


**Figure 3.1:** Equipment and materials used for all three methods of SPPS. [Left] Assembled reactor for 'classical' SPPS. [Centre] Equipment used for US-assisted SPPS. [Right] Equipment used for MW-assisted SPPS.

### 3.1.1.1 Method for Manual SPPS

Peptide S3B was manually obtained by standard Fmoc-based SPPS with Fmoc protecting groups on the α-N of the amino acid and orthogonal side chain protecting groups. The latter were tert-butyloxycarbonyl (OtBu) for glutamic acid, tert-butyl (tBu) for aspartic acid, trityl (Trt) for glutamine and 2,2,4,6,7-pentamethyldihydrobenzofuran-5-sulfonyl group (Pbf) for arginine. All reaction vessels were thoroughly washed using ethanol and dried with an $N_2$ gaseous flow (Air Liquide, Miraflores, Portugal). Immediately after, all vessels were washed three times using DMF, followed by DCM. Subsequently, the filter and Rink Amide MBHA resin LL (100-200 mesh) with a molar substitution of 0.38 mmol/g were added to the reaction vessel.

The first step in the synthesis was the pre-swelling of the resin. The polystyrene-based resin was pre-swollen with DMF and stirred for 30 min by an $N_2$ gaseous flow (Air Liquide, Miraflores, Portugal), followed by a thorough wash using DCM. During the swelling procedure, a 50 mL solution of 20% piperidine (PP) in DMF was prepared. After pre-swelling and washing the resin, approximately 10 mL of the freshly prepared 20% PP in DMF was added to the reactor for Fmoc deprotection. For 25 min, the contents of the reactor vessel were agitated using a gentle continuous flow of $N_2$. While Fmoc deprotection of the resin occurred, HBTU and the first amino acid (3 equivalents) were dissolved in 5 mL of DMF. After homogenization, 10 equivalents of DIPEIA were added to the solution. The mixture was then swirled and incubated at room temperature for 15 min.

After stirring for 25 min in 20% PP in DMF, the resin was thoroughly washed three times using DMF, followed by three times with DCM. After the wash, a few resin beads were transferred to a test tube for synthesis control, using the pre-prepared Kaiser test kit. From A to C, two drops of the reagents were added to the test tube in order, that was immediately put in a 100 ºC distilled water bath for 5 min. Subsequently, a qualitative analysis was made. Examples of the most common results obtained for the Kaiser test during the synthesis can be seen in Figure 3.2.

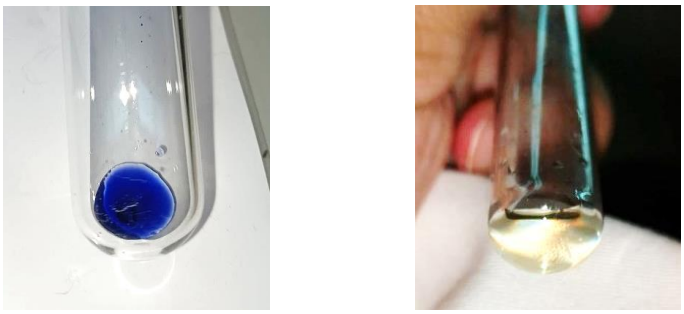

**Figure 3.2:** Kaiser test results during SPPS. [Left] The solution and resin beads emanate a dark blue colour when a primary amine group is present. This means the peptide is deprotected and can accept the subsequent amino acid in the sequence. [Right] The solution presents a translucid colouring if the deprotection was unsuccessful (during the deprotection stage), or if the amino acid was successfully coupled to the chain (coupling step).

When a positive Kaiser test was obtained (dark blue colour) - indicating the α-amine was deprotected - the activated amino acid solution was added to the reactor vessel for the amino acid coupling step. The deprotected resin and activating solution were agitated using $N_2$, for 5 min. The amino acid solution was removed from the reactor, and the resin was washed. Following the wash, a few resin beads were removed from the reactor and added to a new test tube for new synthesis control. Subsequent steps would depend on the Kaiser test result. If the result was positive (blue colour), a new coupling step would take place. The deprotection-coupling cycle was repeated until the desired peptide was assembled.

Succeeding all the amino acid couplings, a final deprotection using 20% PP in DMF was made in preparation for the peptide cleavage. During the final deprotection, the cleavage cocktail was prepared. The cleavage was performed for 4.5 hours, using 10 mL of a standard cleavage cocktail (TFA 92.5% / TIS 2.5% / EDT 2.5% / water 2.5%, *% v/v*). Afterwards, the peptide was precipitated by adding ice-cold diethyl ether and isolated by centrifugation. Obtained crude S3B precipitated as a white residue and was dried under a stream of $N_2$. Finally, the crude peptide S3B (see Table 3.2) was stored at -20 ºC.

**Table 3.2:** Peptide S3B's sequence, chemical formula, and exact mass without the final carboxamide ($CONH_2$) group.

| | **S3B** |
|---|---|
| **Sequence** | RQMATADEA-$NH_2$ |
| **Chemical Formula** (w/out final carboxamide group) | $C_{38}H_{65}N_{13}O_{16}S$ |
| **Exact Mass (Da)** | 991.44 |

### 3.1.1.2 Method for US-Assisted SPPS

During US-SPPS, the same reagents and equivalents of reaction as those used during manual SPPS of reaction were used. The main differences between manual and US-SPPS were the reaction vessels and agitation method. A total of three syntheses were made (S3B and two 3A), having used Rink Amide MBHA resin LL (loading: 0.38 mmol/g) in the first batch (S3B, 3A), and NovaPEG Rink Amide resin (loading: 0.47 mmol/g) on the second (3A).

All synthesis started by washing the polymeric syringe reactor three times with DMF, followed by DCM. Subsequently, the resin was added to the reactor, followed by 3 mL of DMF. When all reagents were inside the reactor, the removable cap was put on to avoid water contamination. Afterwards, a 30-min pre-swelling step was made using the ultrasound bath.

During the swelling procedure, a 50 mL solution of 20% piperidine (PP) in DMF was prepared. After pre-swelling and washing the resin, 3.5 mL of the freshly prepared 20% PP in DMF was added to the reactor for Fmoc deprotection. Under the ultrasound bath, the Fmoc-deprotection step was reduced to 5 min, in comparison with the 'classical' procedure. After deprotection, the resin was washed and synthesis control by colorimetric test was made.

After deprotection confirmation, HBTU and the first amino acid (3 equivalents) were dissolved in 1 mL of DMF. The solution was then homogenized under the ultrasound bath for 2 min, and 10 equivalents of DIPEA were added to the solution. The mixture was agitated under ultrasounds for 10 min. Post agitation, the activated amino acid was added to the reactor and agitated for 5 min. Following the coupling, the resin was washed, and a new colorimetric assessment was made by placing a few resin beads in a test tube for synthesis control, using the pre-prepared Kaiser test kit. From A to C, two drops of the reagents were added to the test tube in order, that was put in a 100 ºC distilled water bath, for 5 min. The deprotection-coupling cycle was repeated until the desired peptide was assembled.

Having coupled all the amino acids, a final deprotection was made using 20% PP in DMF in preparation for the peptide cleavage.

The cleavage cocktail was prepared according to standard procedure, using 4 mL of a standard cleavage cocktail (TFA 92.5% / TIS 2.5% / EDT 2.5% / water 2.5%, *% v/v*). Cleavages took place for 4.5 hours. The peptides were precipitated by ice-cold diethyl ether and isolated by centrifugation. Obtained crudes of peptides S3B and 3A precipitated as a white residue and were dried under a stream of $N_2$. Lastly, the synthesized peptides (see Table 3.3) were stored at -20 ºC.

**Table 3.3:** Peptides S3B and 3A sequence, chemical formula, and exact mass without the final carboxamide ($CONH_2$) group.

| | **S3B** | **3A** |
|---|---|---|
| **Sequence** | RQMATADEA - $NH_2$ | KLFMALVAFLRFLT-RQMPTEDEY - $NH_2$ |
| **Chemical Formula** | $C_{38}H_{65}N_{13}O_{16}S$ | $C_{131}H_{203}N_{31}O_{34}S_2$ |
| **Exact Mass (Da)** (w/o final carboxiamide) | 991.44 | 2818.45 |

### 3.1.1.3 Method for MW-Assisted SPPS

The MW-assisted SPPS (for 3A and 3B) was performed in a CEM Liberty 908505 automated microwave peptide synthesizer. The software Pepdriver was used, and a 0,1 mM resin scale was set up for NovaPEG Rink Amide resin (resin substitution: 0.47 mmol/g). When programming the peptide sequence, several protocols were available, as shown in Table 3.4.

**Table 3.4:** Software pre-set methods for SPPS. Each method presented several different conditions, from temperature to time of exposure, being that some of the methods were amino acid or peptide-dependent.

| **Method** | **Nº of Steps** | **Settings (Microwave Cycles)** |
|---|---|---|
| Deprotection | 1 | **Step 1:** 35 W for 30 seconds at 75 ºC |
| Coupling | 1 | **Step 1:** 25 W for 300 seconds at 75 ºC |
| Coupling (50 ºC) | 2 | **Step 1:** 0 W for 120 seconds at 50 ºC<br>**Step 2:** 25 W for 300 seconds at 50 ºC |
| Couple Arginine | 2 | **Step 1:** 0 W for 1500 seconds at 75 ºC<br>**Step 2:** 25 W for 300 seconds at 75 ºC |
| AA Coupling Long Peptide | 1 | 25 W for 300 seconds at 75 ºC |
| AA Coupling Long Peptide (50 ºC) | 4 | **Step 1:** 0 W for 120 seconds at 50 ºC<br>**Step 2:** 25 W for 240 seconds at 50 ºC<br>**Step 3:** 0 W for 120 seconds at 50 ºC<br>**Step 4:** 25 W for 240 seconds at 50 ºC for 240 |
| Double [Method] | 1 | Chosen method would have double the time settings for each step. |

Several of the procedures were already personalized within the software, such as the arginine coupling method, or the coupling at 50 ºC. These exceptions are made to facilitate - or avoid - certain reactions. For example, arginine is an amino acid quite known for its difficulty in the coupling, and as such, is coupled under harsher conditions. As opposed to arginine, glutamic and aspartic acids are known to easily form unwanted products by cyclization, and as such need to be under milder conditions.

The methods used for MW-assisted SPPS were chosen entirely as a function of the amino acid being conjugated and/or the adjacent amino acid. These chosen methods can be found in Tables 3.5 and 3.6.

**Table 3.5:** Description of the method programmed for peptide 3A's synthesis by MW-assisted SPPS.

| Peptide | Step | Amino acid | Cycle name |
|---|---|---|---|
| **3A** | 1 | - | **Resin Deprotection** |
| | 2 | Tyrosine (Y) | Coupling |
| | 3 | Glutamic Acid (E) | Coupling (50 ºC) |
| | 4 | Aspartic Acid (D) | Coupling (50 ºC) |
| | 5 | Glutamic Acid (E) | Coupling (50 ºC) |
| | 6 | Threonine (T) | Double Coupling |
| | 7 | Proline (P) | Double Coupling |
| | 8 | Methionine (M) | Double Coupling (50 ºC) |
| | 9 | Glutamine (Q) | Double Coupling |
| | 10 | Arginine (R) | Double Couple Arginine |
| | 11 | Threonine (T) | Double Coupling Long Peptide |
| | 12 | Leucine (L) | Double Coupling Long Peptide |
| | 13 | Phenylalanine (F) | Double Coupling Long Peptide |
| | 14 | Arginine (R) | Double Coupling Long Peptide |
| | 15 | Leucine (L) | Double Coupling Long Peptide |
| | 16 | Phenylalanine (F) | Double Coupling Long Peptide |
| | 17 | Alanine (A) | Double Coupling Long Peptide |
| | 18 | Valine (V) | Double Coupling Long Peptide |
| | 19 | Leucine (L) | Double Coupling Long Peptide |
| | 20 | Alanine (A) | Double Coupling Long Peptide |
| | 21 | Methionine (M) | Double Coupling Long Peptide (50 ºC) |
| | 22 | Phenylalanine (F) | Double Coupling Long Peptide |
| | 23 | Leucine (L) | Double Coupling Long Peptide |
| | 24 | Lysine (K) | Double Coupling Long Peptide |
| | **25** | - | **Final Deprotection** |

**Table 3.6:** Description of the method programmed for peptide 3B's synthesis by MW-assisted SPPS.

| Peptide | Step | Amino acid | Cycle name |
|---|---|---|---|
| | **1** | **-** | **Resin** |
| | 2 | Alanine (A) | Coupling |
| | 3 | Glutamic Acid (E) | Coupling (50 ºC) |
| | 4 | Aspartic Acid (D) | Coupling (50 ºC) |
| | 5 | Alanine (A) | Coupling |
| | 6 | Threonine (T) | Double Coupling |
| | 7 | Alanine (A) | Coupling |
| | 8 | Methionine (M) | Double Coupling (50 ºC) |
| | 9 | Glutamine (Q) | Double Coupling |
| | 10 | Arginine (R) | Double Couple Arginine |
| | 11 | Threonine (T) | Double Coupling Long Peptide |
| | 12 | Leucine (L) | Double Coupling Long Peptide |
| **3B** | 13 | Phenylalanine (F) | Double Coupling Long Peptide |
| | 14 | Arginine (R) | Double Coupling Long Peptide |
| | 15 | Leucine (L) | Double Coupling Long Peptide |
| | 16 | Phenylalanine (F) | Double Coupling Long Peptide |
| | 17 | Alanine (A) | Double Coupling Long Peptide |
| | 18 | Valine (V) | Double Coupling Long Peptide |
| | 19 | Leucine (L) | Double Coupling Long Peptide |
| | 20 | Alanine (A) | Double Coupling Long Peptide |
| | 21 | Methionine (M) | Double Coupling Long Peptide (50 ºC) |
| | 22 | Phenylalanine (F) | Double Coupling Long Peptide |
| | 23 | Leucine (L) | Double Coupling Long Peptide |
| | 24 | Lysine (K) | Double Coupling Long Peptide |
| | **25** | **-** | **Final Deprotection** |

Proceeding the synthesis, the resin was removed from the equipment and stored in polymeric syringe reactors. The resin was divided into four samples, two samples being peptides 3A and 3B for cleavage, and two samples for subsequent PEGylation and radiolabelling by US-assisted SPPS. The resins containing peptides 3A and 3B for cleavage were washed with DMF, then DCM. A 4 mL standard cleavage cocktail was prepared (TFA 92.5% / TIS 2.5% / EDT 2.5% / water 2.5%, *% v/v*) and inserted in the syringe reactors. The cleavages lasted for 4.5 hours, followed by precipitation and centrifugation with ice-cold diethyl ether. Crudes of obtained peptides were stored at -20 ºC.

## 3.2 Peptide Purification and Analysis

### 3.2.1 Materials

The RP-HPLC equipment used for analytical control of all peptides and bioconjugates, and purification of bioconjugates C3A and C3B was a PerkinElmer LC pump 200 coupled to a PerkinElmer Series 200 UV/Vis Detector. Additionally, a Supelco Discovery® Bio Wide Pore C18-5 column (250 mm × 4.6 mm, 5 µm) with a flow rate of 1.0 mL $min^{-1}$ and UV detection at λ = 220 nm.

For semi-preparative purification of peptides 3A and 3B, a Waters 2535 Quaternary Gradient Model and Waters 2998 Photodiode Array Detector system were used, coupled with a Supelco Analytical 567209-U C-18 column (250 mm x10 mm x 10 µm, SIGMA-ALDRICH®) with a flow rate of 3.0 mL $min^{-1}$ and UV detection at λ = 220 nm.

Two solutions were prepared to be used as eluents for both methods: (A) 0.1 % TFA in $H_2O$ and (B) 0.1 % TFA in Acetonitrile (ACN). TFA (≥ 99.8%) and ACN (≥ 99.9%) were purchased from Merck®.[54]

### 3.2.2 Methods

The composition of the RP-HPLC mobile phase, both in analytical control and peptide purification, used as eluents: A – 0.1 % TFA (aq) and B – 0.1 % TFA in ACN).[84] The applied binary HPLC gradients used are shown in Figures 3.3 and 3.4.

**Gradient used for peptides 3A, 3B and C3A and C3B:**

- 0 → 5 min, 10% B, flow rate 1.0 mL $min^{-1}$;
- 5 → 25 min, 10–100% B, flow rate 1.0 mL $min^{-1}$;
- 25 → 28 min, 100% B, flow rate 1.0 mL $min^{-1}$;
- 28 → 30 min, 100–10% B, flow rate 1.0 mL $min^{-1}$;

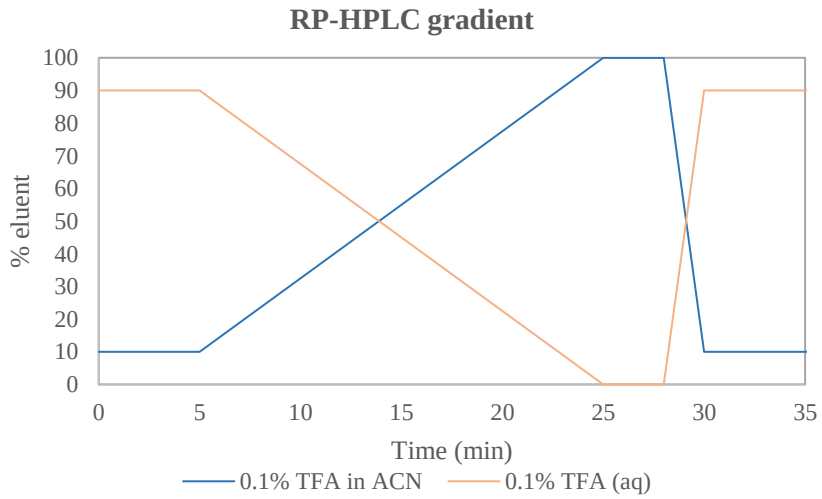


**Figure 3.3:** RP-HPLC method used for peptides 3A, 3B, C3A and C3B.

**Gradient used for peptide S3B:**

- 0 → 5 min, 10% B, flow rate 1.0 mL $min^{-1}$;
- 5 → 25 min, 10–25% B, flow rate 1.0 mL $min^{-1}$;
- 25 → 27 min, 25-100% B, flow rate 1.0 mL $min^{-1}$;
- 27 → 28 min, 100% B, flow rate 1.0 mL $min^{-1}$;
- 28 → 30 min, 100-10% B, flow rate 1.0 mL $min^{-1}$.

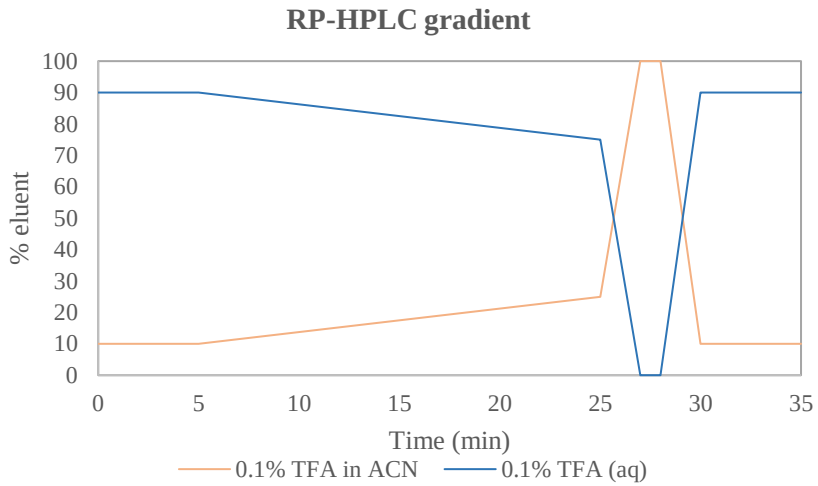


**Figure 3.4:** RP-HPLC method used for peptide S3B.

Analytical control of all peptides was made using the analytical RP-HPLC, whilst purification of peptides 3A and 3B was made by semi-preparative RP-HPLC. Additionally, the purification of bioconjugates C3A and C3B was made by analytical RP-HPLC.

## 3.3 Peptide Concentration Determination by UV-Vis Spectrophotometry

### 3.3.1 Materials

Agilent Technology's Cary 60 UV-Vis Spectrophotometer containing a Xenon source lamp (λ: 190→1100 nm) was used for UV-Vis spectrophotometry. Suprasil® quartz cuvettes (spectral range 200-2500 nm; path length 10 x 2 mm; chamber volume 400 µL) were acquired from SIGMA-ALDRYCH®.

### 3.3.2 Methods

Peptide concentration determination was made by UV-Vis Spectrophotometry. Stock solutions of peptides C3A and C3B were obtained by dilution of the polypeptides in 900 µL and 500 µL of MilliQ water, respectively. For UV-Vis analysis (see Figure 3.5), a 15 µL stock solution sample of C3A, and 10 µL of C3B were further diluted in 400 µL of MilliQ water.

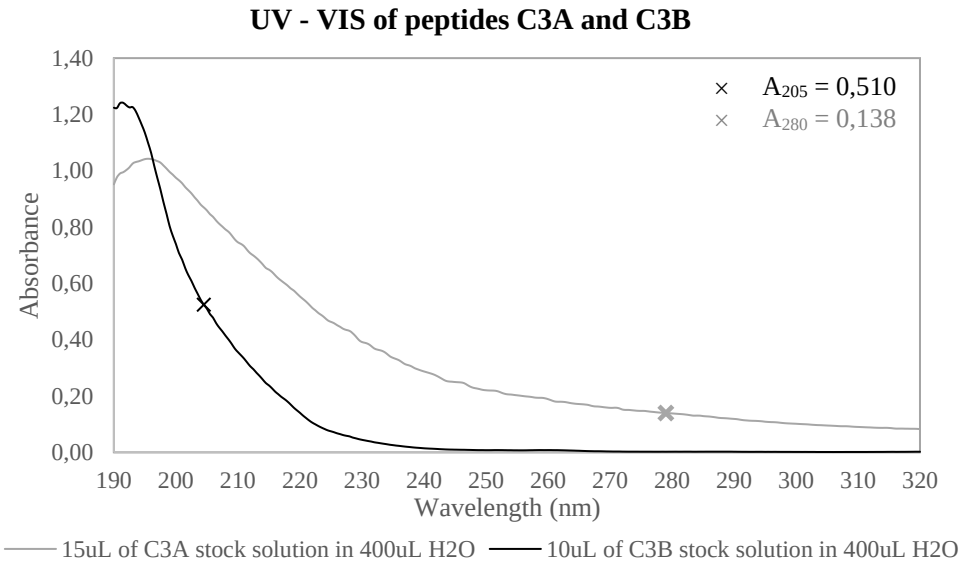


**Figure 3.5:** UV-Vis spectrum obtained from C3A and C3B analysis.

Determination of peptide concentration can be achieved by several methods. Theoretical calculations, however, were made based on the molar extinction coefficients of the absorbing residues constituting the sequence. For C3A (NODAGA-PEG2-KLFMALVAFLRFLTRQMPTEDEY-NH2), calculations were based on the theoretical determination of the extinction coefficient (ε) at 280 nm, which can be calculated up to an accuracy of ± 2% using equation 3.1.

$$\varepsilon_{280} = 5500(nTrp) + 1490(nTyr) + 125(nCys)^2 \quad (3.1)$$

Where *nTrp*, *nTyr* and *nCys* represent the number of residues of tryptophan, tyrosine, and cysteine, respectively. By direct substitution in equation 3.1, the coefficient of molar extinction of C3A at λ = 280 nm is determined as $\varepsilon_{280}$(C3A) = 1490 $M^{-1}$ $cm^{-1}$.

In the case of peptide C3B (NODAGA-$PEG_2$-KLFMALVAFLRFLTRQMATADEA-$NH_2$), which presents none of the abovementioned amino acid residues, calculations of the molar extinction coefficient were made with the assistance of an online protein parameter calculator (http://nickanthis.com/tools/a205.html; Reference 86), that determines $\varepsilon_{205}$ based on equation 3.2.[85]

$$\varepsilon_{205} = \sum[\varepsilon_i n_i] + \varepsilon_{bb}(r-1) \quad (3.2)$$

Where $\varepsilon_i$ represents the molar absorptivity for each amino acid type, $n_i$ the number of amino acid residues in the sequence, $\varepsilon_{bb}$ the molar absorptivity of the backbone peptide bond, and *r* the number of residues in the peptide sequence.[86] At 205 nm, the molar extinction coefficient was determined to be $\varepsilon_{280}$(C3B) = 93720 $M^{-1}$ $cm^{-1}$ for C3B.[86, 99, 100]

Having theoretically determined the extinction coefficients of the peptides and experimentally obtaining their Absorbance (A) at a certain wavelength (λ), the concentration of the peptide dilution (and stock solution) was calculated by the Beer-Lambert law (see equations 3.3 and 3.4).

$$c = \frac{A_\lambda}{\varepsilon_\lambda l} \quad (3.3) \quad \Leftrightarrow \quad c(stock\ solution) = \frac{Diluted\ volume}{Transferred\ stock\ volume} \times \frac{A(\lambda)}{\varepsilon(\lambda) l} \quad (3.4)$$

By substitution of the parameters in equation 3.4, stock solution concentrations were calculated to be 2.56 mM for C3A, and 0.22 mM for C3B. After the procedure, samples were flash frozen and stored at -20 ºC.

## 3.4 Radiolabeling of the Peptides

### 3.4.1 Materials for PEGylayion and Bifunctional Chelating Agent Coupling

Fmoc-Ebes and (R)-NODA-GA(tbBu)$_3$ were purchased from Iris Biotech GMBH and CheMatech, respectively. All other reagents (DCM, DMF, HBTU, DIPEA, Piperidine and Kaiser test reagents) and equipment used (reactors and ultrasonic bath) were those used for US-assisted SPPS and can be found in subchapter 3.1.1.

### 3.4.2 Methods for PEGylayion and Bifunctional Chelating Agent Coupling

The method for PEGylation, and subsequent bifunctional chelating agent coupling of peptides 3A and 3B, was similar to that applied during US-assisted SPPS. After the synthesis of the main peptide sequences by MW-SPPS, two samples of resin containing peptides 3A and 3B were left with their N-terminal deprotected.

[2] The molar extinction coefficients used for calculations were those described in the formula. However, they have been updated. Currently, they stand as $\varepsilon_{280}$ (Trp) = 5690 $M^{-1}cm^{-1}$, $\varepsilon_{280}$ (Tyr) = 1280 $M^{-1}cm^{-1}$ and $\varepsilon_{280}$ (Cys) = 120 $M^{-1}cm^{-1}$.

Using the US-SPPS method, Fmoc-Ebes and NODAGA coupling was made in accordance with the amino acid couplings. HBTU and 2 equivalents of Fmoc-Ebes were dissolved in 1 mL of DMF. The solution was then homogenized under the ultrasound bath for 2 min. Subsequently, 10 equivalents of DIPEA were added to the solution. The mixture was agitated under ultrasounds for 10 min. Post agitation, the activated Fmoc-Ebes solution was added to the reactor and agitated for 15 min. Following the coupling, the resin was washed, and a Kaiser test was performed. After determining if the coupling was successful, deprotection ensued. 3.5 mL of a newly prepared 20% PP in DMF (% v/v) was added to each reactor and agitated under ultrasounds for 5 min. The resins were washed three times with DMF and DCM, and a new Kaiser test was made, to ensure peptide deprotection.

Subsequently, HBTU and 2 equivalents of NODAGA were dissolved in 1 mL of DMF. The solution was homogenized under the ultrasound bath for 2 min, followed by the addition of 10 equivalents of DIPEA to the solution and a 10-min ultrasonication. Afterwards, the activated NODAGA was added to the reactors and agitated under ultrasounds. The coupling was complete after 15 min of agitation in the case of peptide 3B, and 1-hour agitation for peptide 3A.

The resins containing the now bioconjugates, named as C3A and C3B, were washed with DMF and DCM. A 4 mL standard cleavage cocktail was prepared for each cleavage (TFA 92.5% / TIS 2.5% / EDT 2.5% / water 2.5%, % v/v) and inserted in the syringe reactors. The cleavages took place for 4.5 hours. The peptides were precipitated using ice-cold diethyl ether and isolated by centrifugation. Crudes of bioconjugates C3A and C3B obtained precipitated as a white residue and were dried under a gentle stream of $N_2$. Finally, the peptides were stored at -20 ºC.

### 3.4.3 Conversion of $^{67}$Ga-Citrate to $^{67}$Ga-chloride and Radiolabeling

#### 3.4.3.1 Materials

Solution of gallium-67 citrate was purchased from Curium. For conversion of $^{67}$Ga-citrate to $GaCl_3$, SEP-PAK SI cartridges were obtained from Waters, and the solution of hydrochloric acid (HCl) was purchased from SIGMA-ALDRICH®. For pH adjustment of the prepared $GaCl_3$, anhydrous Sodium Acetate (≥ 99%) from Riedel-de Haën™ (Hannover, Germany) was used.

Finally, analytical control of the radiolabelled peptide was achieved on a PerkinElmer LC pump 200 coupled to a Shimadzu SPD-10AV VP UV VIS detector, as well as a Nucleosil 100-10 C18 column (250 mm × 4 mm, 10 µm) with a flow rate of 1.0 mL $min^{-1}$ and UV detection at $\lambda$ = 220 nm attached to a PerkinElmer NCI 900 Network Chromatography Interface Analog to Digital Convertor, which received flow-through radioactivity data from a BERTHOLD TECHNOLOGIES Radioflow Detector LB509. As eluents, two fresh solutions were prepared: (A) 0.1 % TFA in H2O and (B) 0.1 % TFA in Acetonitrile (ACN). TFA (≥ 99.8%) and ACN (≥ 99.9%) were purchased from Merck ®.

#### 3.4.3.2 Methods

The method used for the conversion of gallium-67 citrate into its chloride solution was accomplished through the adaptation of simple methods developed by Kim Chan and Igor Gonda (1991), and Vladimir S. with Johan E. van Lier.[87-89]

Approximately 2.2 mL of $^{67}$Ga-Citrate (3.1 mCi) was placed in a SEP-PAK SI cartridge (Waters) that had previously been conditioned with 10 mL of $H_2O$. Following the addition of the $^{67}$Ga-citrate, 10 mL of $H_2O$ was passed through the cartridge to remove excess of citrate and subsequently dried with air. This was followed by the addition and collection of 5 x 500 µL of 0.1 M HCl to the column, after which the five fractions were separated. Afterwards, the activity of each portion was measured using a CRC®-$^{77}$Thr Dose Calibrator.

For radiolabelling C3A and C3B, the fraction with the highest activity per µL was chosen, containing 1.37 mCi in 440 µL. The pH of the solution was then adjusted to pH = 6, by adding approximately 10.5 mg of sodium acetate [99%; Riedel-de Haën™ (Hannover, Germany)]. After neutralization, the fraction was divided into two samples of 200 µL each. 10 µL of C3A (c = 2.56 mM) and 100 µL of C3B (c = 0.22 mM) were added to their respective recipients, shaken, and left incubating for at least 30 min at room temperature, in preparation for RP-HPLC analysis.

RP-HPLC analysis of $GaCl_3$ and the radiolabelled peptides used as eluents: A - 0.1 % TFA (aq) – and B – 0.1 % TFA in ACN) -. The applied gradient (see Figure 3.6) was in all cases as follows:

- 0 → 5 min, 5% B, flow rate 1.0 mL $min^{-1}$;
- 5 → 20 min, 5-100% B, flow rate 1.0 mL $min^{-1}$;
- 20 → 25 min, 100% B, flow rate 1.0 mL $min^{-1}$;
- 25 → 26 min, 100-5% B, flow rate 1.0 mL $min^{-1}$;
- 26 → 30 min, 5% B, flow rate 1.0 mL $min^{-1}$.

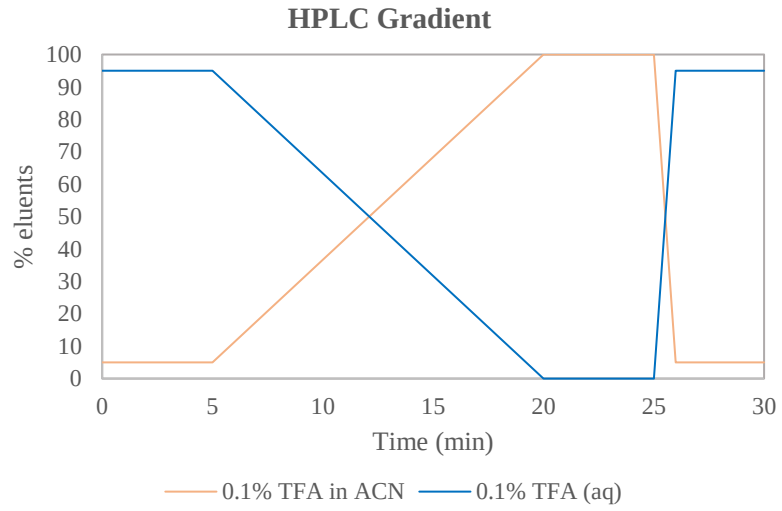


**Figure 3.6:** RP-HPLC method used for the analysis of $GaCl_3$, and radiolabelled C3A and C3B.

## 3.5 Nuclear Imaging

### 3.5.1 SPECT Technical Specifications

The FLEX™ Triumph™ pre-clinical imaging system is a PET-SPECT-CT system used for molecular imaging, biomedical and pharmaceutical research, and development. In Tables 3.7 and 3.8, a general overview of the SPECT Gamma Camera properties, and the specifications of all the collimators available for testing can be seen, respectively.

**Table 3.7:** FLEX™ Triumph™ SPECT system specifications.[90]

| **SPECT specifications** | |
|---|---|
| **Detector Size (cm)** | 18.2 x 19.7 x 13.3 |
| **Detector Material** | CZT (Cadmium Zinc Telluride, CdZnTe) |
| **Active Area (cm)** | 12.7 x 12.7 |
| **Array Size** | 5-by-5 CZT modules |
| **Pixel Size (mm)** | 1.5 |
| **Pixel Pitch (mm)** | 1.6 |
| **Pixel Array** | 80-by-80 |
| **Detector Weight (kg)** | 11.8 |

**Table 3.8:** FLEX™ Triumph™ SPECT gamma camera collimators, and respective specifications.[90]

| **SPECT Gamma camera collimators** | |
|---|---|
| **HRES: High-Resolution Parallel-Hole** | 1.2 mm hex holes, 25.4 mm hole length, 0.2 mm septal thickness |
| **HSEN: High-Sensitivity Parallel-Hole** | 2 mm hex holes, 25.3 mm hole length, 0.2 mm septal thickness |
| **N1F90A10** | 1 pinhole, 90 mm focal length, 1 mm aperture |
| **N5F65A10** | 5 pinholes, 65 mm focal length, 1 mm aperture |
| **N5F75A10** | 5 pinholes, 75 mm focal length, 1 mm aperture |

Presented in Figure 3.7, is the inside view of the equipment during a geometric alignment of CT and SPECT.

**Figure 3.7:** Interior view of the FLEX™ Triumph™ equipment. In the Figure, the gamma camera can be seen with the N5F75A10 collimator, prepared to acquire the image of a phantom.

### 3.5.2 Calibrations

To ensure the best system performance, several calibrations of the equipment were made periodically. These are fundamental to ensure the full functionality of the equipment, as well as to detect and correct possible errors and parameters from the several components. As such, all calibrations were exactly followed as recommended by the manufacturer, which were:

- Gantry Calibration
- Uniformity Correction Table
- QC-Quality Check

#### 3.5.2.1 Gantry Calibration

The gantry calibrations can be made by several methods. From the available methods, the most straightforward was by accessing the user interface Triumph SPECT™ , as demonstrated in Figure 3.8.


**Figure 3.8:** Triumph SPECT$^{TM}$ gantry calibration window.

When executed, the software top tab would open. As indicated in Figure 3.8, the calibration menu would pop-up, and the gantry calibration was initiated by clicking *start*. By clicking *start*, both the patient bed and gantry bed would move to their *zero* position - first the bed, and then the gantry. To ensure an accurate gantry functioning, a gantry calibration is recommended to be performed monthly, or whenever the gantry is powered off. However, the gantry was calibrated before every acquisition, and after any major calibration.

### 3.5.2.2 Camera Calibration – Uniformity Correction Table (UCT) and Quality Check (QC)

One of the most important parameters to maintain up to date is the gamma camera uniformity. This type of calibration must be updated due to small artifacts that can accumulate over time due to electronic components within the equipment. The UCT is a uniformity correction method for a particular radionuclide that is acquired for a considerable number of counts. This method uses the acquisition computer to evaluate the high-count flood and mean counts per pixel. Subsequently, the system stores a pixel-by-pixel correction factor based on the variation of counts within the matrix from the correction flood, which is used for future image acquisitions. For the best quality of the acquisitions, system nonuniformity should be maintained at a 1-3% range.[91]

For multi-pinhole collimators (N5F65A10 and N5F75A10), the equipment UCT required the use of intrinsic images (images with a point source and without a collimator). Therefore, following the manufacturers specifications, a ~10 μCi point source was positioned on top of the mouse bed, and the gamma camera was adjusted so that the average count rate would be 5000-8000 cps. Additionally, the total count value was set to 10 000 kilo counts for UCT and 3000 kilo counts for QC. For single pinhole and parallel hole collimators, the system required extrinsic images (images taken with a flood phantom and the respective collimator). Hence, for extrinsic calibration of single pinhole collimators, a liquid 2’’x2’’ flood phantom (Trifoil) filled with 10 mCi of the element to calibrate was used. In the case of parallel collimators (HRES), a 5’’x5’’ flood phantom (Trifoil) filled with 5 mCi of the respective radioelement was used.

UCT’s were performed bimonthly, at a pre-determined date, for every radioelement and collimator to be used during that time. QCs were performed after every UCT, as part of the calibration procedure.

Additionally, quality checks were also made immediately before any acquisition – to ensure no significant changes occurred in the gamma camera since the aforehand UCT.

### 3.5.3 Validation Study – Phantom Acquisitions

To evaluate the performance of the SPECT equipment, several pre-validation tests were made. These consisted of acquisitions of *in-house made* phantoms of different sizes and shapes, and containing different radioisotopes. Before the acquisition, the protocol was set according to the desired specifications, as the example shown in Figure 3.9.

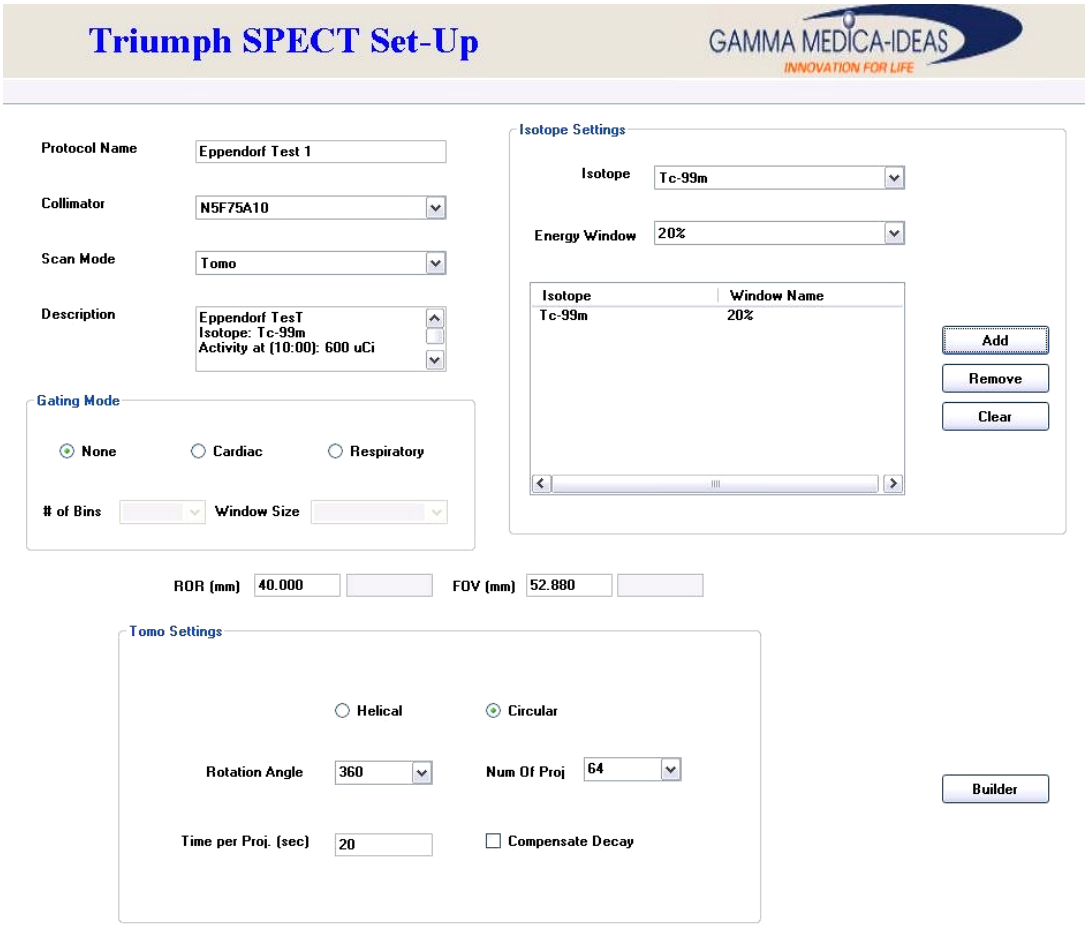


**Figure 3.9:** Triumph SPECT™ window used to set-up acquisition protocols. In this case, a protocol for the acquisition of an Eppendorf tube phantom filled with $^{99m}$Tc was set, with a time per projection of 20 seconds.

During all acquisitions, Tomography settings were fixed and set to circular, with a rotation angle of 360º and 64 projections, as recommended in the Gamma Medica-Ideas Triumph X-SPECT® User's Manual. As for the parameters of the radius of rotation (ROR), the field of view (FOV), collimator, isotope, and energy window, these were variable according to the size of the phantom or the radioisotope being used. However, as a default, ROR was manually set to 40 mm when using N5F75A10 collimator with an energy window of 20%.

When the scan icon was selected, another window would appear, the Triumph SPECT Camera Status. This window allowed visualization of sections of the object inside the equipment. Additionally, it also showed the energy spectra detected by the equipment, the count rate, and several other parameters that can be edited as deemed necessary (see Figure 3.10).

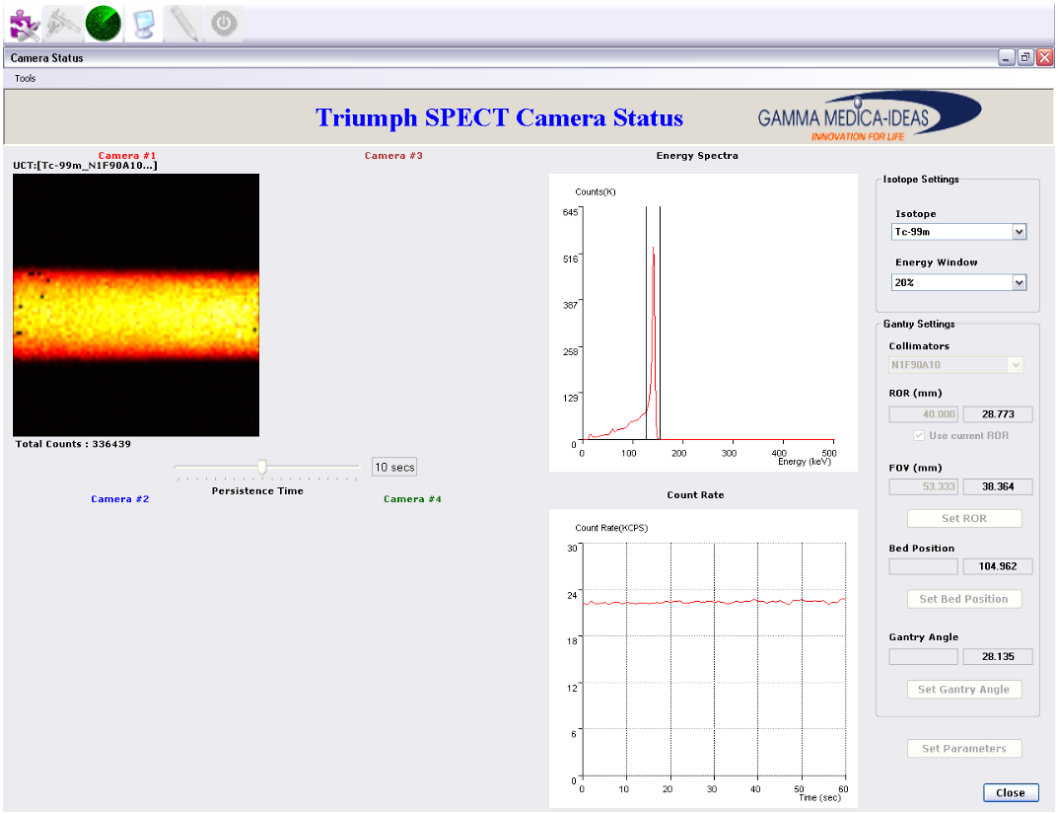


**Figure 3.10:** Triumph SPECT™ SPECT camera status window. As seen in the Figure, the current projection can be seen, as well as the energy spectra of the element, and the count rate.

After the acquisition was finished, the sinogram would become available in the software *Data Viewer* tab (see Figure 3.11). Subsequently, data would be exported for reconstruction.

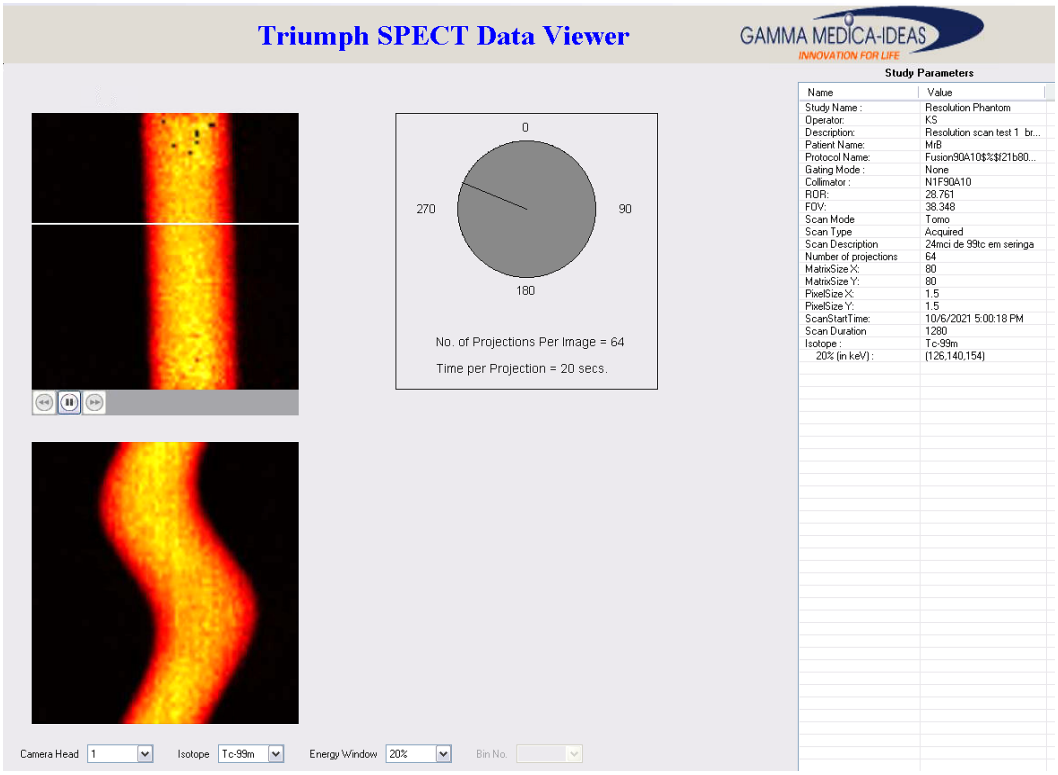


**Figure 3.11:** Triumph SPECT™ data viewer window. Visible in this window are all the specifications used during the acquisition (e.g., the radius of rotation and field of view), as well as the projections and sinogram obtained.

After exporting the data from the data viewer to the provided software for image reconstruction (Triumph$^{TM}$ SPECT Reconstruction Application Version 1.0.8.0), the image was reconstructed. One of two available reconstruction methods could be chosen, either being Filtered Backprojection (FBP), or Ordered Subset-Expectation Maximization (OSEM).

FBP is an analytical method extensively used in SPECT image reconstruction (see Figure 3.12). This method consists of two steps: data filtering and back projection of the filtered data. Since in a 2D acquisition, each row of projections represents the sum of all counts along a straight line through the depth of the object being image, by applying a back projection reconstruction, a redistribution of the number of counts at each point is being made, for all pixels and angles. [92,93]

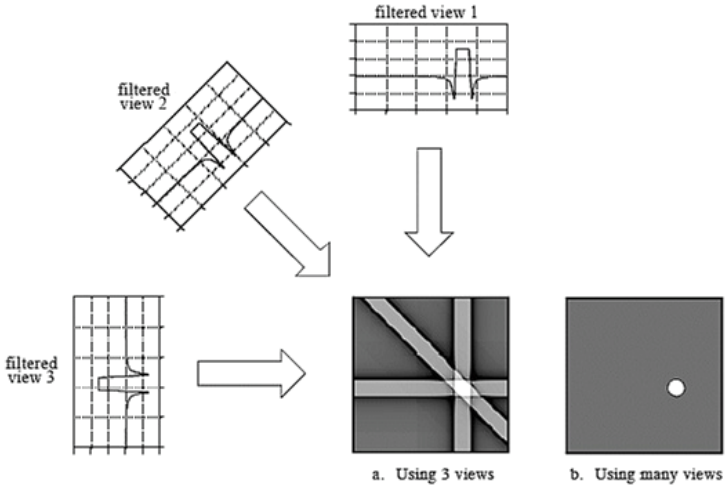


**Figure 3.12:** Schematic representation of the filtered backprojection image reconstruction. Adapted from [93].

As opposed, OSEM is an iterative algorithm that aims at numerical solutions to improve image quality, by iteration processes. An initial estimation of the tomographic image is made. Afterwards, several corrections are applied to the data, such as attenuation and blur corrections due to the collimator aperture. The estimated projection data set is then compared with the actual projection of the main peak (the rationale behind the importance of frequent UCT calibrations). After comparison, the photo peak data is updated, generating new estimations of the reconstructed image. This iteration is repeated until true values are obtained (see Figure 3.13).

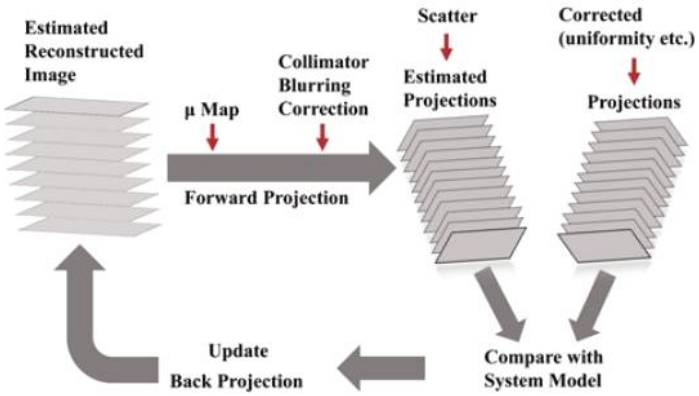


**Figure 3.13:** Schematic representation of the OSEM image reconstruction method. Adapted from [94].

Two main reasons led to the choice of the OSEM reconstruction method. The first was the reports of a slight advantage in OSEM regarding image quality.[94, 95] The second was that, in some instances, the provided software did not allow FBP reconstruction. Hence, for result consistency, all reconstructions

were made using OSEM with the standard parameters already pre-set in the equipment (2 iterations, 8 subsets), as shown in Figure 3.14.

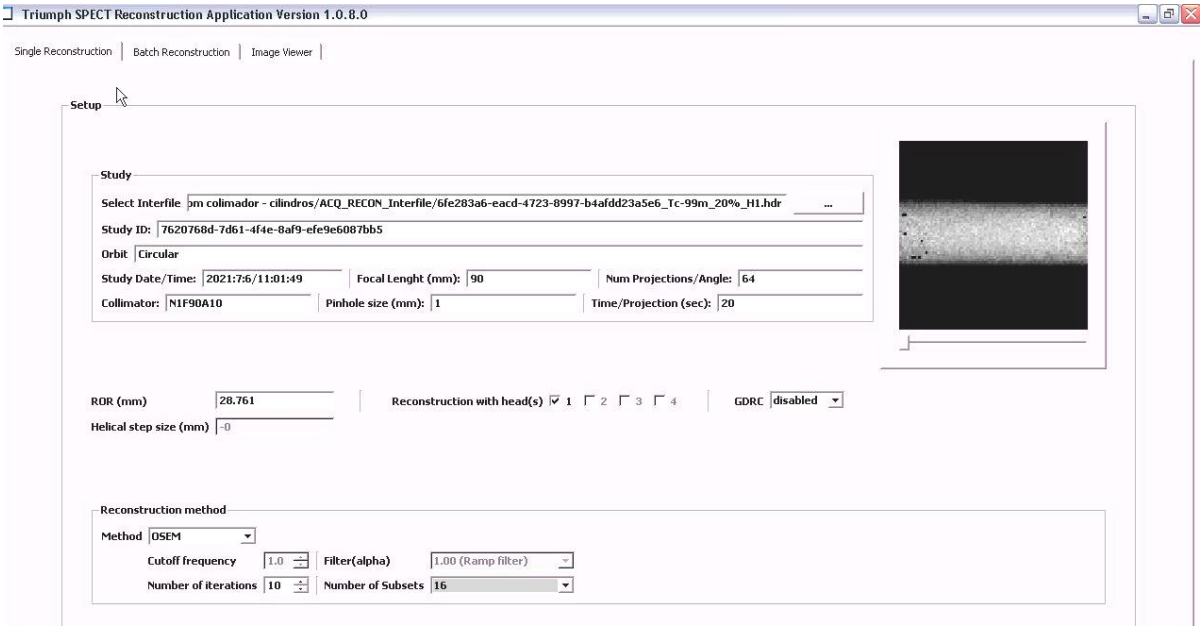


**Figure 3.14:** Triumph$^{TM}$ SPECT Reconstruction Application Version 1.0.8.0 interface.

After image reconstruction, the file was opened using Amide or Vivid software.

### 3.5.4 Methods for SPECT-CT Validation

Inspired by T. Uehara et al., S. Díez-Villarez et al. and Z. Ritter et al.[96-98], to validate the SPECT-CT equipment for *in-vivo* animal models, a $^{67}$Ga test was conducted to simulate a tumour. In this study, a 40 mL syringe was filled with 0.3 mL of a solution containing 20 MBq of $^{67}$Ga. Subsequently, the syringe was sealed in a 50 mL Eppendorf tube filled with water (see Figure 3.15). This test was conducted to simulate the existence of a 0.3 cm$^3$ tumour inside a mouse. Measurements were made over the course of 24 h, at 1 h and 24 h p.i., 64 projections, and a time per projection of 60 s and 84 s, respectively. The chosen collimator was the N5F75A10, with an ROR of 69 mm, and the chosen algorithm of reconstruction was the in-built 3D-OSEM method, using 2 subsets and 8 iterations.

**Figure 3.15:** Phantom used to simulate a tumour inside a mouse.

### 3.5.5 *In Vivo* Animal Model Imaging using CT-SPECT

As it will be further discussed in the Results section, the radiolabelling procedure of bioconjugates C3A and C3B was unsuccessful. However, several other compounds within the scope of cancer research

are also being studied, namely gold nanoparticles of the type $^{67}$Ga-AuNP-BBN-Pt1. Although the imaging of peptides C3A and C3B was not possible, it was considered that in preparation for future studies, the equipment could still be validated. As such, to validate the quality of in vivo studies, a mouse prepared for traditional biodistribution was imaged for result confirmation and comparison with traditional biodistribution. The used animal model was from the Balb/c lineage, with PC-3 cell xenotransplants (prostate adenocarcinoma cells of human origin). Moreover, the investigated compound was named $^{67}$Ga-AuNP-BBN-Pt1, a gold nanoparticle (AuNP) radiolabelled with $^{67}$Ga. The objective was to assess the radiopharmaceutical distribution at 1- and 24-hours post-injection (p.i).$^{67}$Ga-AuNP-BBN-Pt1 was intra-tumourally administered in 2 different tumour sites.

To perform the acquisitions, a FLEX® Triumph® II (Trifoil Imaging) SPECT/CT imaging system was used. The system was equipped with one Cadmium Zinc Telluride (CZT) detector and a five-pinhole (1.0 mm) collimator (N5F75A10). The SPECT data acquisitions were performed at 60 s per projection, with the stepwise rotation of 64 projections over 360º, accounting for the decay of $^{67}$Ga at 24 h – 84 s per projection. Cone-beam CT images were acquired in a gantry fly motion mode (512 projections, 110 ms/projection, 70 kVp, 340 μA), 2X2 binning, 1184 x 1120 matrix. SPECT Triumph Reconstruction Application v1.0.8.0 (Trifoil Inc.) was used to obtain the transaxial, coronal, and sagittal slices, using a 3D-ordered subset expectation maximization (3D-OSEM) reconstruction algorithm with 8 subsets and 5 iterations. Vivid Amira 4.1 software was used to perform the post-processing analysis, as well as the coregistration of SPECT images in conjunction with the corresponding CT images. A gauss filter with a 0.6 sigma, 3x3 kernel, was applied to the CT slices at a threshold of 1300.

The animal study was approved by the local ethics committee, and all procedures were made whilst supervised by duly accredited staff members from C$^2$TN-IST to ensure all procedures were according to the Guide for the Care and Use of Laboratory Animals. The animal was first scanned in SPECT, followed by an immediate CT scan for SPECT-CT fusion.

Section

# 4 Results And Discussion

## 4.1 Synthesis of Peptide S3B by '*Classical*' SPPS *versus* US-Assisted-SPPS

We were able to fully synthesize the 9-mer peptide S3B (RQMATADEA-$NH_2$) by both 'classical' SPPS and US-assisted SPPS, with the methods described above in subchapters 3.1.1.1 and 3.1.1.2 respectively. The conjugation times of the amino acids constituting peptide S3B, synthesized by manual SPPS and US-assisted SPPS, are compared in Figure 4.1.

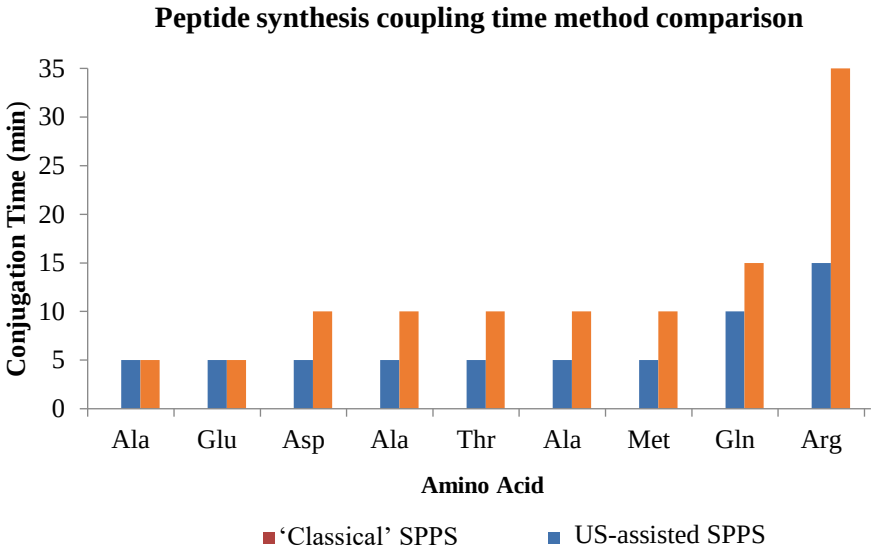


**Figure 4.1:** Conjugation times (min) for each amino acid of peptide S3B prepared by "Classical" SPPS and by US-SPPS.

The first major difference between procedures arose during the deprotection step, which for manual SPPS was 25 min, and for US-assisted SPPS could be reduced up to 5 min, a more than fivefold decrease in the required time. As for the conjugation times, differences became more noticeable only after the third amino acid coupling, aspartic acid, possibly due to the growth of the peptide chain.

In total, results show that there is up to a fourfold time reduction during peptide S3B assembly, as the classical SPPS method (365 min) was replaced by US-SPPS (85 min). Although conjugation times show some decrease in the US-assisted procedure, the reduction in the deprotection step has a prevalent impact on the total time required for assembly.

Apart from the time consumed, an important factor to consider is the chromatographic profile of the final product, representative of the synthesis, purity, and quality. Analytical RP-PLC (Figure 4.2) revealed an 84% versus 72% purity for the crude peptide S3B achieved by manual SPPS and US-assisted SPPS, respectively. At 15 min (Figure 4.2), it is possible to observe an impurity not present in the classical product. Due to the local increase in temperature, associated to ultrasound irradiation, and the presence of aspartic acid residue, we can speculate that the decrease in purity is mainly due to aspartimide formation. Aspartic acid and other basic amino acids are prone to aspartimide formation by cyclization of the residue side chains. This is intensified when a new amino acid is conjugated to aspartic acid (the α-amine of aspartic acid is free) under higher temperatures. To confirm this hypothesis, this

impurity needed to be purified and analysed by ESI-MS. Unfortunately, it was not possible to evaluate such impurity.

This decrease in purity for crude of S3B, although significant, is offset by the substantial decrease in time of synthesis, but also reagent usage, which is much more sustainable in the case of US-assisted SPPS.

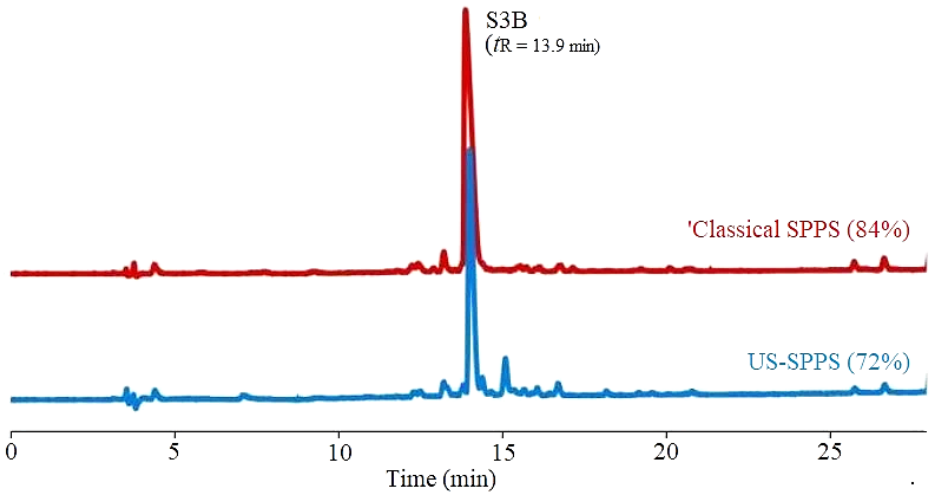


**Figure 4.2:** Comparison of analytical RP-HPLC obtained for crude S3B peptide ($t_R$ = 13.9 min) using manual SPPS and US-SPPS.[54]

## 4.2 US-Assisted SPPS of Peptide 3A

Two attempts were made for the synthesis of peptide 3A (KLFMALVAFLRFLTRQMPTEDEY-$NH_2$) by US-assisted SPPS. During both attempts, the first segment of the peptide (RQMPTEDEY) showed slightly higher conjugation times, in comparison with S3B (see Figure 4.3). Additionally, stable increments in amino acid coupling times were also observed at the start of the second section of the peptide, up until the first phenylalanine. This phenomenon was expected, as in a growing peptide sequence, it becomes more difficult to couple a new residue to the resin-bound chain.

During the first attempt, abrupt transitions in coupling times started appearing during the first arginine of the second segment (KLFMALVAFL**R**FLT-RQMPTEDEY), taking up to 6 hours of conjugation. Given such unexpected results, several modifications were made in an attempt to ameliorate synthesis time, such as the doubling of the activator and amino acid solution concentration, as well as using brand new reagents (DIPEA and protected amino acid). After finally coupling said arginine, the subsequent leucine conjugation seemed to accelerate once again, in line with its precursors. However, during adjacent phenylalanine coupling (KLFMALVA**F**LRFLT-RQMPTEDEY), even further aggravation in coupling times took place, taking up to a '*working'* day for a single conjugation. After phenylalanine, conjugation times seemed to once again stabilize, having only one exception, the last phenylalanine.

Considering the difficulty of the first synthesis, a second attempt was made using a different resin, which was indicated to possess excellent swelling properties in DMF, DCM and water, and good results with hydrophobic peptides - the NovaPEG Rink Amide resin (loading: 0.47 mmol/g). In fact, a slight improvement was observed during the first twelve amino acid conjugations, as shown in Figure 4.3. However, when coupling the first arginine from the second section of the peptide (KLFMALVAFL**R**FLT-RQMPTEDEY), similar issues as those of the first synthesis arose. Exceedingly high conjugation times surged, which led to an incomplete coupling of arginine after 2.5 working days. The problems persisted even after doubling the equivalents of amino acid, DIPEA and

HBTU of the activated amino acid solution. Once presented with such results, the synthesis was stopped and disregarded, in the pursuit of alternative procedures of synthesis.

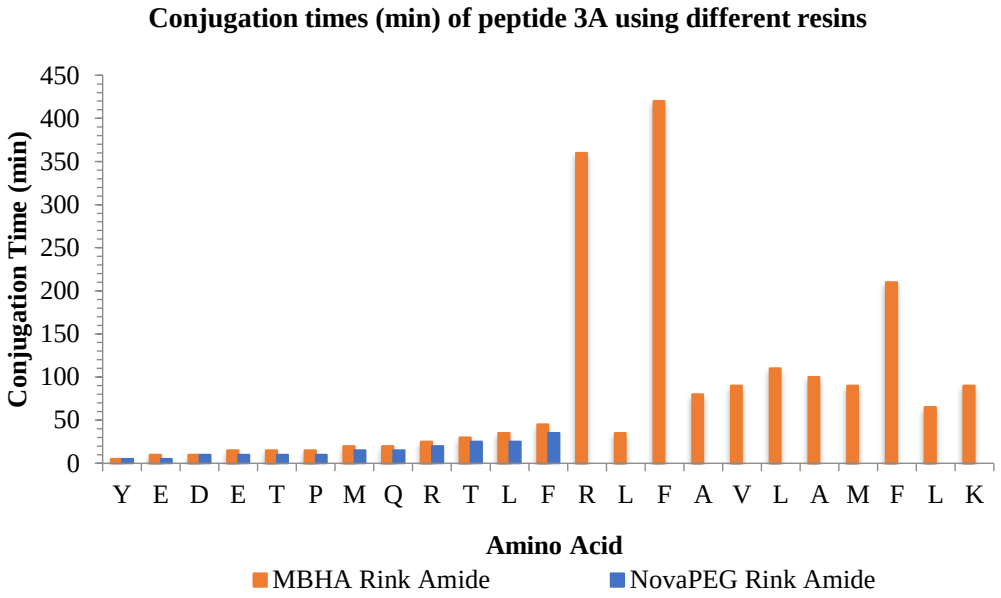


**Figure 4.3:** Graphical comparison of conjugation times obtained for the amino acids constituting peptide 3A by US-assisted SPPS using Rink Amide MBHA resin and NovaPEG Rink Amide resin.

After bringing the second synthesis to a halt, the first batch was cleaved for RP-HPLC analytical control (Figure 4.4).

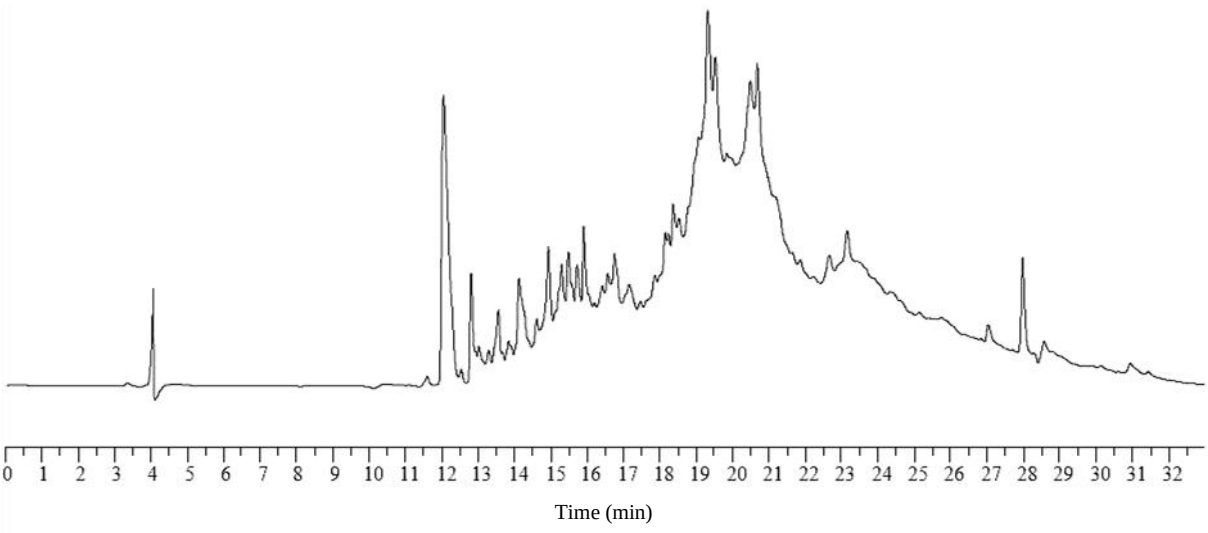


**Figure 4.4:** Analytical RP-HPLC obtained for crudes of peptide 3A, using Rink Amide MBHA resin.

By analysing Figure 4.4 it was concluded that even if peptide 3A had been synthesized, it would be present in very poor yields. To determine whether peptide 3A was present, the two most probable samples recovered during RP-HPLC were analysed by Electrospray Ionisation Mass Spectrometry (ESI-MS). The first sample (S1) corresponds to elution times ranging from min 12 up to min 12.5, which comprises the first major peak. The second sample (S2) was recovered comprising all compounds eluted after min 17 up to min 23. ESI-MS spectra analysis (positive mode) of both acquired samples was inconclusive. For demonstration purposes of the calculation procedure, presented below is the ESI-MS

spectrum obtained from the analysis of S1. Obtained full-size ESI-MS spectra of S1 and S2, can be found under appendixes 1 and 2, respectively.

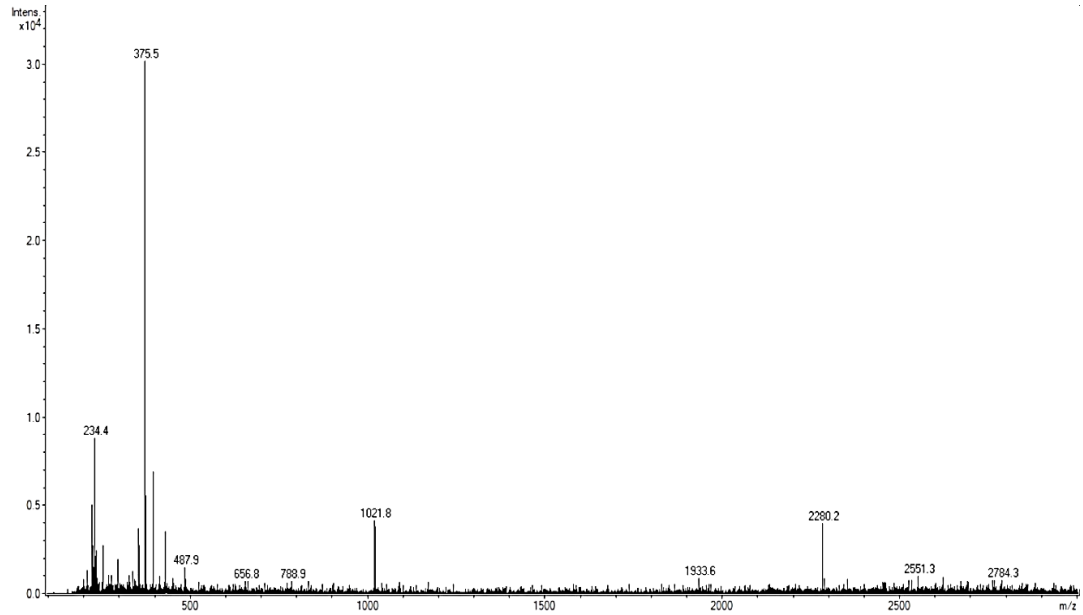


**Figure 4.5:** ESI-MS spectrum obtained for peptide 3A crude sample S1 analysis.

The first step of the analysis consisted of calculating the molecular weight of the simplest positive ionic species that the peptide could acquire. That is, the molecular weight cations that resulted from proton interaction.

$$M_w(N+) = \frac{M_w(Peptide) + N \cdot M_w(H+)}{Charge} \quad (4.1)$$

Where $M_w$(Peptide) and $M_w(H^+)$ represent the molecular weight of the peptide and proton, respectively. N is the number of protons present in the cationic species, and Charge is the charge of the resulting cation, which should be equal to N. Substituting $M_w$(Peptide) by the exact mass of 3A, and $M_w(H^+)$ by 1.01, the molecular weight of cations +1 up to +4 were calculated, as shown in Table 4.1.

**Table 4.1:** Calculated exact masses of cationic forms of peptide 3A.

| Cation | Calculated exact mass (Cation) (Da) |
|---|---|
| $[M + H^+]^+$ | 2819.45 |
| $[M + 2H^+]^{2+}$ | 1410.23 |
| $[M + 3H^+]^{3+}$ | 940.49 |
| $[M + 4H^+]^{4+}$ | 705.62 |

By comparing the calculated $M_w$ of each cation with those obtained in the ESI-MS analysis, none of the masses coincided. Therefore, it is concluded that peptide 3A is not present in fraction S1 at least in its simplest cationic forms. Analysis of other molecular ion adducts often observed in ESI-MS spectra was also assessed, some of which exemplified in Table 4.2.

**Table 4.2:** Calculated exact mass of molecular ion adducts commonly found in peptide crude analysis for peptide 3A.

| Molecular Ion Adducts | Charge | Exact Mass (Da) |
|---|---|---|
| $[M + K^+]^+$ | +1 | 2857.42 |
| $[M + Na^+]^+$ | +1 | 2841.44 |
| $[M + H^+ + Na^+]^{2+}$ | +2 | 1421.23 |
| $[M + ACN + 2H^+]^{2+}$ | +2 | 1430.75 |

Using equation 4.1, calculations with the molecular weight of the compounds detected by ESI-MS can also be made, to determine correlations between the different compounds contained in each fraction. For instance, by analysing the isotope pattern surrounding the 375.5 m/z peak of Figure 4.6, the following peaks were identified:

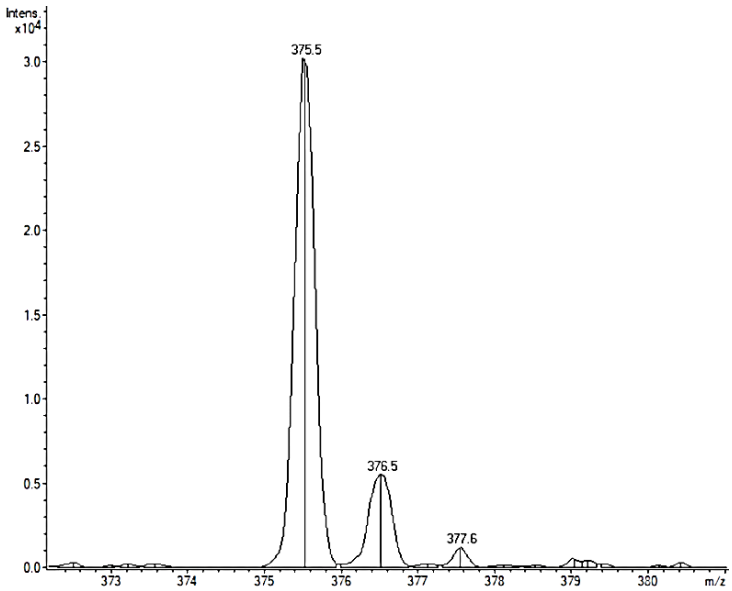


**Figure 4.6:** ESI-MS analysis of the main peak found in sample S1 of peptide 3A crude.

Considering the isotopic distribution shows increments of 1 m/z between species, it is perceivable that the compound being analysed could be the monocharged species $[M + H^+]^{+1}$. Further analysis indicates no correlation between each compound present within the full chromatogram. The assessment made for sample S1 was also applied during sample S2 analysis. After further consideration, it was determined that the peptide did not seem to have been synthesized during the US-assisted SPPS procedure. Additionally, considering the difficulties that arose during the synthesis, no further attempts of synthesizing peptide 3A by this method were made.

Albeit not having synthesized the peptides, with exception of S3B, up to this point in the procedure, several observations were noteworthy for further discussion. During the deprotection stage of the peptide synthesis, sporadic incomplete deprotections occurred. This issue was easily overcome by simply repeating the deprotection procedure. After the peptide cleavage, and in preparation for RP-HPLC analysis, peptide 3A was dissolved in ultrapure water. In some instances, and in the similar concentration of peptide, this would not be the case, acquiring what could be described as a cloudy appearance. Such occurrence could be managed by adding a residual amount of TFA to the solution (0.01 to 0.1% *v/v*). More interestingly, was that this effect would also irregularly occur at room temperature. At a first instance, attempts of dissolving the precipitate were made by ultrasonication. This procedure would sometimes cope with the issue. However, in other situations, only by adding an additional amount of TFA to the solution, this precipitation could be dissolved. Finally, a few hours after RP-HPLC procedures were conducted, cases of a substantial increase in pressure (>20%) on the HPLC column were reported. As such, a more thorough wash had to be established, using 0.1% TFA in ACN eluent.

Several of these observations point towards a common - but complex - occurrence in peptide synthesis, a phenomenon known as peptide aggregation.

## 4.3 Synthesis of Peptides 3A and 3B by MW-Assisted SPPS

Considering the difficulties that arose during US-assisted SPPS, a more automated method of synthesis was conducted for peptides 3A and 3B development, the MW-assisted SPPS. Synthesis by

MW-assisted SPPS took place for approximately two *working days*. To ensure peptides 3A and 3B were synthesized, a small portion of resin of each peptide was isolated and cleaved for 4.5 h. The remaining resin was stored at -20 ºC in preparation for PEGylation. RP-HPLC analysis of peptides 3A and 3B was performed immediately after cleavage and can be found in Figures 4.7 and 4.11, respectively.

### 4.3.1 Analysis of Peptide 3A

The RP-HPLC chromatogram of 3A displays a moderate purity of ca. 53% (Figure 4.7). A particular region of interest was identified, namely the compound eluting at 20.7 min. Compounds eluted before the 15$^{th}$ min were disregarded.

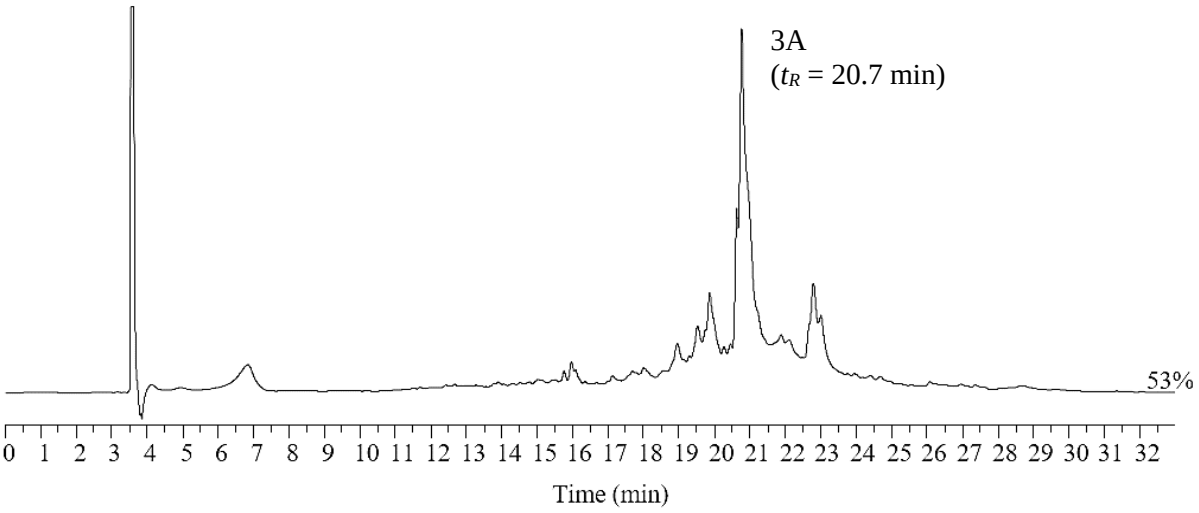


**Figure 4.7:** Analytical RP-HPLC of crude peptide 3A obtained by MW-assisted SPPS.

A sample of the main peak was collected, and it was possible to identify the presence of ionic forms of peptide 3A in the corresponding ESI-MS spectrum (Figure 4.8).

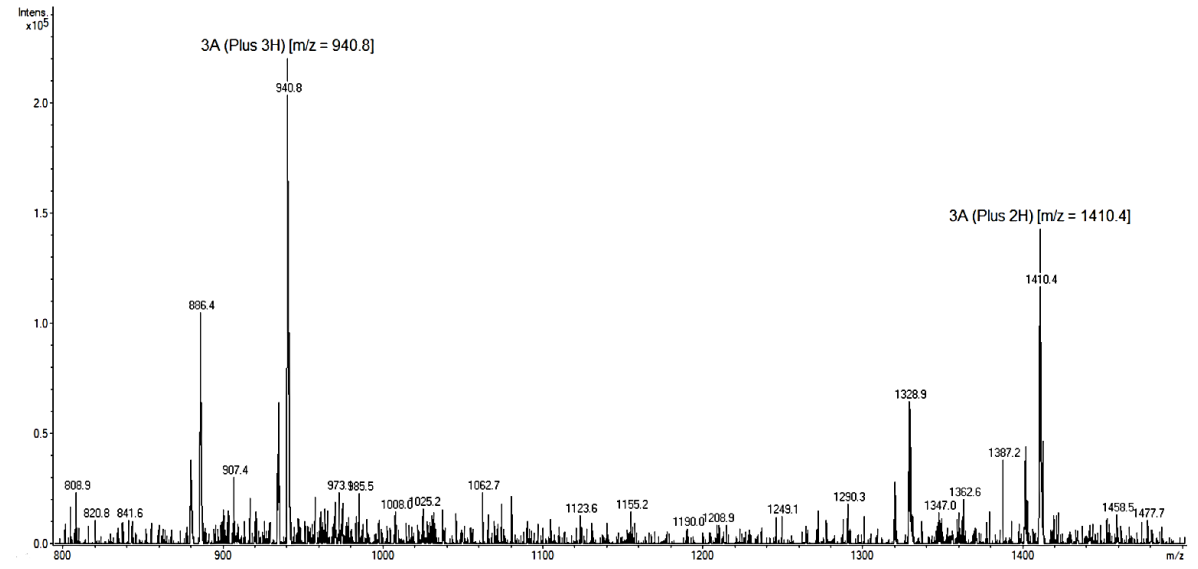


**Figure 4.8:** ESI-MS chromatogram obtained from analysis of a sample recovered from the main peak of peptide 3A crude, synthesized by MW-assisted SPPS.

Moreover, also present in the same sample, there are two other peptide species with molecular weights of 1328.9 m/z and 886.4 m/z, which correspond to peptide 3A with no initial Tyrosine (Table 4.3).

**Table 4.3:** Calculated exact mass of cationic forms of peptide 3A.

| Cation | M | $[M + 2H^+]^{2+}$ | $[M + 3H^+]^{3+}$ |
|---|---|---|---|
| **Exact Mass 3A (Da)** | 2818.45 | 1410.23 | 940.49 |
| **Exact Mass 3A (w/o Y) (Da)** | 2655.28 | 1328.65 | 886.10 |

Focusing on the 1410.4 Da peak obtained in the ESI-MS, the expected isotopic mass distribution pattern was found (Figure 4.9).

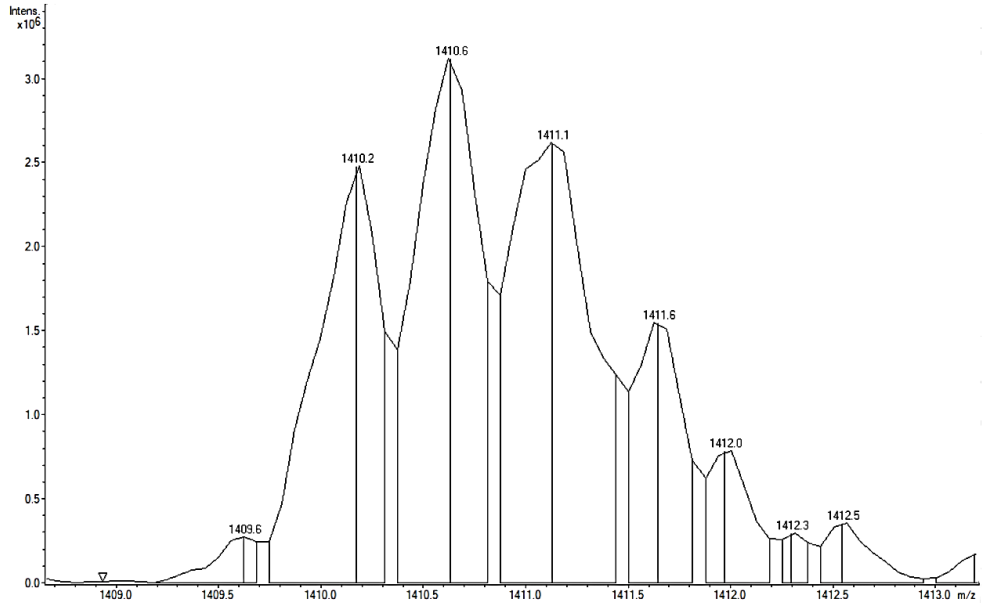


**Figure 4.9:** Isotopic distribution surrounding 1410.4 Da peak of 3A crude (MW-assisted SPPS).

Purification of peptide 3A was performed by semi-preparative RP-HPLC, whose crude chromatogram can be found in appendix 3. The comparison between analytical RP-HPLC obtained before and after purification can be seen below. As presented in Figure 4.10, the maximum purity achieved for peptide 3A was ca. 92.3%.

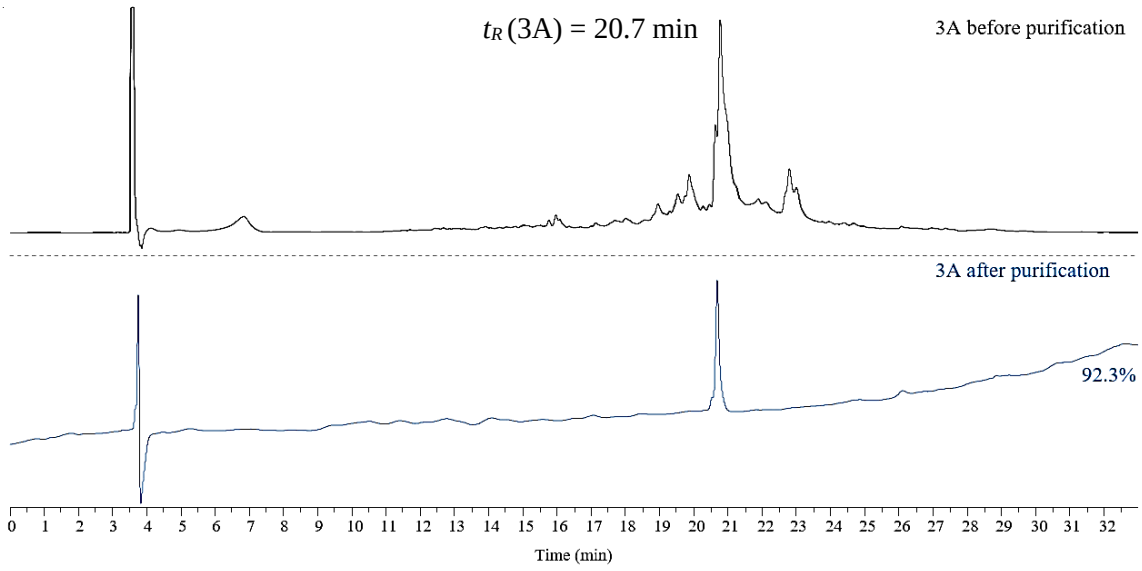


**Figure 4.10:** RP-HPLC chromatograms of peptide 3A before and after purification.

After purification, the recovered eluate was lyophilized and the resulting lyophilized solid stored at -20 ºC.

### 4.3.2 Analysis of Peptide 3B

The synthesis, analytical control, and purification of peptide 3B followed the same procedures as those used for 3A. The RP-HPLC chromatographic profile of crude peptide 3B is shown in Figure 4.11.

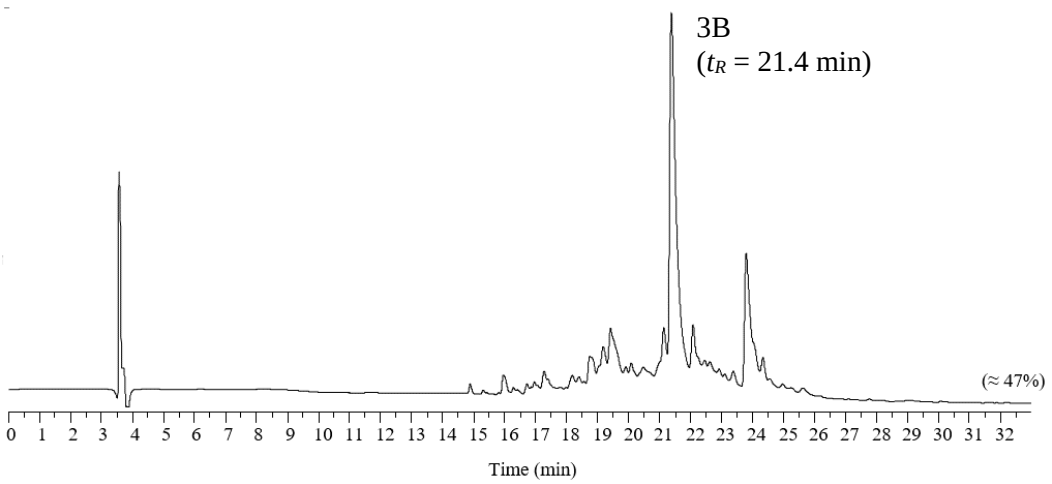


**Figure 4.11:** Analytical RP-HPLC chromatogram of crude peptide 3B obtained by MW-assisted SPPS.

The main peak ($t_R$ = 21.4 min) was recovered and analysed by ESI-MS (Figure 4.12). By calculating peptide 3B's simplest cationic forms (Table 4.4), and comparing it to the isotopic distribution surrounding the 1322.5 Da mass (Figure 4.13), it was concluded that peptide 3B was present in the sample.

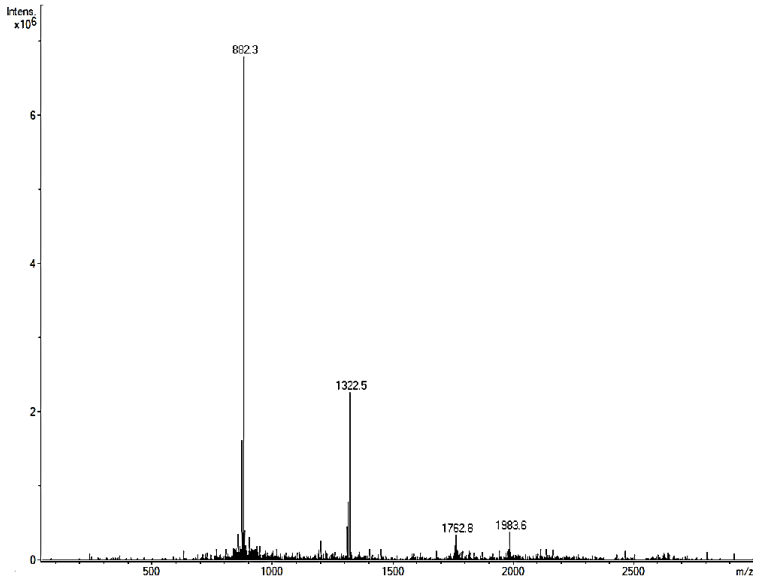


**Figure 4.12:** ESI-MS chromatogram obtained from analysis of a sample recovered from the main peak of peptide 3B crude, synthesized by MW-assisted SPPS.

**Table 4.4:** Calculated exact masses of cationic forms of peptide 3B.

| Cation | Calculated exact mass (Cation) (Da) |
|---|---|
| $[M + H^+]^+$ | 2643.42 |
| $[M + 2H^+]^{2+}$ | 1322.21 |
| $[M + 3H^+]^{3+}$ | 881.81 |
| $[M + 4H^+]^{4+}$ | 661.61 |

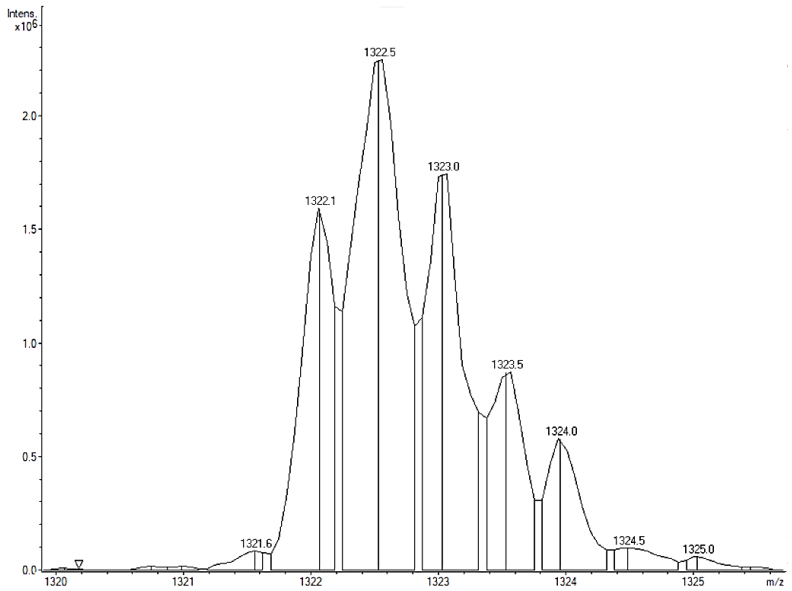


**Figure 4.13:** Isotopic distribution surrounding 1322.5.4 Da peak of crude 3B (MW-assisted SPPS).

After determining that peptide 3B was successfully synthesized, purification was ensued by semi-preparative RP-HPLC, whose crude chromatogram can be found in appendix 4. The comparison between analytical RP-HPLC obtained before and after purification is shown below in Figure 4.14. Peptide 3B was obtained with a final purity of approximately 86%. After purification, the peptide was lyophilized and stored at -20 ºC.

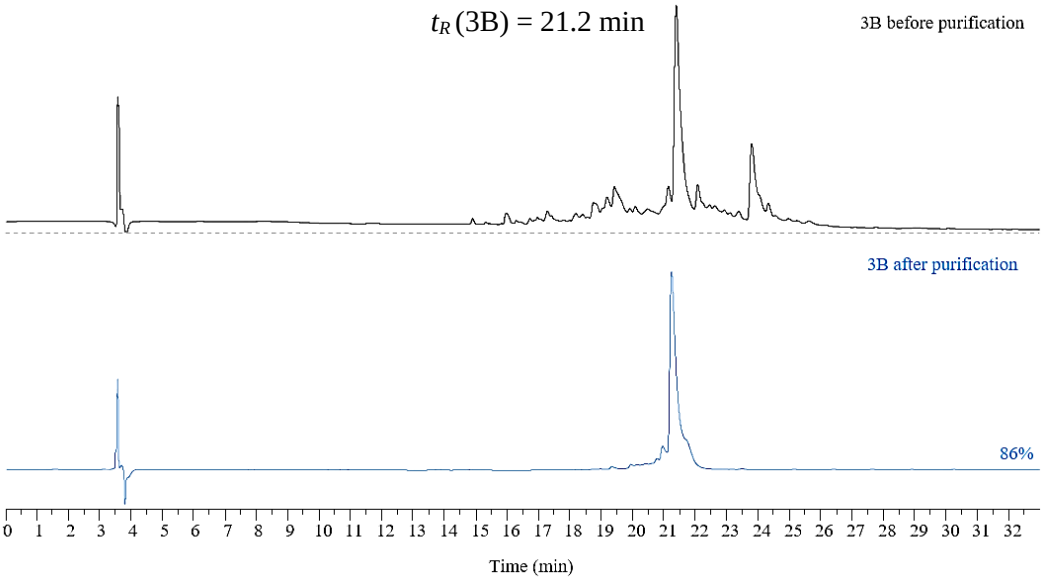


**Figure 4.14:** RP-HPLC chromatograms of crude peptide 3B before and after purification.

## 4.4 Radiolabeling Peptides C3A and C3B

### 4.4.1 PEGylation and NODAGA Conjugation

After assembling the amino acid sequences corresponding to peptides 3A and 3B on the resin, the preparation of the conjugates C3A and C3B involved sequential conjugation to **(i)** FMOC-Ebes and NODAGA coupling; followed by **(ii)** analytical control by RP-HPLC and purification; and **(iii)** determination of the concentration of conjugates C3A, C3B for radiolabelling.

As mentioned in the methods, Fmoc-Ebes and NODAGA coupling by US-assisted SPPS were made similarly to the coupling of a Fmoc-AA. The main difference between the reactions was the stoichiometric ratios of each reagent used. In the case of an amino acid, the rule was 3 equivalents, whilst for Fmoc-Ebes and NODAGA, the equivalents of reaction were of a factor of 2, and 1.7, respectively. The coupling of Fmoc-Ebes was successful for both peptides in approximately 15 min. As for the NODAGA coupling, the reaction was completed in 15 min for peptide 3B, whilst for 3A taking place for 1 hour. Subsequently, a portion of each of the now C3A and C3B were cleaved and stored at -20 ºC for purification in semi-preparative RP-HPLC, and subsequent analytical RP-HPLC analytical control.

### 4.4.2 RP-HPLC Analysis and Purification of the Peptide Conjugates

The analytical RP-HPLC chromatograms obtained before and after purification of C3A (89.5% purity) and C3B (> 90% purity) are presented in Figures 4.15 and 4.17. The characterization of the peptides by ESI-MS is given in Tables 4.5 and 4.6, and the corresponding ESI-MS spectra are shown in Figures 4.16 and 4.18.

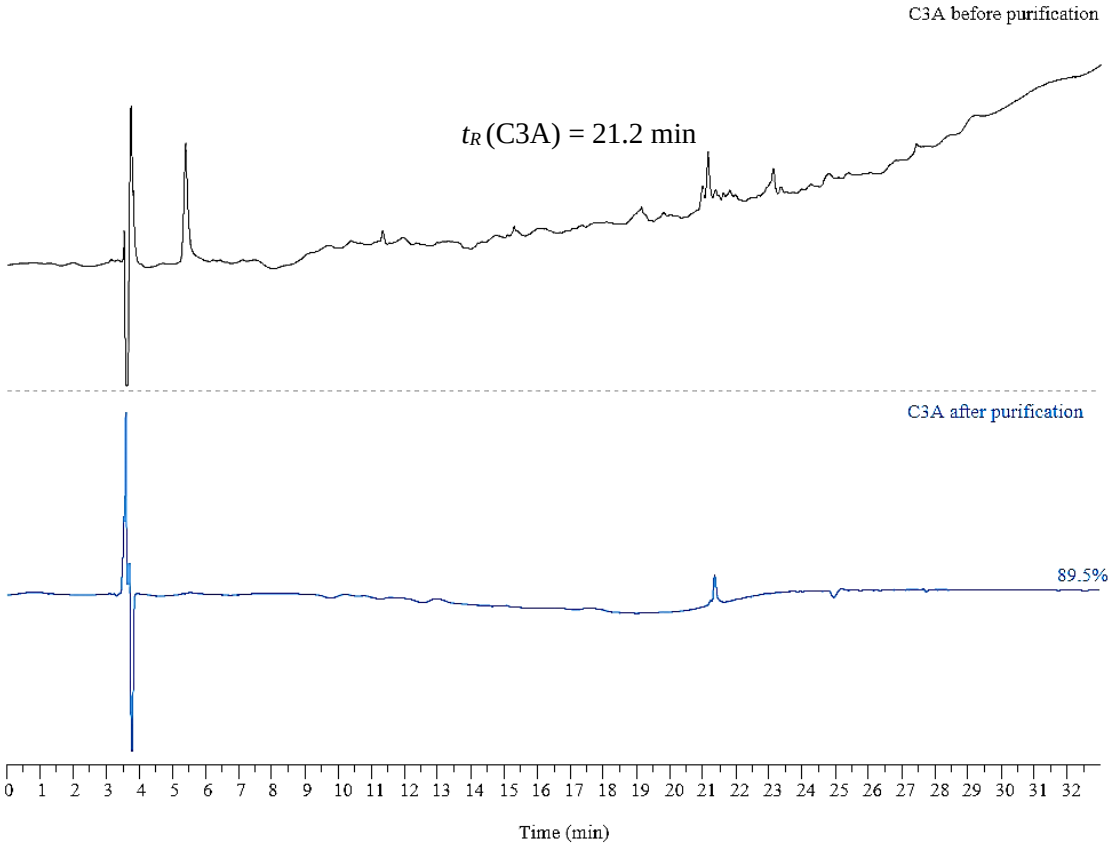


**Figure 4.15:** RP-HPLC chromatograms of crude C3A before and after purification.

**Table 4.5:** Calculated exact masses of cationic forms of C3A.

| Cation | Calculated exact masses $M_w$(Cation) (Da) |
|---|---|
| $[M + H^+]^+$ | 3406.74 |
| $[M + 2H^+]^{2+}$ | 1703.88 |
| $[M + 3H^+]^{3+}$ | 1136.25 |
| $[M + 4H^+]^{4+}$ | 852.44 |

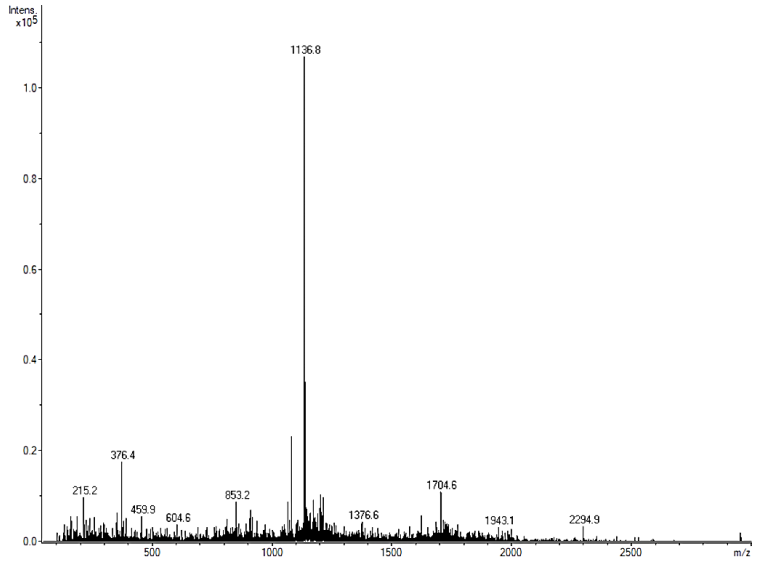


**Figure 4.16:** ESI-MS chromatogram obtained from analysis of a sample recovered from the main peak of C3A crude.

The mass spectrum of the fraction does reveal molecular ions with a molecular weight of 1704.6 Da, 1136.8 Da and 853.2 Da, all of which seem to coincide with three of the calculated exact masses, which proves C3A was successfully synthesized.

As for conjugate C3B, a similar assessment was made. A sample of the RP-HPLC's main peak (Figure 4.17; $t_R$ = 21.7 min) was collected for ESI-MS analysis. By comparing the calculated masses (see Table 4.6) with the ESI-MS spectrum obtained from the main peak analysis (see Figure 4.18), it was concluded that conjugate C3B was successfully synthesized.

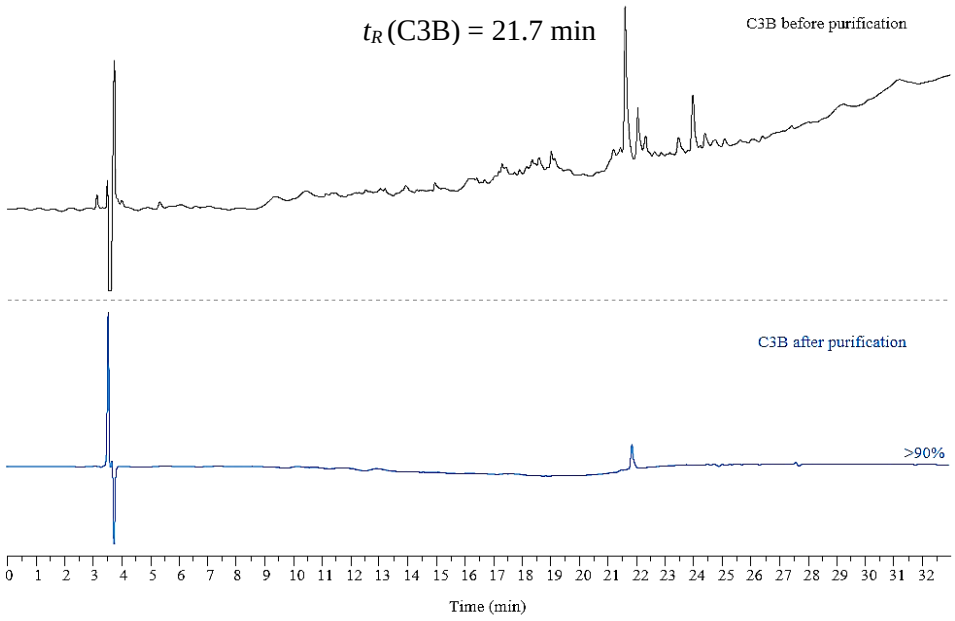


**Figure 4.17:** RP-HPLC chromatograms of crude conjugate C3B and purified bioconjugate C3B.

**Table 4.6:** Calculated exact masses of cationic forms of C3B.

| Cation | Calculated exact masses $M_w$(Cation) (Da) |
|---|---|
| $[M + H^+]^+$ | 3230.70 |
| $[M + 2H^+]^{2+}$ | 1615.85 |
| $[M + 3H^+]^{3+}$ | 1077.57 |
| $[M + 4H^+]^{4+}$ | 808.43 |

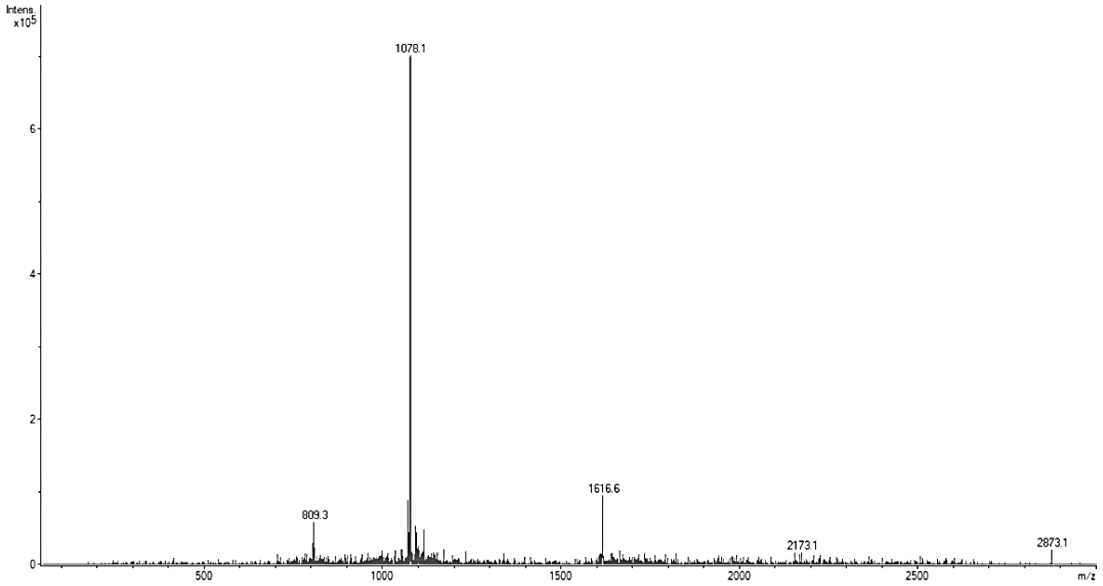


**Figure 4.18:** ESI-MS chromatogram obtained from analysis of the main peak of C3B crude.

### 4.4.3 Radiolabeling Bioconjugates C3A and C3B With $^{67}$Ga

The first step of the radiolabelling procedure involved the preparation of the radioactive precursor $^{67}GaCl_3$, which was obtained by conversion of commercially available $^{67}$Ga-citrate solution (Curium) to $^{67}GaCl_3$ following the methods developed by Kim Chan and Igor Gonda (1991), and Vladimir S. with Johan E. van Lier.[87-89] (see subchapter 3.4.3)

The $^{67}$Ga-labeled conjugates $^{67}$Ga-C3A and $^{67}$Ga-C3B were prepared under gentle stirring upon incubation of solutions of the respective peptide, with a solution of $^{67}GaCl_3$ at room temperature ($c_{FinalC3A}$ = 122 µM; $c_{FinalC3B}$ = 73.3 µM). Figure 4.19 displays the RP-HPLC chromatogram of the precursor $GaCl_3$ chromatogram (Retention time = 2.7 min)

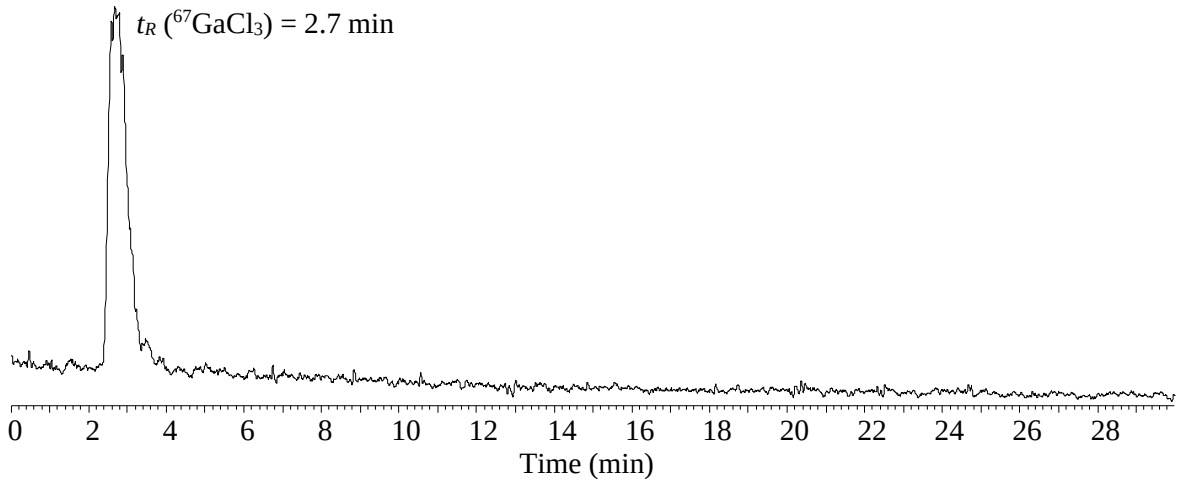


**Figure 4.19:** Analytical RP-HPLC of $GaCl_3$ solution.

The radiolabelled conjugate $^{67}$Ga-C3A was obtained in moderate radiochemical yield (ca. 49%) only after 75 min of incubation, with a concentration of 206 µM (Figure 4.20). In the case of $^{67}$Ga-C3B (Figure 4.21), a radiochemical yield as high as 78% was obtained after 30 min of incubation with a $c_{FinalC3B}$ = 73.3 µM.

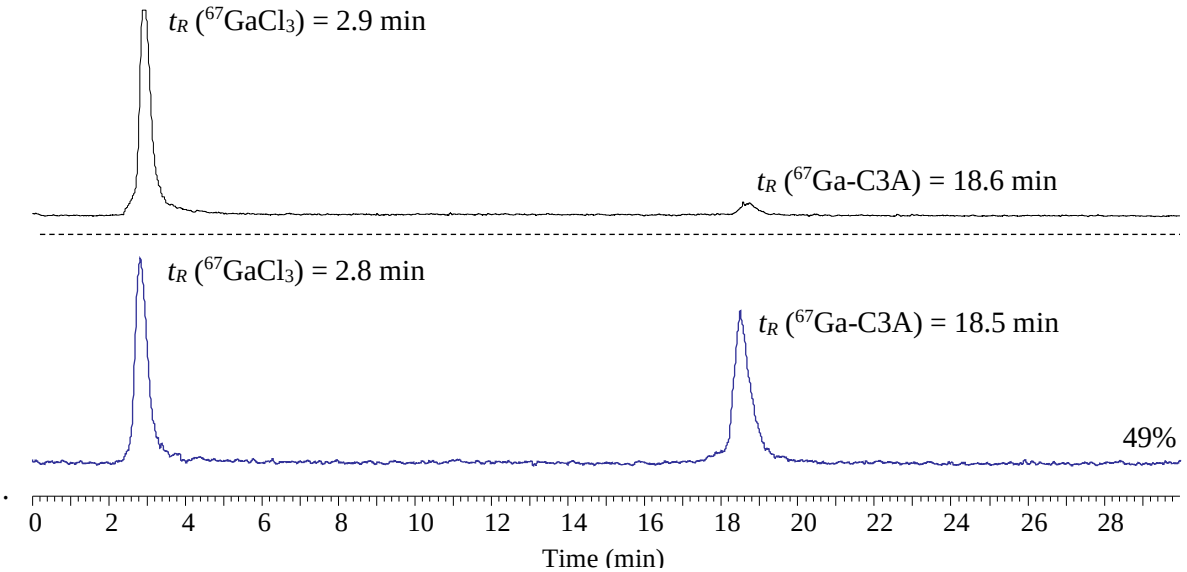


**Figure 4.20:** RP-HPLC chromatograms of $^{67}$Ga-C3A. Highlighted in black is the chromatogram obtained with an incubation time of 30 min ($c_{FinalC3A}$ = 122 µM). Highlighted in blue, is a second attempt of radiolabelling after 75 min of incubation ($c_{FinalC3A}$ = 206 µM).

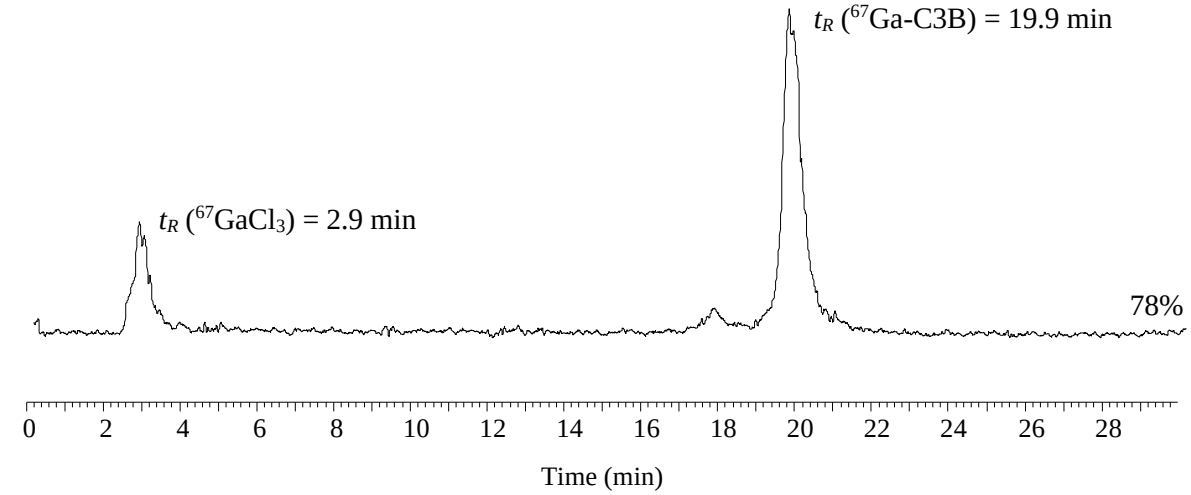


**Figure 4.21:** RP-HPLC chromatogram of $^{67}$Ga-C3B obtained after 30 min incubation ($c_{FinalC3B}$ = 73.3 µM) at room temperature.

A further optimization study is needed towards improving the radiochemical yield and purity (> 95%) of both $^{67}$Ga-C3A and $^{67}$Ga-C3B in order to proceed with the biodistribution and imaging studies in healthy mice. One of the most important parameters to be optimized is concentration, and higher peptide concentrations should be tested. However, considering that peptide and peptide-conjugate overall synthetic yields were low, assigned mainly to long and laborious purification procedures, it is mandatory to prepare higher amounts of both peptides and respective conjugates. Due to time constraints, it has not been possible to synthesize extra batches of C3A and C3B and, consequently, prepare $^{67}$Ga-C3A and $^{67}$Ga-C3B to continue to *in vivo* imaging studies.

As an academic alternative, we have used target-specific $^{67}$Ga-labeled gold nanoparticles decorated with a bombesin derivative ($^{67}$Ga-AuNP-BBN-Pt) to proceed for the biodistribution studies.

## 4.5 $^{67}$Ga Validation Study for *In Vivo* Animal Model

To simulate the imaging of a mouse with a tumour, a sealed syringe containing 20 MBq of $^{67}$Ga (20 MBq; 0.3 mL) was inserted inside a water-filled falcon tube. Figure 4.22 shows the acquisition made 1

hour “post-injection”, with a time per projection of 60 seconds, of the phantom shown in Figure 3.14. The 64 projections were acquired along a 360º circular geometry, with a 20% energy window for all gallium-67 peaks.

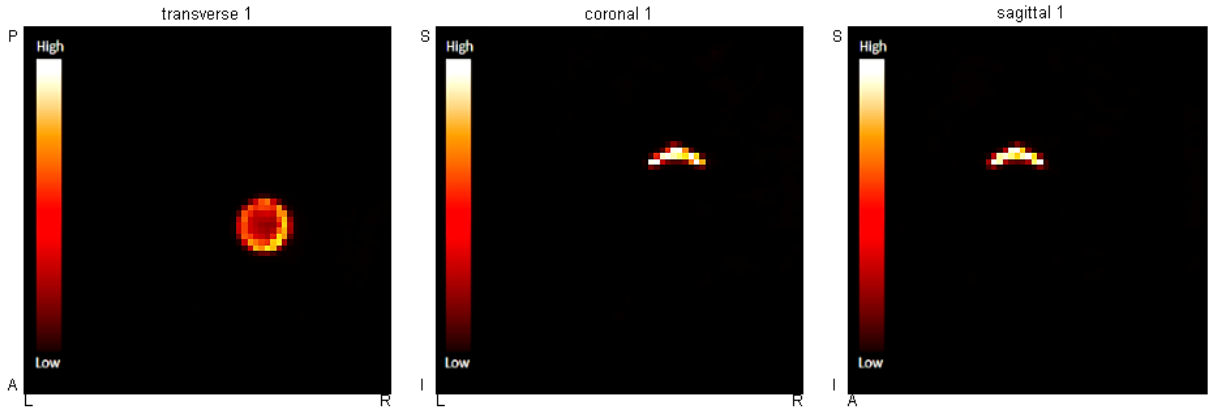


**Figure 4.22:** SPECT acquisition of the designed phantom, 1 hour post injection (p.i).

Isolated CT and CT-SPECT fusion were also evaluated, to ensure camera alignment and quality. The CT camera was calibrated to 70 keV and 110 ms exposure time, with a 2 x 2 binning. Acquired data was reconstructed in an in-built software from by Trifoil, with default settings (2 subsets, 8 iterations). Figure 4.23 shows the isolated CT acquisition, and Figure 4.24 shows the CT-SPECT fusion, where the isosurface of the activity inside the syringe can be clearly seen.

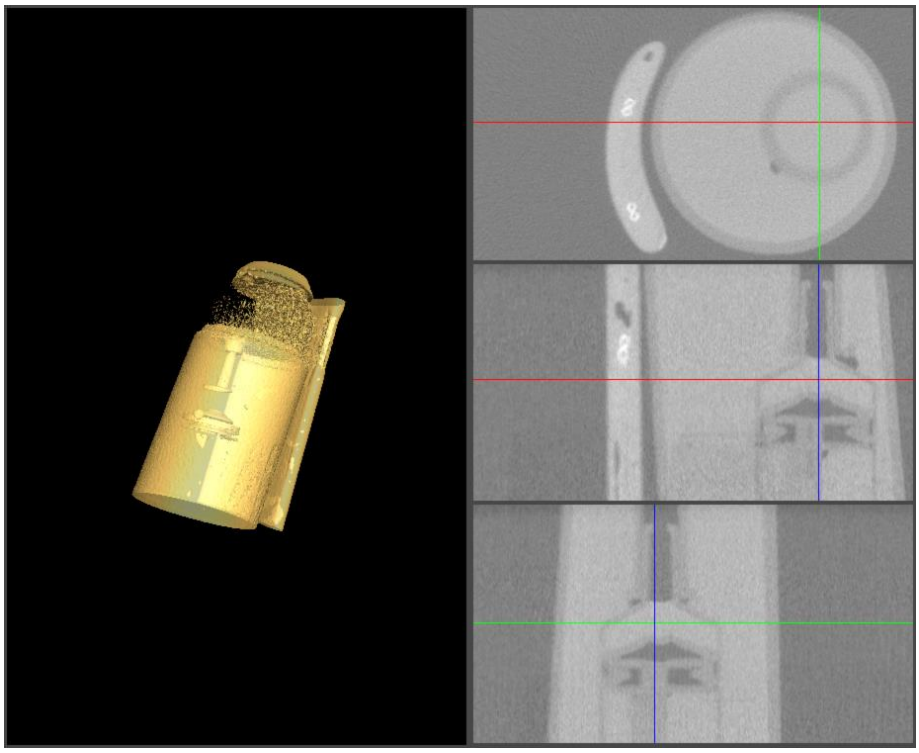

**Figure 4.23:** CT image acquired of the designed phantom. [Left] 3D reconstruction of the phantom using a threshold of 403. [Right] CT slices acquired of the phantom.

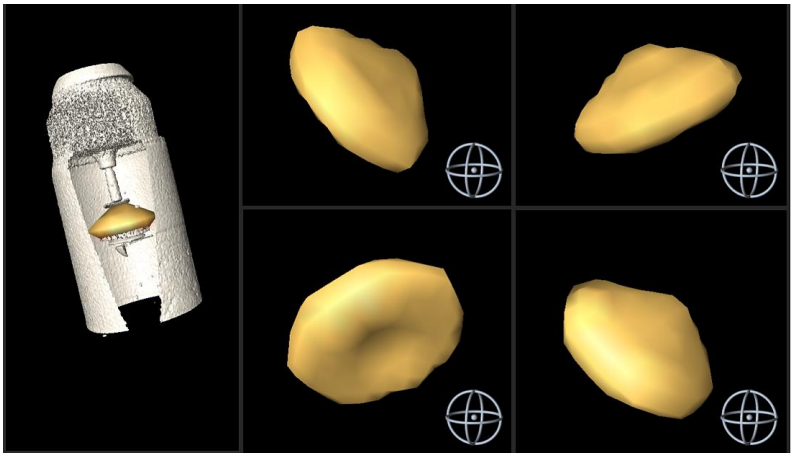

**Figure 4.24:** CT-SPECT fusion of the acquisition of the designed phantom. On the left image coloured in white, is the 3D reconstruction of the CT acquisition using a threshold of 413. With a brown colour is the isosurface of the $^{67}$Ga activity contained inside the syringe.

Several other acquisitions were made to explore the equipment's performance, and to validate the equipment. These acquisitions can be found in appendix 5.

## 4.6 Results Of *In Vivo* Animal Model Acquisition

Registered in Figures 4.25 and 4.26, are the SPECT-CT reconstructed images acquired 1-hour p.i. of the compound $^{67}$Ga-AuNP-BBN-Pt (see subsection 3.5.5 for methods).

By observing Figure 4.25, the sites of injection of the radiolabelled compound can be seen in the 3D SPECT-CT fusion. The uptake of tracer is perceived mainly in the tumour at 1-hour p.i.

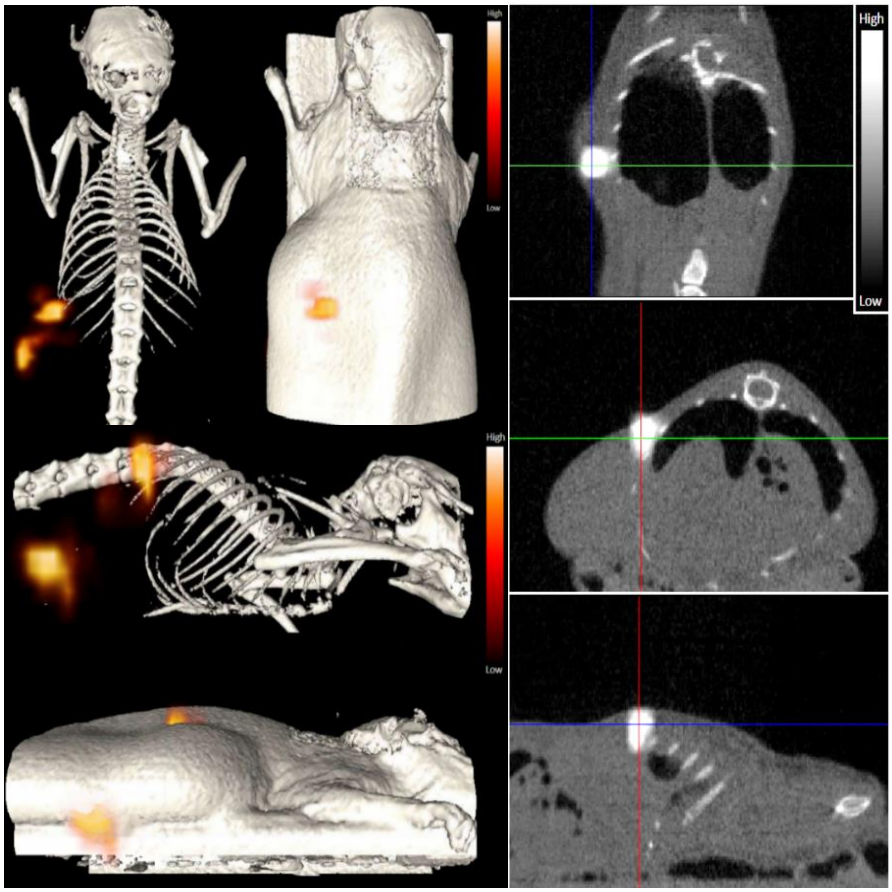


**Figure 4.25:** SPECT-CT fusion acquisition made 1 h p.i of a male Balb/c mice injected with $^{67}$Ga-AuNP-BBN-Pt.

By analysing the acquisition made at 24 hours p.i., a migration of the compound can be observed. By comparison, at 1 hour p.i two main regions of interest are seen. However, 24 hours p.i, the $^{67}$Ga-AuNP-BBN-Pt compound seems to be shifting towards a new region, leading to three distinguishable points.

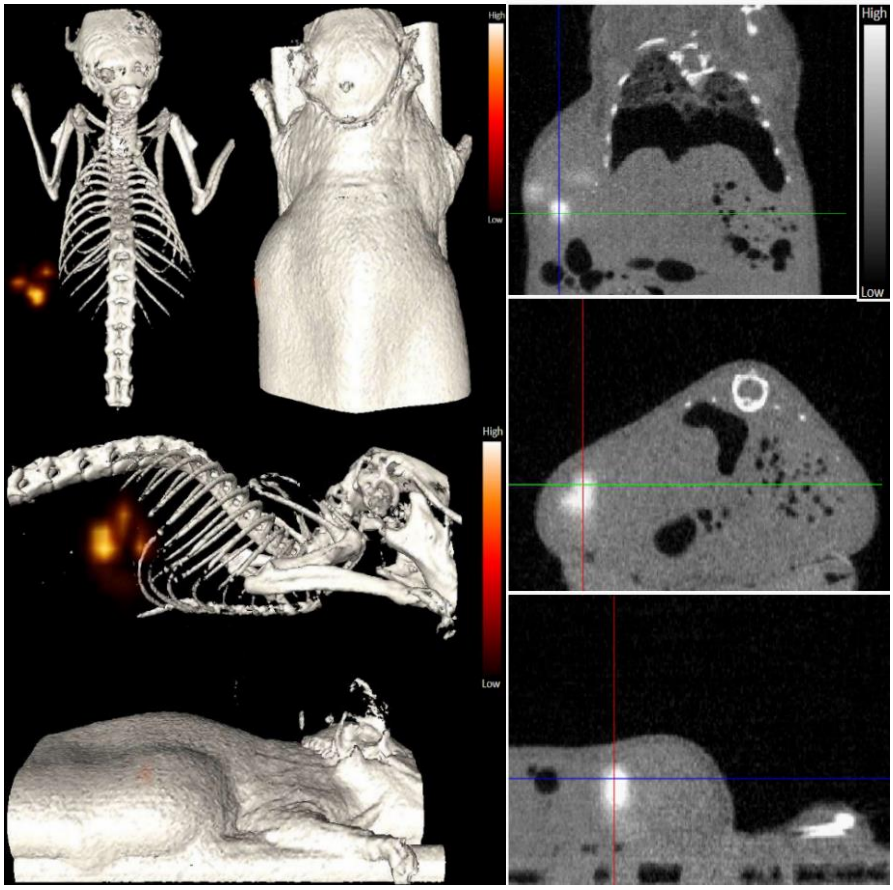


**Figure 4.26:** SPECT-CT fusion acquisition made 24 hours p.i of a male Balb/c mouse injected with $^{67}$Ga-AuNP-BBN-Pt.

Image comparison shows substantial retention of $^{67}$Ga-AuNP-BBN-Pt1 at the tumour site, and negligible dissemination in surrounding organs and tissues, even after 24 hours. The obtained SPECT-CT fusion acquisitions are supported by traditional biodistribution results, available in appendix 6. Further information regarding this acquisition can be found in reference 102.

Section

# 5 Conclusion

## 5.1 Conclusions and Perspectives

The model peptide 3B (S3B) was synthesized by two different methods, namely US-assisted SPPS and 'Classical' SPPS. During the deprotection step, which for manual SPPS was 25 min, for US-assisted SPPS could be reduced to 2-5 min. This reduction allows a more than fivefold decrease in time just in amino acid deprotection. As for the conjugation times, differences became noticeable only at the third amino acid coupling, aspartic acid. Interestingly, no issues arose during the US-assisted SPPS. During this synthesis, a lower crude purity was observed by analytical RP-HPLC: 72% for US-assisted SPPS versus the 84% obtained for 'classical' SPPS. This can be explained by a local heating phenomenon associated with US-assisted SPPS. Albeit having a lower crude purity, the US-assisted SPPS presented itself as a viable alternative to the 'classical' SPPS, allowing synthesis to be completed approximately four times faster. This work resulted in an article published by the time of writing this thesis.[54]

Having successfully synthesized peptide S3B by both 'classical' SPPS and US-SPPS, the method of choice for the more complex peptides 3A and 3B selected was the US-based methodology, as it allowed faster reaction times with less reagent usage. Unexpectedly, the synthesis of 3A was not accomplished in any of the two attempts. In the first attempt, the synthesis was finalized with difficulty, reaching coupling times of over 6 hours per residue. Although finished, ESI-MS did not show the existence of the desired peptide in the product cleaved from the resin, and even if it were, it would be present in very low yields. Hence, a second attempt was made, where several parameters were modified, also to no avail.

Not being able to obtain the desired peptide by US-assisted SPPS, a different approach was taken: MW-assisted SPPS. Impressively, the synthesis was finalized in approximately two working days. Analytical RP-HPLC presented a crude purity of 53% for peptide 3A, and 47% for 3B. Even though MW-assisted SPPS presented itself as a successful method for larger peptide chains, this process required major amounts of reagents, raising questions concerning sustainability. Such fact should give place to US-assisted SPPS method optimization and automation.

Besides sustainability concerns that MW-assisted SPPS arose, other topics should be assessed. Particularly, the reasons that led to the difficulty of coupling during US-assisted SPPS. The two-hypothesis deemed more likely were either the interference of water entering from crevices of the syringe, or peptide aggregation. For the time being, only the first hypothesis was assessed. During the synthesis, besides using a syringe cap to close the syringe containing the peptide, water entry points were covered with Parafilm sealing film. This, however, is not the ideal method to address the water infiltration issue, as water infiltration is always prone to occur. Even though unlikely, this possibility should be considered. The second hypothesis, which is an extensively documented problem arising during peptide synthesis, was peptide aggregation. Peptide aggregation was considered in the case of 3A, but not deemed as a definitive cause, considering that to determine it as a definite cause would require experimentation outside of this project's scope. This consideration led to the necessity of adjusting some procedures, such as avoiding the manipulation of high concentrations of peptide, flash freeze procedures after the peptide's usage, and the addition of trace amounts of TFA when the peptide's handling seemed to become more difficult. The handling and manipulation of peptide 3A during the

determination of peptide concentration by UV-Vis spectrophotometry did in fact present difficulties. The peptide seemed to spontaneously precipitate. This phenomenon became evident by spontaneous formations of *cloud-like* clusters, visible by the naked eye, after approximately 20 min at room temperature. This could be mitigated by adding trace amounts of diluted TFA (0.1% TFA in Milli-Q water) to the solution, followed by 10 min of sonification. Attempts of adding DMSO (dimethyl sulfoxide) were also made, interestingly with no avail.

With the synthesised peptides 3A and 3B, the subsequent steps were conjugation to the PEG linker (spacer) and the bifunctional chelator (NODAGA) to prepare the respective conjugates C3A and C3B. Although the US-assisted SPPS was not successful in synthesizing the 23-mer peptides, it is still a valid method for SPPS. As such, to finalize the synthesis of the conjugates, the spacer and the chelator were conjugated to the resin using ultrasound irradiation.

The $^{67}$Ga-labeled conjugates $^{67}$Ga-C3A (ca. 49 % radiochemical yield) and $^{67}$Ga-C3B (ca. 78% radiochemical yield) were prepared upon incubation of solutions of the respective peptide with a solution of $^{67}GaCl_3$, which was obtained by conversion of commercially available $^{67}$Ga-citrate solution (Curium) to $^{67}GaCl_3$. Due to time constraints, it has not been possible to synthesize higher amounts of C3A and C3B to improve the radiochemical yield and purity of $^{67}$Ga-C3A and $^{67}$Ga-C3B to continue to *in vivo* imaging studies.

Notwithstanding, since the objective herein contained was to have an overview of the whole process from the amino acid to radiolabelled peptide, and finally a nuclear image, it was proposed to use target-specific $^{67}$Ga-labeled gold nanoparticles decorated with a bombesin derivative ($^{67}$Ga-AuNP-BBN-Pt) to proceed for the biodistribution studies as described below. $^{67}$Ga-AuNP-BBN-Pt is comprised of $^{67}$Ga-labeled gold nanoparticles containing DOTA derivates, a bombesin derivate (BBN), and a Pt(IV) pro-drug.

In parallel to the synthetic work, we performed the complete calibration of the CT and SPECT cameras of the FLEX™ Triumph™ Trifoil equipment, as well as several mock tests. These mock tests consisted in the imaging of several objects – such as Eppendorf tubes and hand-made phantoms– using the CT and SPECT imaging modalities, as well as CT-SPECT fusions. This testing led to a last and final test image, inspired by previously published scientifical articles.[96-98] The last, and final mock acquisition, consisted of a 50 mL falcon tube filled with water. Enclosed inside the water-filled falcon, was a syringe filled with a 0.3 mL solution of 20 MBq of $^{67}$Ga. This phantom was constructed as a representation of a mouse with a 0.3 $cm^3$ tumour, injected intratumorally with 20 MBq of $^{67}$Ga. This experiment established a baseline for the test statistic needed to obtain an image with adequate quality.

For the SPECT acquisition, an N5F75A10 collimator was used rotating along a stepwise circular 360º motion, with an ROR of 68 mm. The number of projections was 64, with a 60 s per projection being considered based on the acquisitions made by Uehara et al.[96] The acquired image was reconstructed using the inbuilt software, with a 3D-OSEM algorithm using the system's defaulted settings (2 subsets and 8 iterations). Observing the reconstructed image (Figure 4.24), a clear cone-like shape is seen. This represented shape indicates the region in which radioactivity is detected, which in this case is concentrated near the bottom portion of the syringe's piston, acquiring the same shape as the syringe.

$^{67}$Ga-AuNP-BBN-Pt was injected in two different sites, into male Balb/c mice bearing SY tumour xenografts (n ¼ 2) for traditional biodistribution. By observing the image acquired 1 h p.i (see Figure 4.25), the locations of injection are notably distinguishable, characterized by the two regions where the radioactivity was more concentrated. Intriguingly, the acquisition made 24 h p.i (see Figure 4.26) seems to show a migration of the $^{67}$Ga-AuNP-BBN-Pt towards a more central region of the tumour, without spreading to adjacent tissues or organs. This observation encourages further investigation involving the molecule, as an image-guided nanocarrier to deliver prodrugs to tumours. Finally, it is noteworthy that the acquired images are the first pre-clinical micro-SPECT-CT images fully developed in $C^2$TN-IST,

surging as a multi-year cooperation. Future potential is evident, the underlying question is which study will follow.

## 5.2 Work to Be Developed

Due to time constraints, there were several possible studies to be made that would both supplement the present work and lead to interesting research. Presented below, are a few ideas that would complement and add to the project:

**Peptide synthesis**

- **Automation of US-SPPS method –** The method of US-SPPS presented itself as an alternative to MW-SPPS and "classical" SPPS. There is, however, a lack of automation in the process, which leads to a researcher being in the constant presence of the equipment – e.g., to check water bath temperature and switch amino acids for coupling. An excellent project would be to develop an automated system for SPPS, that would not need supervision.
- **Study 3A behaviour –** Peptide 3A showed a very particular behaviour in all processes during this project. As such, studies of peptide 3A's behaviour in different conditions, pH, and possible aggregation properties would be interesting.

**Medical Imaging using the Triumph system**

- **Further optimize the protocols –** The equipment was installed recently in $C^2$TN-IST. As such, there is still much room for process optimization and equipment validation. Here follow some ideas for future studies:
    - Detailed comparison of images between isotopes on PET and SPECT. For instance, $^{111}$In, $^{99m}$Tc, $^{67}$Ga, $^{177}$Lu and $^{64}$Cu.
    - Perform comparative studies using the different collimators.
    - Perform evaluative studies on the extremes of activities (with extremely high activity and extremely low) to further study the detector's response.

# References


1 Coleman, R E. “Metastatic bone disease: clinical features, pathophysiology and treatment strategies.” *Cancer treatment reviews* vol. 27,3 (2001): 165-76. doi:10.1053/ctrv.2000.0210.

2 Weilbaecher, Katherine N et al. “Cancer to bone: a fatal attraction.” *Nature reviews. Cancer* vol. 11,6 (2011): 411-25. doi:10.1038/nrc3055

3 Hong, Soojung et al. “Bone metastasis and skeletal-related events in patients with solid cancer: A Korean nationwide health insurance database study.” *PloS one* vol. 15,7 e0234927. (2020), doi:10.1371/journal.pone.0234927

4 Seider, Michael J et al. “Randomized phase III trial to evaluate radiopharmaceuticals and zoledronic acid in the palliation of osteoblastic metastases from lung, breast, and prostate cancer: report of the NRG Oncology RTOG 0517 trial.” *Annals of nuclear medicine* vol. 32,8 (2018): 553-560. doi:10.1007/s12149-018-1278-4

5 Salerno, M et al. “Bone-targeted doxorubicin-loaded nanoparticles as a tool for the treatment of skeletal metastases.” Current cancer drug targets vol. 10,7 (2010): 649-59. doi:10.2174/1568009107936057676 Gisbert-Garzarán, M., Manzano, M., &Vallet-Regí, M. (2020). Mesoporous Silica Nanoparticles for the Treatment of Complex Bone Diseases: Bone Cancer, Bone Infection and Osteoporosis. Pharmaceutics, 12(1), 83. https://doi.org/10.3390/pharmaceutics12010083

6 Rao, V Srinivasa et al. “Protein-protein interaction detection: methods and analysis.” International journal of proteomics vol. 2014 (2014): 147648. doi:10.1155/2014/147648

7 Armstrong, Allison P et al. “A RANK/TRAF6-dependent signal transduction pathway is essential for osteoclast cytoskeletal organization and resorptive function.” The Journal of biological chemistry vol. 277,46 (2002): 44347-56. doi:10.1074/jbc.M202009200

8 Ye, Hong et al. “Distinct molecular mechanism for initiating TRAF6 signalling.” *Nature* vol. 418,6896 (2002): 443-7. doi:10.1038/nature00888

9 Neves, Vera et al. “Novel Peptides Derived from Dengue Virus Capsid Protein Translocate Reversibly the Blood-Brain Barrier through a Receptor-Free Mechanism.” ACS Chemical Biology (2017):12(5):1257-1268. doi: 10.1021/acschembio.7b00087. PMID: 28263555

10 Boyce, Brendan F, and Lianping Xing. “Biology of RANK, RANKL, and osteoprotegerin.” *Arthritis research & therapy* vol. 9 Suppl 1, Suppl 1 (2007): S1. doi:10.1186/ar2165

11 Wu, Xiaoqiu et al. “RANKL/RANK System-Based Mechanism for Breast Cancer Bone Metastasis and Related Therapeutic Strategies.” *Frontiers in cell and developmental biology* vol. 8 76. (2020), doi:10.3389/fcell.2020.00076

12 Steen, Brandon M. et al. “The Role of the Immune System in Fracture Healing.” *Osteoimmunology*, (2011), pp. 343–367. www.sciencedirect.com/science/article/pii/B9780123756701100123, 10.1016/b978-0-12-375670-1.10012-3

13 McClung, Michael. “Role of RANKL inhibition in osteoporosis.” Arthritis research & therapy vol. 9 Suppl 1,Suppl 1 (2007): S3. doi:10.1186/ar2167

14 Thermo Fischer Sientific – US. “Rank Signaling in Osteoclasts.” https://www.thermofisher.com/pt/en/home/life-science/antibodies/antibodies-learning-center/antibodies-resource-library/cell-signaling-pathways/rank-signaling-osteoclasts.html [Retrived August 28, 2022]

15 Boyce, Brendan F, and Lianping Xing. “Functions of RANKL/RANK/OPG in bone modeling and remodeling.” *Archives of biochemistry and biophysics* vol. 473,2 (2008): 139-46. doi:10.1016/j.abb.2008.03.018

16 Schoppet, Michael et al. “RANK ligand and osteoprotegerin: paracrine regulators of bone metabolism and vascular function.” *Arteriosclerosis, thrombosis, and vascular biology* vol. 22,4 (2002): 549-53. doi:10.1161/01.atv.0000012303.37971.da

17 Udagawa, Nobuyuki et al. “Osteoclast differentiation by RANKL and OPG signaling pathways.” *Journal of bone and mineral metabolism* vol. 39,1 (2021): 19-26. doi:10.1007/s00774-020-01162-6

18 Casimiro, Sandra et al. “RANKL/RANK/MMP-1 molecular triad contributes to the metastatic phenotype of breast and prostate cancer cells in vitro.” *PloS one* vol. 8,5 e63153. (2013), doi:10.1371/journal.pone.0063153

19 Bucay, N., Sarosi et al. *“Osteoprotegerin-deficient mice develop early onset osteoporosis and arterial calcification”. Genes & development, 12*(9), 1260–1268. (1998), doi:10.1101/gad.12.9.1260

20 Bradley, J R, and J S Pober. “Tumor necrosis factor receptor-associated factors (TRAFs).” Oncogene vol. 20,44 (2001): 6482-91. doi:10.1038/sj.onc.1204788

21 Zapata, J M et al. “TNFR-associated factor family protein expression in normal tissues and lymphoid malignancies.” *Journal of immunology (Baltimore, Md. : 1950)* vol. 165,9 (2000): 5084-96. doi:10.4049/jimmunol.165.9.5084

22 Pereira, Mafalda I. A., “*Design of Peptides to interfere with the RANK-TRAF6 Pathway: An Integrated Approach*.” Faculdade de Ciências e Tecnologia da Universidade Nova de Lisboa (FCT) (2018).

23 Casimiro, Sandra et al. “The Roadmap of RANKL/RANK Pathway in Cancer.” *Cells* vol. 10,8 1978. (2021), doi:10.3390/cells10081978

24 Casimiro, Sandra et al. “Molecular Mechanisms of Bone Metastasis: Which Targets Came from the Bench to the Bedside?.” *International journal of molecular sciences* vol. 17,9 1415. (2016), doi:10.3390/ijms17091415

25 Maurizi, Antonio, and Nadia Rucci. “The Osteoclast in Bone Metastasis: Player and Target.” Cancers vol. 10,7 218. (2018), doi:10.3390/cancers10070218

26 Baker, Rebecca G et al. “NF-κB, inflammation, and metabolic disease.” *Cell metabolism* vol. 13,1 (2011): 11-22. doi:10.1016/j.cmet.2010.12.008

27 Hayden, Matthew S, and Sankar Ghosh. “Shared principles in NF-kappaB signaling.” Cell vol. 132,3 (2008): 344-62. doi:10.1016/j.cell.2008.01.020

28 Wang, Manni et al. “Molecular mechanisms and clinical management of cancer bone metastasis.” Bone research vol. 8,1 30. (2020), doi:10.1038/s41413-020-00105-1

29 MedlinePlus. (n.d.). “Denosumab Injection”. MedlinePlus - Denosumab Injection. https://medlineplus.gov/druginfo/meds/a610023.html [Retrieved November 12, 2020]

30 Varenna, M, and D Gatti. “Il ruolo dell'inibizione del rank-ligando nel trattamento dell'osteoporosi postmenopausale” [The role of rank-ligand inhibition in the treatment of postmenopausal osteoporosis]. Reumatismo vol. 62,3 (2010): 163-71. doi:10.4081/reumatismo.2010.163

31 Anastasilakis, Athanasios D et al. “Denosumab Discontinuation and the Rebound Phenomenon: A Narrative Review.” *Journal of clinical medicine* vol. 10,1 152. 4 (2021), doi:10.3390/jcm10010152

32 Atkins, Jones, Laverman, P., L. ,. L. *“Chemical Principles: The Quest for Insight. 7th ed.”*, New York, W. H. Freyman, (2016), pp.817.

33 “IUPAC-IUB Joint Commission on Biochemical Nomenclature (JCBN). Nomenclature and symbolism for amino acids and peptides. Recommendations 1983.” *The Biochemical journal* vol. 219,2 (1984): 345-73. doi:10.1042/bj2190345

34 Gunawardena, Gamini. Libretexts. (2020). N-Terminal. ChemistryLibreTexts. https://chem.libretexts.org/Bookshelves/Ancillary_Materials/Reference/Organic_Chemistry_Glossary/N-Terminal [Accessed: 20/04/2022]

35 Bachem. Bachem Peptide Guide. In: BioConnect (2016), pp. 1–60

36 Martin, V., Egelund, P. H. G., Johansson, H., Thordal Le Quement, S., Wojcik, F., & Sejer Pedersen, D. (2020). Greening the synthesis of peptide therapeutics: an industrial perspective. RSC Advances, 10(69), 42457–42492. https://doi.org/10.1039/d0ra07204d

37 Isidro-Llobet, A., Alvarez, M., & Albericio, F. (2009). Amino acid-protecting groups. *Chemical reviews*, *109*(6), 2455–2504.

38 Conda-Sheridan M., Krishnaiah M. (2020) Protecting Groups in Peptide Synthesis. In: Hussein W., Skwarczynski M., Toth I. (eds) Peptide Synthesis. Methods in Molecular Biology, vol 2103. Humana, New York, NY. https://doi.org/10.1007/978-1-0716-0227-0_7

39 Synthesis Notes aapptec. *“Practical Synthesis Guide to Solid Phase Peptide Chemistry.”* AAPPTEC, LLC. www.peptide.com/custdocs/aapptec%20synthesis%20guide%202-0%20%282%29.pdf [Acessed: November 29, 2021]

40 Ragnarsson, Ulf and Grehn, Leif. “*Dual protection of amino functions involving Boc*”. RSC Advances. 3. 18691. doi:10.1039/c3ra42956c.

41 OC Chemie Uni Regensburg. “*Boc - Solid Phase Peptide Synthesis (SPPS), Strategies, resins, and comparison with Fmoc-Strategy*” [Slides]. (2020). http://www-oc.chemie.uni-regensburg.de/OCP/ch/chv/oc22/script/SS05/Topic5.pdf

42 Thermo Fischer Sientific – US. “Peptide Synthesis” https://www.thermofisher.com/pt/en/home/life-science/protein-biology/protein-biology-learning-center/protein-biology-resource-library/pierce-protein-methods/peptide-synthesis.html [Accessed: August 28, 2022]

43 Behrendt, Raymond et al. *“Advances in Fmoc solid-phase peptide synthesis.”* Journal of peptide science: an official publication of the European Peptide Society vol. 22,1 (2016): 4-27. doi:10.1002/psc.2836

44 Amblard, Muriel et al. *“Methods and protocols of modern solid phase Peptide synthesis.” Molecular biotechnology* vol. 33,3 (2006): 239-54. doi:10.1385/MB:33:3:239

45 Fields, G B. *"Methods for removing the Fmoc group." Methods in molecular biology (Clifton, N.J.)* vol. 35 (1994): 17-27. doi:10.1385/0-89603-273-6:17

46 Eissler, Stefan et al. *"Substitution determination of Fmoc-substituted resins at different wavelengths." Journal of peptide science : an official publication of the European Peptide Society* vol. 23,10 (2017): 757-762. doi:10.1002/psc.3021

47 AAPPTEC. *"Monitoring of Peptide Coupling and Capping; Coupling Tests."* https://www.peptide.com/resources/solid-phase-peptide-synthesis/monitoring-of-peptide-coupling-and-capping/. [Accessed: November 29, 2021]

48 ChemPep Inc. *"Peptide Synthesis, Custom Peptide, Fmoc Amino Acids". www.chempep.com*, Chempep Inc., www.chempep.com/ChemPep-Fmoc-Solid-Phase-Peptide-Synthesis.htm#C231.

49 Cruzan, Jeff. *"Proteins."*, xaktly, (2016). xaktly.com/Proteins.html [Acessed November 31, 2021]

50 A.G.N. Montalbetti, C. and Falque, V. *"Amide bond formation and peptide coupling."* Tetrahedron, 61(46), (2005): 10827–10852. https://doi.org/10.1016/j.tet.2005.08.031

51 Valeur, Eric, and Mark Bradley. "Amide bond formation: beyond the myth of coupling reagents." *Chemical Society reviews* vol. 38,2 (2009): 606-31. doi:10.1039/b701677h

52 Chan, Weng C., and Peter White. *Fmoc Solid Phase Peptide Synthesis*. Cary, Oxford University Press, (2000).

53 Ghaderi, Shirin. *"Development of fluorescent nanoparticles 'quantum dots' for biomedical application."* (2012).

54 Silva, Rúben D M et al. "*Ultrasonication Improves Solid Phase Synthesis of Peptides Specific for Fibroblast Growth Factor Receptor and for the Protein-Protein Interface RANK-TRAF6*." *Molecules (Basel, Switzerland)* vol. 26,23 7349. (2021), doi:10.3390/molecules26237349

55 de la Hoz, Antonio, et al. *"Microwaves in Organic Synthesis. Thermal and Non-Thermal Microwave Effects." Chem. Soc. Rev.*, vol. 34, no. 2, pp. 164–178, 10.1039/b411438h, (2005), doi: 10.1039/b411438h.

56 Langa, Fernando, et al. "Microwave Irradiation: More than Just a Method for Accelerating Reactions." *Contemporary Organic Synthesis*, vol. 4, no. 5, (1997) pp. 373–386, pubs.rsc.org/en/content/articlepdf/1997/co/co9970400373, 10.1039/CO9970400373.

57 Microwave-Assisted Synthesis. Anton Paar GmbH, wiki.anton-paar.com/en/microwave-assisted-synthesis/. [Accessed: 30/11/2021]

58 Mason, Timothy J. "Ultrasound in Synthetic Organic Chemistry." Chemical Society Reviews, vol. 26, no. 6, (1997), pp. 443–451, pubs.rsc.org/en/content/articlelanding/1997/CS/cs9972600443, 10.1039/CS9972600443. [Accessed 31/08/2022]

59 Merlino, Francesco, et al. "Boosting Fmoc Solid-Phase Peptide Synthesis by Ultrasonication." *Organic Letters*, vol. 21, no. 16, (2019), pp. 6378–6382, 10.1021/acs.orglett.9b02283.

60 de Mello, Heber et al. "Sonodynamic and Photodynamics Used as a Combined Therapy in the Treatment of Malignant Neoplasms: Facts and Open Questions". Photodynamic Therapy - From

Basic Science to Clinical Research, edited by Natalia Inada et al, IntechOpen, (2020), doi:10.5772/intechopen.94600.

61 NIBIB. *"Nuclear Medicine."* National Institute of Biomedical Imaging and Bioengineering, (2017), www.nibib.nih.gov/science-education/science-topics/nuclear-medicine. [Accessed: 31/08/2022]

62 © Encyclopædia Britannica, Inc *,"Computerized Axial Tomography: Computed X-Ray Tomography (CT) Scanner."* Britannica Kids, kids.britannica.com/students/assembly/view/54158. [Accessed: 31/08/2022]

63 Åkerman, Ludvig Larsson, *"A Technical Validation of The PET/SPECT/CT (Triumph) Scanner"*. (2011). Uppsala Universitet.

64 Faria, Daniele de Paula et al. *"PET imaging in multiple sclerosis."* Journal of neuroimmune pharmacology: the official journal of the Society on NeuroImmune Pharmacology vol. 9,4 (2014): 468-82. doi:10.1007/s11481-014-9544-2

65 Serway, R. A., Moses, C. J., & Moyer, C. A. (2014). Modern physics (Third edition, pp. 491–492). Cengage.

66 National Research Council (US) Committee on Medical Isotope Production Without Highly Enriched Uranium, *'Medical Isotope Production without Highly Enriched Uranium.'* Washington (DC): National Academies Press (US); 2009. 2, Molybdenum-99/Technetium-99m Production and Use: https://www.ncbi.nlm.nih.gov/books/NBK215133/

67 National Research Council (US) and Institute of Medicine (US) Committee on the Mathematics and Physics of Emerging Dynamic Biomedical Imaging. *'Mathematics and Physics of Emerging Biomedical Imaging.'* Washington (DC): National Academies Press (US); 1996. Chapter 5, Single Photon Emission Computed Tomography. https://www.ncbi.nlm.nih.gov/books/NBK232492/

68 Kostelnik, Thomas I, and Chris Orvig. *"Radioactive Main Group and Rare Earth Metals for Imaging and Therapy."* Chemical reviews vol. 119,2 (2019): 902-956. doi:10.1021/acs.chemrev.8b00294

69 Veronese, Francesco M, and Gianfranco Pasut. *"PEGylation, successful approach to drug delivery." Drug discovery today* vol. 10,21 (2005): 1451-8. doi:10.1016/S1359-6446(05)03575-0

70 Wikipedia Contributors. *"Polyethylene Glycol." Wikipedia*, Wikimedia Foundation, (2019), en.wikipedia.org/wiki/Polyethylene_glycol. [Accessed: 31/08/2022]

71 Abuchowski, A et al. *"Alteration of immunological properties of bovine serum albumin by covalent attachment of polyethylene glycol."* The Journal of biological chemistry vol. 252,11 (1977): 3578-81

72 Abuchowski, A et al. *"Effect of covalent attachment of polyethylene glycol on immunogenicity and circulating life of bovine liver catalase."* The Journal of biological chemistry vol. 252,11 (1977): 3582-6.

73 Xue, Ying et al. *"Effect of poly(ethylene glycol) (PEG) spacers on the conformational properties of small peptides: a molecular dynamics study."* Langmuir : the ACS journal of surfaces and colloids vol. 27,1 (2011): 296-303. doi:10.1021/la103800h

74 Pfister, David, and Massimo Morbidelli. "*Process for protein PEGylation*." Journal of controlled release: official journal of the Controlled Release Society vol. 180 (2014): 134-49. doi:10.1016/j.jconrel.2014.02.002

75 Rajan, Rahul S et al. *"Modulation of protein aggregation by polyethylene glycol conjugation: GCSF as a case study."* Protein science: a publication of the Protein Society vol. 15,5 (2006): 1063-75. doi:10.1110/ps.052004006

76 Price, Eric W, and Chris Orvig. *"Matching chelators to radiometals for radiopharmaceuticals."* Chemical Society reviews vol. 43,1 (2014): 260-90. doi:10.1039/c3cs60304k

77 "Research - Eric Price Research Group - Department of Chemistry - University of Saskatchewan." *Research-Groups.usask.ca*, research-groups.usask.ca/price/research.php. [Accessed: 31/08/2022]

78 Correia, João D. G., et al. *"Radiometallated Peptides for Molecular Imaging and Targeted Therapy."* Dalton Transactions, vol. 40, no. 23, (2011), pp. 6144–6167, pubs.rsc.org/en/content/articlelanding/2011/DT/c0dt01599g, doi:10.1039/C0DT01599G

79 Liu, S, and D S Edwards. *"Bifunctional chelators for therapeutic lanthanide radiopharmaceuticals."* Bioconjugate chemistry vol. 12,1 (2001): 7-34. doi:10.1021/bc000070v

80 Shokeen, Monica, and Carolyn J Anderson. "*Molecular imaging of cancer with copper-64 radiopharmaceuticals and positron emission tomography (PET)."* Accounts of chemical research vol. 42,7 (2009): 832-41. doi:10.1021/ar800255q

81 Mewis, R. E., & Archibald, S. J. "*Biomedical applications of macrocyclic ligand complexes*." Coordination Chemistry Reviews, *254*(15-16), (2010). 1686–1712. https://doi.org/10.1016/j.ccr.2010.02.025

82 Wadas, T. J., Wong, E. H., Weisman, G. R., & Anderson, C. J. (2010). *"Coordinating Radiometals of Copper, Gallium, Indium, Yttrium and Zirconium for PET and SPECT Imaging of Disease."* Chemical Reviews, *110*(5), 2858–2902. doi: 10.1021/cr900325h

83 AAPPTec. Technical Bulletins. AAPPTec Complete Peptide Product Source; AAPPTec. https://www.peptide.com/custdocs/1188%20ninhydrin%20test.pdf [Accessed 18/08/2022]

84 Issaq, Haleem J et al. *"Separation, detection and quantitation of peptides by liquid chromatography and capillary electrochromatography."* Journal of chromatography. A vol. 1216,10 (2009): 1825-37. doi:10.1016/j.chroma.2008.12.052

85 Liyanage, Mangala R et al. *"Ultraviolet absorption spectroscopy of peptides."* Methods in molecular biology (Clifton, N.J.) vol. 1088 (2014): 225-36. doi:10.1007/978-1-62703-673-3_15

86 Anthis, Nicholas J, and G Marius Clore. "*Sequence-specific determination of protein and peptide concentrations by absorbance at 205 nm."* Protein science: a publication of the Protein Society vol. 22,6 (2013): 851-8. doi:10.1002/pro.2253

87 Scasnár, V, and J E van Lier. *"The use of SEP-PAK SI cartridges for the preparation of gallium chloride from the citrate solution."* European journal of nuclear medicine vol. 20,3 (1993): 273. doi:10.1007/BF00170012

88 Ben Azzouna, Rana et al. *"Synthesis, gallium labelling and characterization of P04087, a functionalized phosphatidylserine-binding peptide."* EJNMMI radiopharmacy and chemistry vol. 2,1 (2017): 3. doi:10.1186/s41181-016-0021-5

89 Chan, K, and I Gonda. *"A simple method for the preparation of gallium chloride from the citrate solution."* European journal of nuclear medicine vol. 18,10 (1991): 860. doi:10.1007/BF00175068

90 FLEX$^{TM}$ Triumph$^{TM}$ pre-clinical imaging system User Manual

91 Bolstad, Randy et al. *"Extrinsic Versus Intrinsic Uniformity Correction for γ-cameras."* Journal of nuclear medicine technology vol. 39,3 (2011): 208-12. doi:10.2967/jnmt.110.084814

92 Wang, Miao et al. *"Impact of reconstruction parameters on spatial resolution and its comparison between cadmium-zinc-telluride SPECT/CT and conventional SPECT/CT." Nuclear medicine communications* vol. 43,1 (2022): 8-16. doi:10.1097/MNM.0000000000001484

93 Qiu, Dejian and Seeram Euclid. *"Impact of Reconstruction Parameters on Spatial Resolution and Its Comparison between Cadmium-Zinc-Telluride SPECT/CT and Conventional SPECT/CT." Www.researchsquare.com*, (2021), www.researchsquare.com/article/rs-375105/v1.

94 Onoguchi, et al. *"Technical Aspects: Image Reconstruction. Annals Of Nuclear Cardiology"*, (2016). doi:10.17996/ANC.02.01.68.

95 Bai, J et al. *"Comparison of image reconstruction algorithms in myocardial perfusion scintigraphy."* Annals of nuclear medicine vol. 15,1 (2001): 79-83. doi:10.1007/BF03012138

96 Uehara, Tomoya et al. *"A Gallium-67/68-Labeled Antibody Fragment for Immuno-SPECT/PET Shows Low Renal Radioactivity Without Loss of Tumor Uptake."* Clinical cancer research : an official journal of the American Association for Cancer Research vol. 24,14 (2018): 3309-3316. doi:10.1158/1078-0432.CCR-18-0123

97 Díez-Villares, Sandra et al. *"Biodistribution of $^{68/67}$Ga-Radiolabeled Sphingolipid Nanoemulsions by PET and SPECT Imaging."* International journal of nanomedicine vol. 16 5923-5935. 26 Aug. 2021, doi:10.2147/IJN.S316767

98 Ritter, Zsombor et al. *"In situ lymphoma imaging in a spontaneous mouse model using the Cerenkov Luminescence of F-18 and Ga-67 isotopes."* Scientific reports vol. 11,1 24002. 14 Dec. 2021, doi:10.1038/s41598-021-03505-3

99 ProtParam. "ExPASy - ProtParam Tool." *ProtParam*, web.expasy.org/protparam. [Accessed: 4/09/2022]

100 Anthis, N. J., and G. M. Clore. "*Nick Anthis - Protein Parameter Calculator*." Protein Parameter Calculator, nickanthis.com/tools/a205.html. Accessed 4 Sept. 2022.

101 Radiology (ACR), Radiological Society of North America (RSNA) and American College of. "Glossary." Radiologyinfo.org, www.radiologyinfo.org/en/glossary-index. [Accessed: 19/02/2023]

102 Silva F, Mendes C, D'Onofrio A, Campello MPC, Marques F, Pinheiro T, Gonçalves Kyle, Figueiredo S, Gano L, Ravera M, Gabano E, Paulo A. Image-Guided Nanodelivery of Pt(IV) Prodrugs to GRP-Receptor Positive Tumors. Nanotheranostics 2023; 7(1):22-40. doi:10.7150/ntno.78807. https://www.ntno.org/v07p0022.htm

# Appendix 1

## 3A - ESI-MS Spectra of sample S1 obtained by US-assisted SPPS

Generic Display Report

**Analysis Info**

| | | | |
|---|---|---|---|
| Analysis Name | C:\Data\Ruben\210323_Kyle_1_P1.d | Acquisition Date | 23-03-2021 17:31:18 |
| Method | DEF_MS_NEW.M | Operator | User |
| Sample Name | 210323_Kyle_1_P1 | Instrument | HCT |
| Comment | 3A<br>2820.36 g/mol<br><br>H2O/ACN | | |

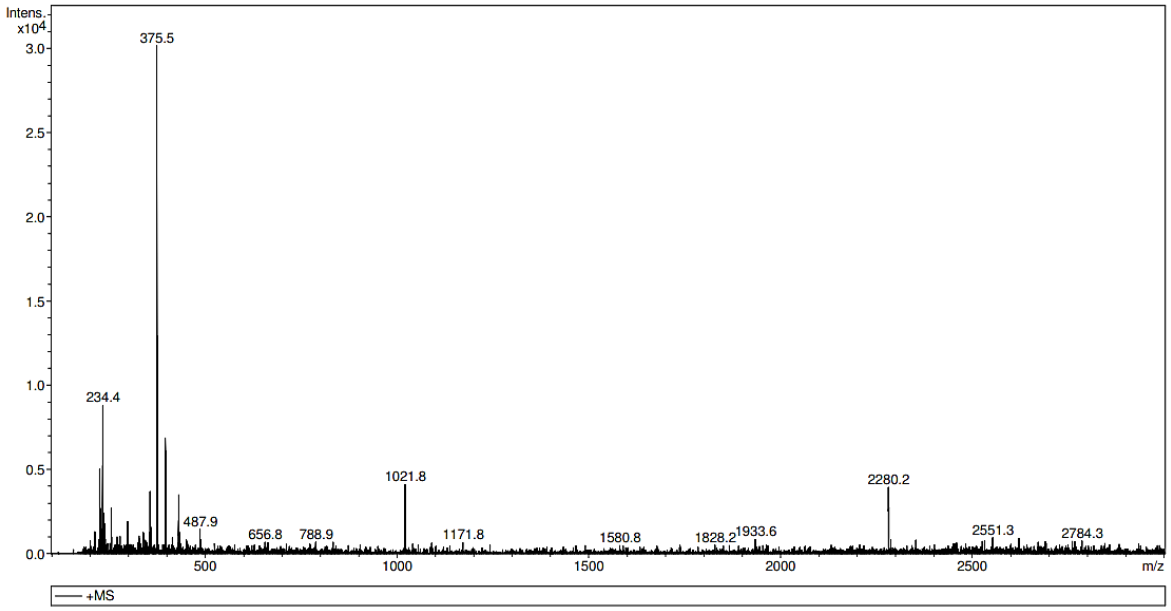

# Appendix 2

## 3A - ESI-MS Spectra of sample S2 obtained by US-assisted SPPS

Generic Display Report

**Analysis Info**

| | | | |
|---|---|---|---|
| Analysis Name | C:\Data\Ruben\210323_Kyle_2_P.d | Acquisition Date | 23-03-2021 17:36:23 |
| Method | DEF_MS_NEW.M | Operator | User |
| Sample Name | 210323_Kyle_2_P | Instrument | HCT |
| Comment | 3A<br>2820.36 g/mol<br><br>H2O/ACN | | |

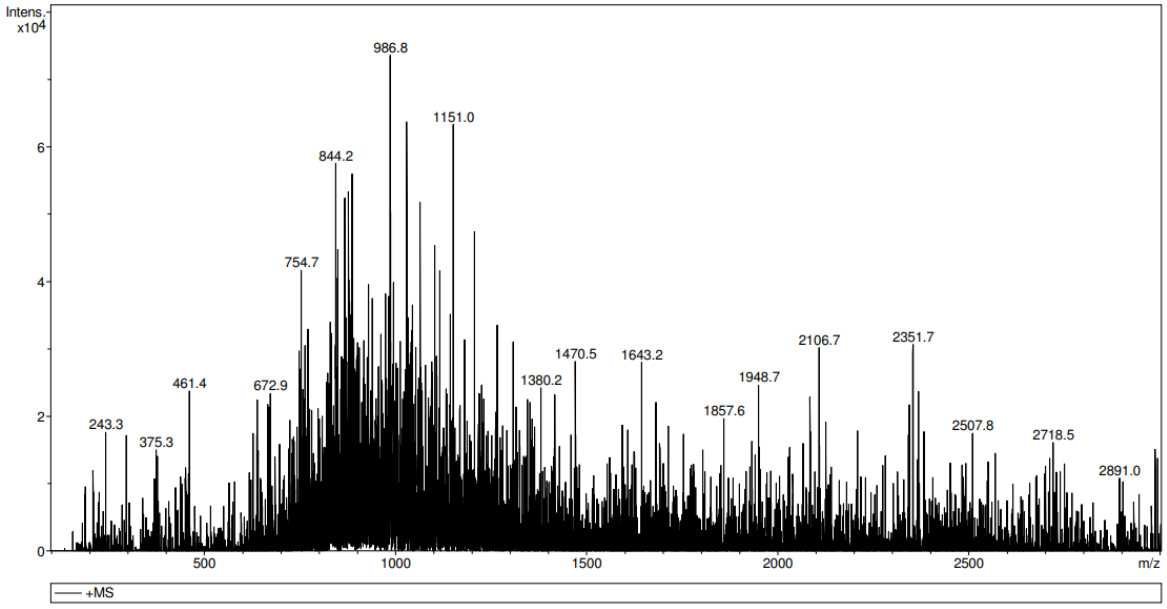

# Appendix 3

## Preparative RP-HPLC chromatogram of peptide 3A crude

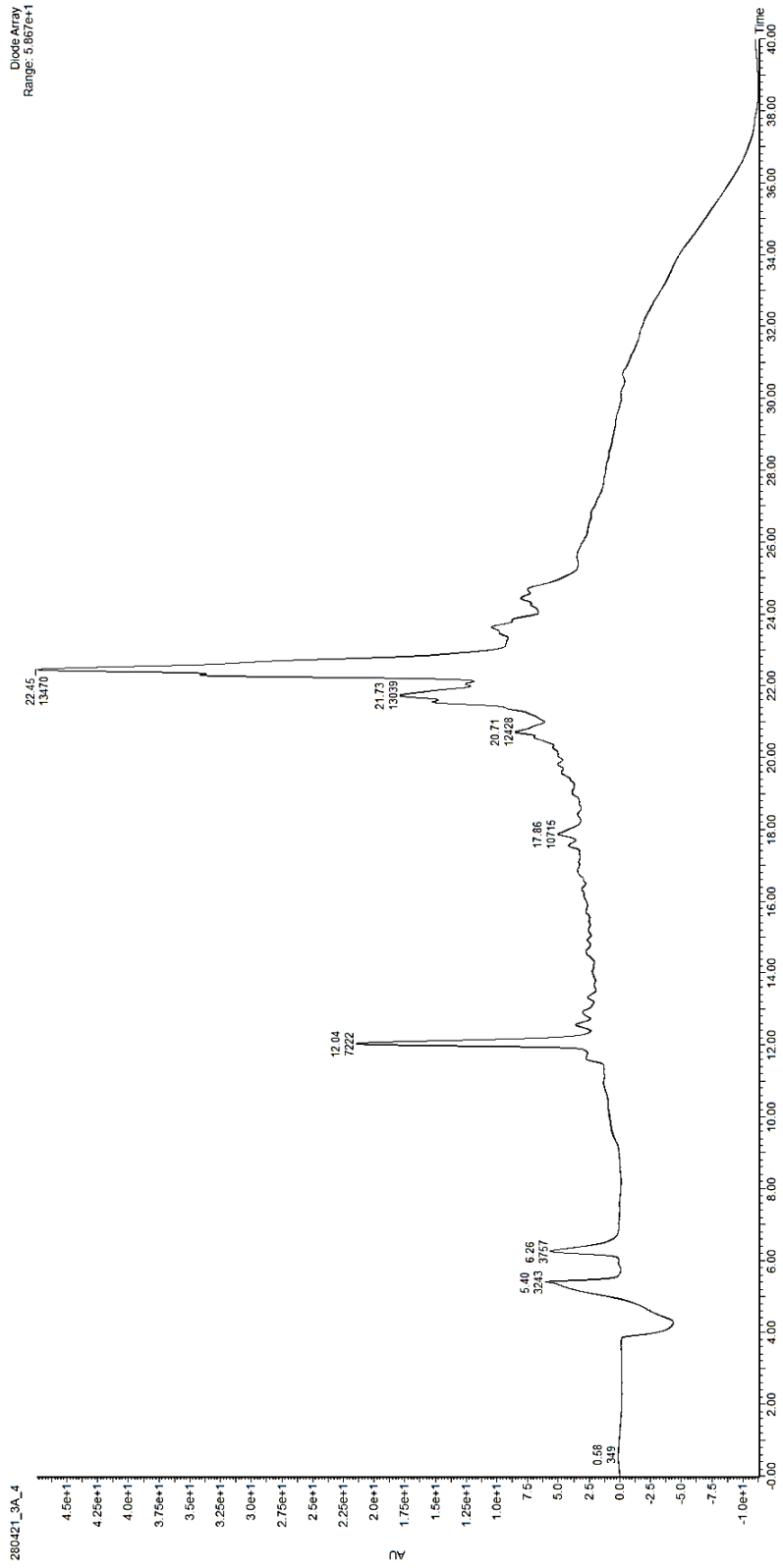

# Appendix 4

## Preparative RP-HPLC chromatogram of peptide 3B crude

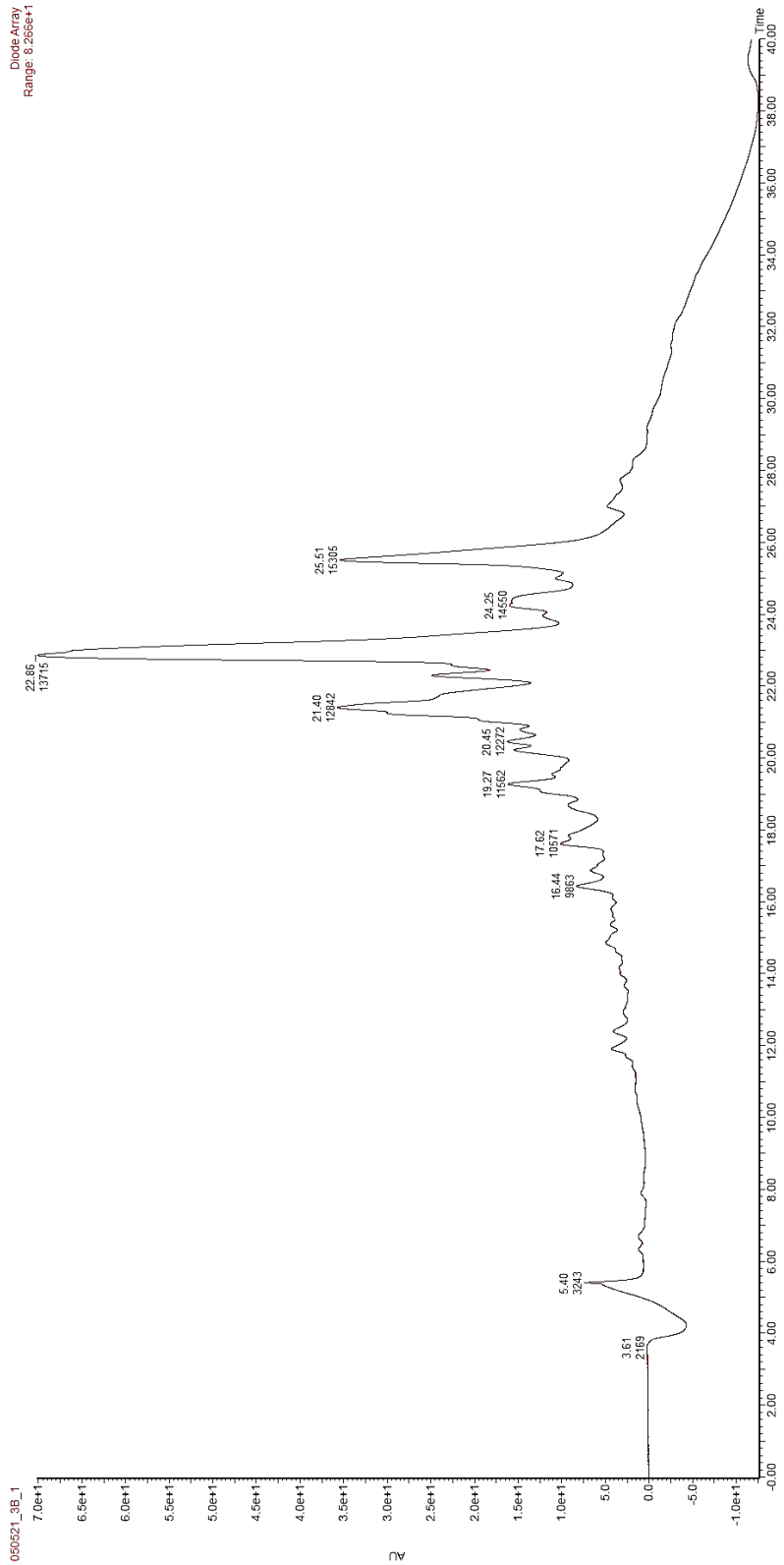

# Appendix 5
## CT and SPECT additional acquisitions

**(A)** SPECT acquisition of a $^{99m}$Tc filled syringe (25mCi). The used reconstruction method was OSEM (10 iterations, 16 subsets).

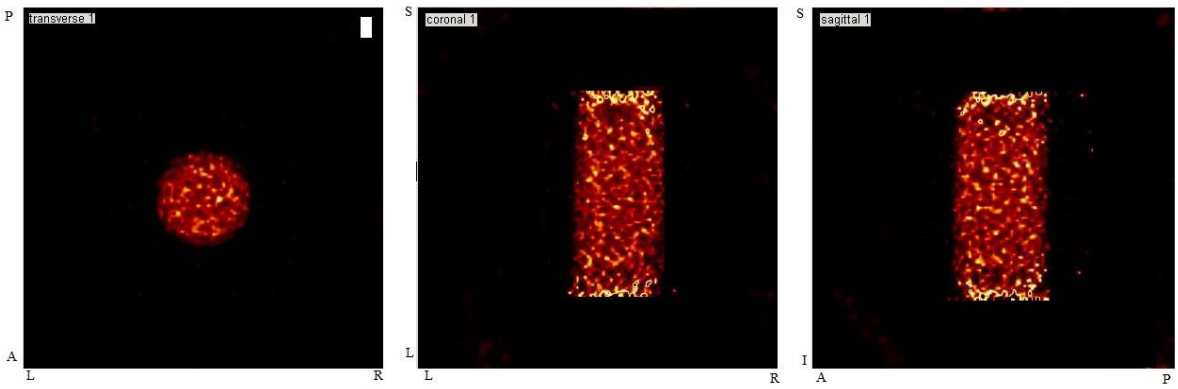


(B) CT Reconstruction of a wool doll.

**(C)** SPECT image of a mouse after injection of 99mTc-tetrofosmin (1.2 mCi). Images obtained 2 h p.i. Accumulation of activity is visible. Kidneys (Ki) and heart (H). The used reconstruction method was 3D-OSEM (10 iterations, 16 subsets).

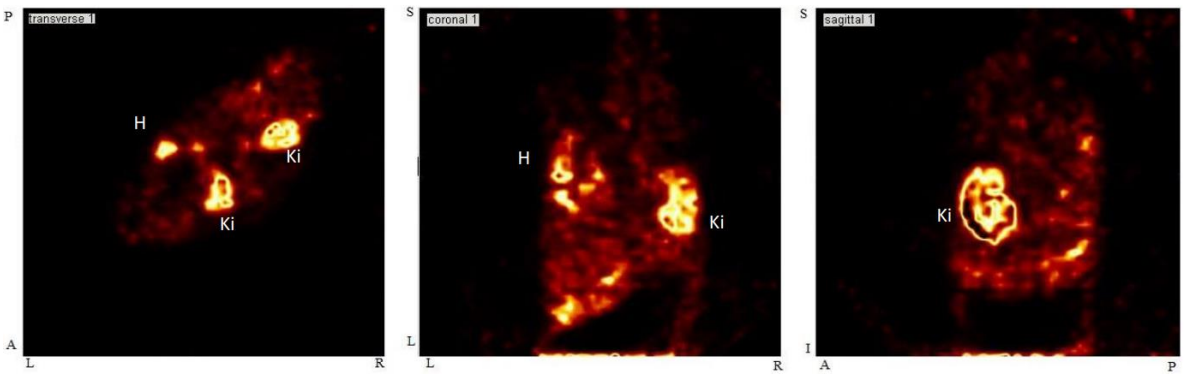

# Appendix 6
## Biodistribution of $^{67}$Ga-AuNp-BBN-Pt

**Animal model:** Balb/c mice with PC3-xenographs

**Administration:** intratumoral (50 µL)

| Organ | % Injected Activity / organ | | |
|---|---|---|---|
| | **1 h** | **24 h** | **72 h** |
| **Blood** | 3.4 ± 0.7 | 1.29 ± 0.02 | 0.43 ± 0.08 |
| **Liver** | 0.7 ± 0.3 | 7.0 ± 0.9 | 4.7 ± 0.6 |
| **Intestine** | 0.9 ± 0.4 | 3.1 ± 0.2 | 2.3 ± 0.2 |
| **Spleen** | 0.04 ± 0.01 | 0.43 ± 0.01 | 0.17 ± 0.02 |
| **Heart** | 0.14 ± 0.01 | 0.05 ± 0.01 | 0.06 ± 0.01 |
| **Lung** | 0.16 ± 0.07 | 1.1 ± 0.2 | 0.20 ± 0.07 |
| **Kidney** | 0.3 ± 0.1 | 1.1 ± 0.1 | 1.3 ± 0.1 |
| **Muscle** | 2.3 ± 1.0 | 2.2 ± 0.1 | 2.5 ± 0.3 |
| **Bone** | 0.9 ± 0.3 | 4.6 ± 0.7 | 8.3 ± 1.0 |
| **Stomach** | 0.13 ± 0.05 | 0.28 ± 0.03 | 0.25 ± 0.02 |
| **Pancreas** | 0.08 ± 0.02 | 0.19 ± 0.06 | 0.22 ± 0.09 |
| **Brain** | 0.03 ± 0.01 | 0.05 ± 0.01 | 0.04 ± 0.01 |
| **Tumor** | **77.5 ± 0.7** | **34.3 ± 1.6** | **25.6 ± 10.6** |
| **Excretion** | **2.2 ± 1.0** | **34.5 ± 0.8** | **40.7 ± 2.6** |

# Appendix 7

## Chemical Structure of peptides 3A and 3B

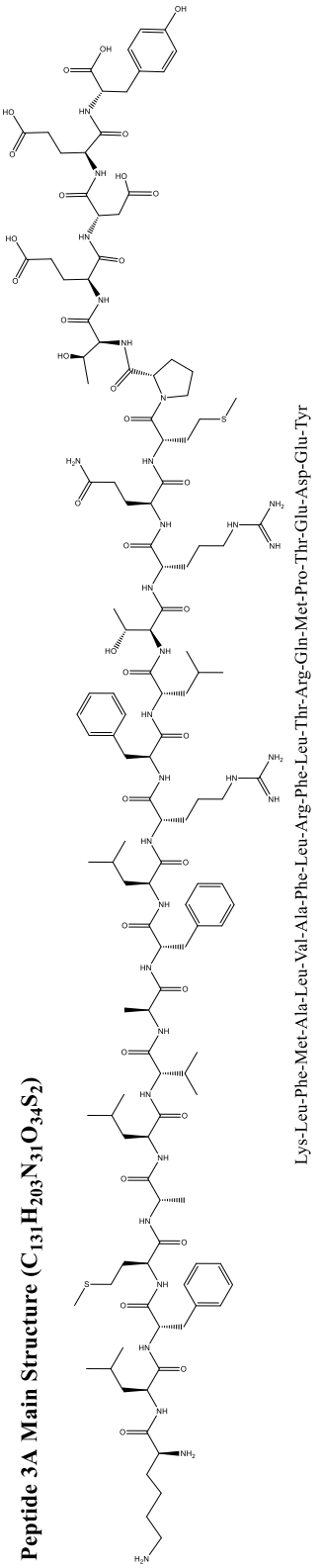

**Peptide 3A Main Structure ($C_{131}H_{203}N_{31}O_{34}S_2$)**

Lys-Leu-Phe-Met-Ala-Leu-Val-Ala-Phe-Leu-Arg-Phe-Leu-Thr-Arg-Gln-Met-Pro-Thr-Glu-Asp-Glu-Tyr

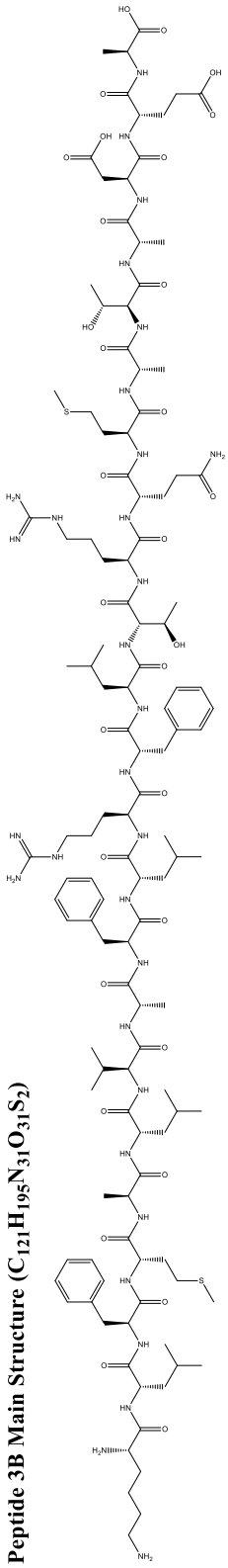

**Peptide 3B Main Structure ($C_{121}H_{195}N_{31}O_{31}S_2$)**

Lys-Leu-Phe-Met-Ala-Leu-Val-Ala-Phe-Leu-Arg-Phe-Leu-Thr-Arg-Gln-Met-Ala-Thr-Ala-Asp-Glu-Ala

# Appendix 8

## Bioconjugates C3A and C3B structure

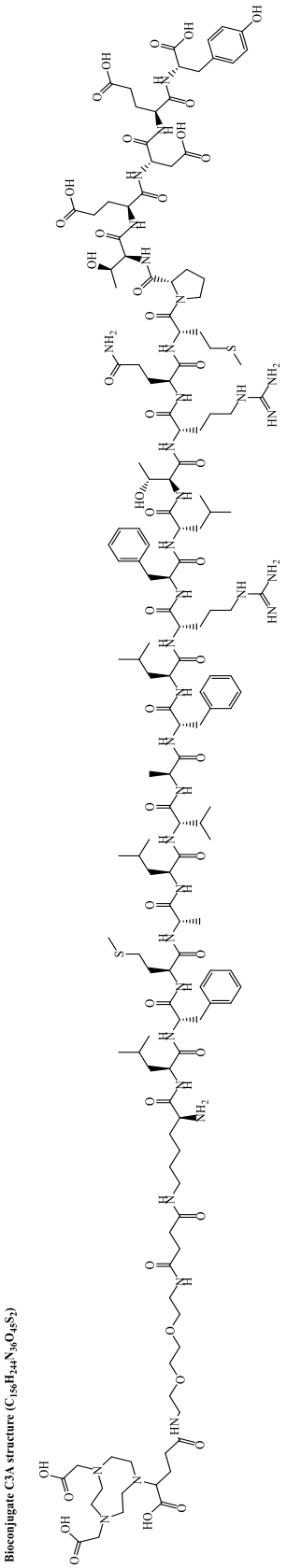

Bioconjugate C3A structure ($C_{156}H_{244}N_{36}O_{45}S_2$)

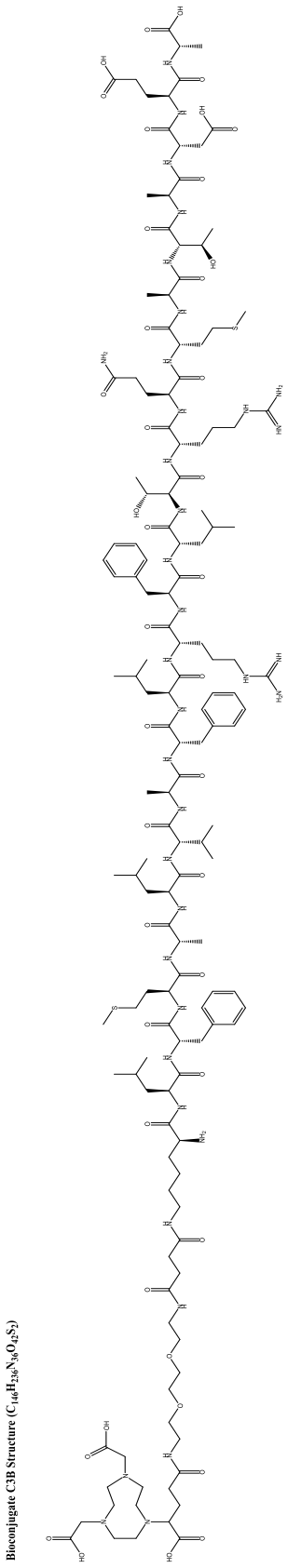

Bioconjugate C3B Structure ($C_{146}H_{236}N_{36}O_{42}S_2$)